Literature Review on Microwave and Sub-millimetre Spectroscopy for MetOp Second Generation

Emma Turner[1], Stuart Fox[1], Vinia Mattioli[2], Domenico Cimini[3]

Met Office[1], EUMETSAT[2], National Research Council of Italy[3]

This documentation was developed within the context of the EUMETSAT Satellite Application Facility on Numerical Weather Prediction (NWP SAF), under the Cooperation Agreement dated 7 December 2016, between EUMETSAT and the Met Office, UK, by one or more partners within the NWP SAF. The partners in the NWP SAF are the Met Office, ECMWF, DWD and Météo France.

Change record			
Version	Date	Author / changed by	Remarks
v1.0	26/01/2022	E. Turner	final draft

Abstract

A review of the recent research surrounding clear-sky spectroscopy between 0–1000 GHz, motivated by the forthcoming MetOp Second Generation suite of microwave and sub-millimetre instruments, is presented. The three on-board sensors: ICI, MWI and MWS build on the heritage of existing space-borne microwave instruments and expand to new frequencies, including water vapour features between 200 and 700 GHz and the little exploited 118-GHz oxygen line. The three principle molecules relevant to the spectral region: water vapour, ozone and oxygen, are reviewed in turn. Line parameters from four databases and five absorption models are compared alongside results from recent studies derived both in-situ and in the laboratory. A maximum brightness temperature range of 1.2 $\pm$0.6 K in the 200–300 GHz window is estimated from analysis of eleven water vapour continuum models. Two models are recommended to take forward for further assessment: the latest empirically constrained set of parameters from AER including the MT-CKD continuum model; and the most recent update of the Rosenkranz model, which includes parameters derived from laboratory based studies.

Contents

1 MetOp Second Generation microwave instruments 5

1.1 Ice Cloud Imager (ICI) . . . 5
1.2 MicroWave Imager (MWI) . . . 8
1.3 MicroWave Sounder (MWS) . . . 9

2 Radiative transfer models and line databases 10

2.1 Line-by-line models . . . 10
2.1.1 AMSUTRAN . . . 10
2.1.2 ARTS . . . 11
2.1.3 ATM . . . 11
2.1.4 MonoRTM (AER) . . . 12
2.1.5 Rosenkranz models . . . 12
2.1.6 LBL Comparisons . . . 13
2.2 Line databases . . . 13
2.2.1 HITRAN . . . 14
2.2.2 AER . . . 14
2.2.3 GEISA . . . 14
2.3 Fast radiative transfer models . . . 15
2.3.1 RTTOV . . . 15
2.4 Radiative Transfer Summary . . . 17

3 Water vapour 19

3.1 Water vapour lines . . . 20
3.1.1 Line shape . . . 22
3.1.2 Line parameters . . . 24
3.1.3 22.235 GHz line ($6_{16} \leftarrow 5_{23}$) . . . 24
3.1.4 183.311 GHz line ($3_{13} \leftarrow 2_{20}$) . . . 29
3.1.5 325.15 GHz line ($5_{15} \leftarrow 4_{24}$) . . . 33
3.1.6 448.00 GHz line ($4_{23} \leftarrow 3_{20}$) . . . 34
3.1.7 556.94 GHz line ($1_{10} \leftarrow 1_{01}$) . . . 36
3.1.8 752.03 GHz line ($2_{11} \leftarrow 2_{01}$) . . . 37
3.1.9 HITRAN 2020 . . . 38
3.1.10 Line absorption . . . 38
3.1.11 Water vapour lines summary . . . 44
3.2 Water vapour continuum . . . 46
3.2.1 Dimers . . . 46
3.2.2 MT-CKD . . . 47
3.2.3 Continuum models . . . 50
3.2.4 Water vapour continuum summary . . . 55

3.3 Continuum and line comparison . . . 56

4 Ozone **61**
4.1 HITRAN 2016 . . . 62
4.2 JPL 2005 v4 . . . 63
4.3 Absorption models . . . 65
4.4 JPL 2005 with broadening parameters . . . 65
4.5 Ozone lines summary . . . 67

5 Oxygen **69**
5.1 HITRAN 2016 . . . 70
5.2 Absorption models . . . 71
5.3 Line mixing . . . 71
5.4 118.75 GHz (N = 1-) . . . 72
5.5 Zeeman effect . . . 75
5.6 Oxygen lines summary . . . 76

6 Recommendations and Uncertainties **78**
6.1 Recommended models . . . 78
6.2 Parameter uncertainties . . . 81
6.3 Recommendations to spectroscopists . . . 83
6.4 Recommendations and Uncertainties summary . . . 85

7 Summary and conclusions **86**

Appendices **89**

A Profile datasets **89**

References **90**

1 MetOp Second Generation microwave instruments

Table 1: ICI channel spectral characteristics.

Channel number	Centre frequency (GHz)	Frequency offset (GHz)	Bandwidth (GHz)	Polarisation	Feature
1	183.31	7.0	2.0	V	H_2O
2	183.31	3.4	1.5	V	H_2O
3	183.31	2.0	1.5	V	H_2O
4*	243.2	2.5	3.0	V,H	H_2O continuum
5	325.15	9.5	3.0	V	H_2O
6	325.15	3.5	2.4	V	H_2O
7	325.15	1.5	1.6	V	H_2O
8	448.0	7.2	3.0	V	H_2O
9	448.0	3.0	2.0	V	H_2O
10	448.0	1.4	1.2	V	H_2O
11*	664.0	4.2	5.0	V,H	H_2O continuum

* Some sources defines channels with dual polarisation (V & H) as two separate channels.

Table 2: MWI channel spectral characteristics.

Channel number	Centre frequency (GHz)	Frequency offset (GHz)	Bandwidth (GHz)	Polarisation at 53° downwards view	Feature
1*	18.7		0.2	V,H	H_2O continuum
2*	23.8		0.4	V,H	H_2O
3*	31.4		0.2	V,H	H_2O continuum
4*	50.3		0.4	V,H	window/O_2
5*	52.61		0.4	V,H	O_2
6*	53.24		0.4	V,H	O_2
7*	53.75		0.4	V,H	O_2
8*	89.0		4.0	V,H	H_2O continuum
9	118.7503	3.2	0.5	V	O_2
10	118.7503	2.1	0.4	V	O_2
11	118.7503	1.4	0.4	V	O_2
12	118.7503	1.2	0.4	V	O_2
13	165.5	0.75	1.35	V	H_2O continuum
14	183.31	7.0	2.0	V	H_2O
15	183.31	6.1	1.5	V	H_2O
16	183.31	4.9	1.5	V	H_2O
17	183.31	3.4	1.5	V	H_2O
18	183.31	2.0	1.5	V	H_2O

* Some sources defines channels with dual polarisation (V & H) as two separate channels.

1.1 Ice Cloud Imager (ICI)

ICI is a conical scanning radiometer that will fly on the MetOp-SG-B satellite with five bands comprising 11 channels measuring in the 183–664 GHz range (Accadia et al., 2020; Bergadá et al., 2016; Thomas et al., 2014). Channel characteristics and clear-sky features are listed in Table 1. The primary purpose of ICI will be to measure ice clouds and this will fill an observational gap for meteorology by sensing different altitudes of cloud depending on frequency, and estimate cloud ice water path and mean ice particle size (Eriksson et al., 2020; Wang et al., 2017). ICI presents new challenges for spectroscopy, not only for hydrometeors, but for the clear-sky too, as past improvements have almost exclusively focused on the region below 200 GHz. Apart from a handful of exceptions including: SMR (Submillimeter and Millimeter Radiometer), still operating on Odin, the Swedish smallsat launched in 2001 (Frisk et al., 2003); SMILES (Superconducting Submillimeter-Wave Limb-Emission Sounder), deployed on the International Space Station for seven months (Kikuchi et al., 2010); and MLS (Microwave Limb Sounder), which has operated on the Aura satellite since 2004 (Froidevaux et al., 2006); this has traditionally been the upper spectral limit of atmospheric microwave radiometers. As the astronomical community relies on this region for radio-telescope measurements some insights may be gleaned from the cross-over to higher frequencies. A review of sub-millimetre atmospheric observations from Top-of Atmosphere (TOA) and ground vantage points can be found in Turner et al. (2016).

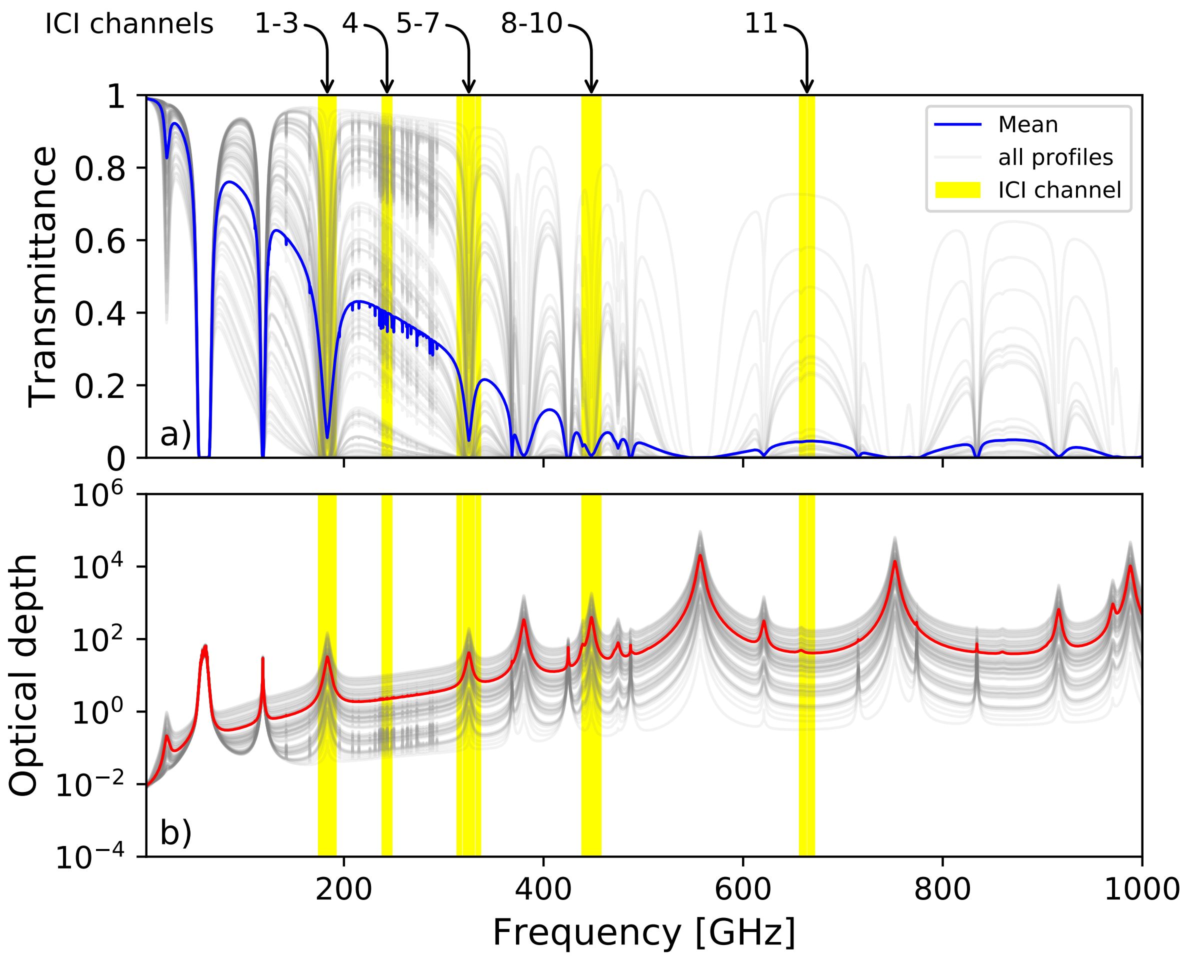

Figure 1: Total surface to space a) transmittance and b) optical depth for 83 diverse atmospheric profiles (grey lines) and their mean (bold lines), produced by the AMSUTRAN line-by-line model using the spectroscopic configuration described in section 2.1.1. The coverage of ICI channels are shaded yellow.

Although there is a lack of satellite data covering the sub-millimetre region, observations with which to test the new configuration may be sought from aircraft measurements. Fox et al. (2017b) presents a comparison of simulations calculated using a variety of spectroscopic combinations with measurements from the airborne instrument International SubMillimetre Airborne Radiometer (ISMAR) (Fox et al., 2017a), which is a demonstrator built to inform decisions on the design of ICI.

Figure 1 shows the location of ICI channels in the sub-millimetre (>300 GHz), and microwave spectrum. The five bands are strategically positioned to take advantage of the varying absorption of water vapour, with three straddling major spectral lines at 183.31, 325.15 and 448.00 GHz, and two centered over window regions at 243.20 and 664.00 GHz, even though the latter will be affected by strong neighbouring lines at 556.94 and 752.03, both will be affected by the water vapour continuum. The 83 atmospheric profiles used in the absorption calculations (grey lines) were selected to represent the diverse range of possible atmospheric conditions (Matricardi, 2008). This dataset is used for all radiative calculations shown throughout this review and are described in Appendix A.

Table 3: MWS channel spectral characteristics.

Channel number	**Centre frequency (GHz)**	**Frequency offset (GHz)**	**Bandwidth (GHz)**	**Polarisation downwards view**	**Feature**
1	23.8		0.27	V or H	H_2O
2	31.4		0.18	V or H	H_2O continuum
3	50.3		0.18	V or H	window/O_2
4	52.8		0.4	V or H	O_2
5	53.246	0.08	0.14	V or H	O_2
6	53.596	0.115	0.17	V or H	O_2
7	53.948	0.081	0.142	V or H	O_2
8	54.4		0.4	V or H	O_2
9	54.94		0.4	V or H	O_2
10	55.5		0.33	V or H	O_2
11	57.290344		0.33	V or H	O_2
12	57.290344	0.217	0.4	V or H	O_2
13	57.290344	0.3222±0.048	0.36	V or H	O_2
14	57.290344	0.3222±0.022	0.16	V or H	O_2
15	57.290344	0.3222±0.010	0.08	V or H	O_2
16	57.290344	0.3222±0.0045	0.03	V or H	O_2
17	89.0		4.0	V or H	H_2O continuum
18	165.5	0.725	1.35	V or H	H_2O continuum
19	183.31	7.0	2.0	V or H	H_2O
20	183.31	4.5	2.0	V or H	H_2O
21	183.31	3.0	1.0	V or H	H_2O
22	183.31	1.8	1.0	V or H	H_2O
23	183.31	1.0	0.5	V or H	H_2O
24	229.0		2.0	V or H	H_2O continuum

There is a considerable amount of variation in transmittance and optical depth between atmospheric profiles, but in general, beyond 200 GHz the atmospheric transmittance from surface to space falls off rapidly, due to the opacity from pure rotational transitions of water vapour. Even with a dry atmosphere there will be little transmittance from the surface at frequencies higher than 500 GHz, however, there are two ‘partial’ windows centred around 650 and 850 GHz that transmit a small amount (around 10%) in very low humidity conditions.

1.2 MicroWave Imager (MWI)

MetOp-SG-B satellite will also carry the MWI instrument, which is a conical scanning total power microwave radiometer, providing calibrated and geolocated measurements in 18 channels (26 if the dual polarised channels are separated). Channels are listed in Table 2. Its primary objective is to measure precipitation including snow, drizzle, light precipitation and the height and depth of the melting layer, over sea and land. It will also sense water vapour profiles and surface imagery including sea-ice and snow. Channels 9–12 on MWI are centred at 118.75 GHz, which is an oxygen line that has not been exploited for temperature measurements nearly as much as the lower frequency O_2 band at 50–60 GHz. Only a handful of instruments in orbit measure around this line, including: MHWS-2 (Micro-Wave Humidity Sounder-2) on the Chinese Feng-Yun 3C and 3D satellites, MLS on Aura, and the GEMS-1 (Global Environmental Monitoring System-1) cubesat from Orbital MicroSystems[1].

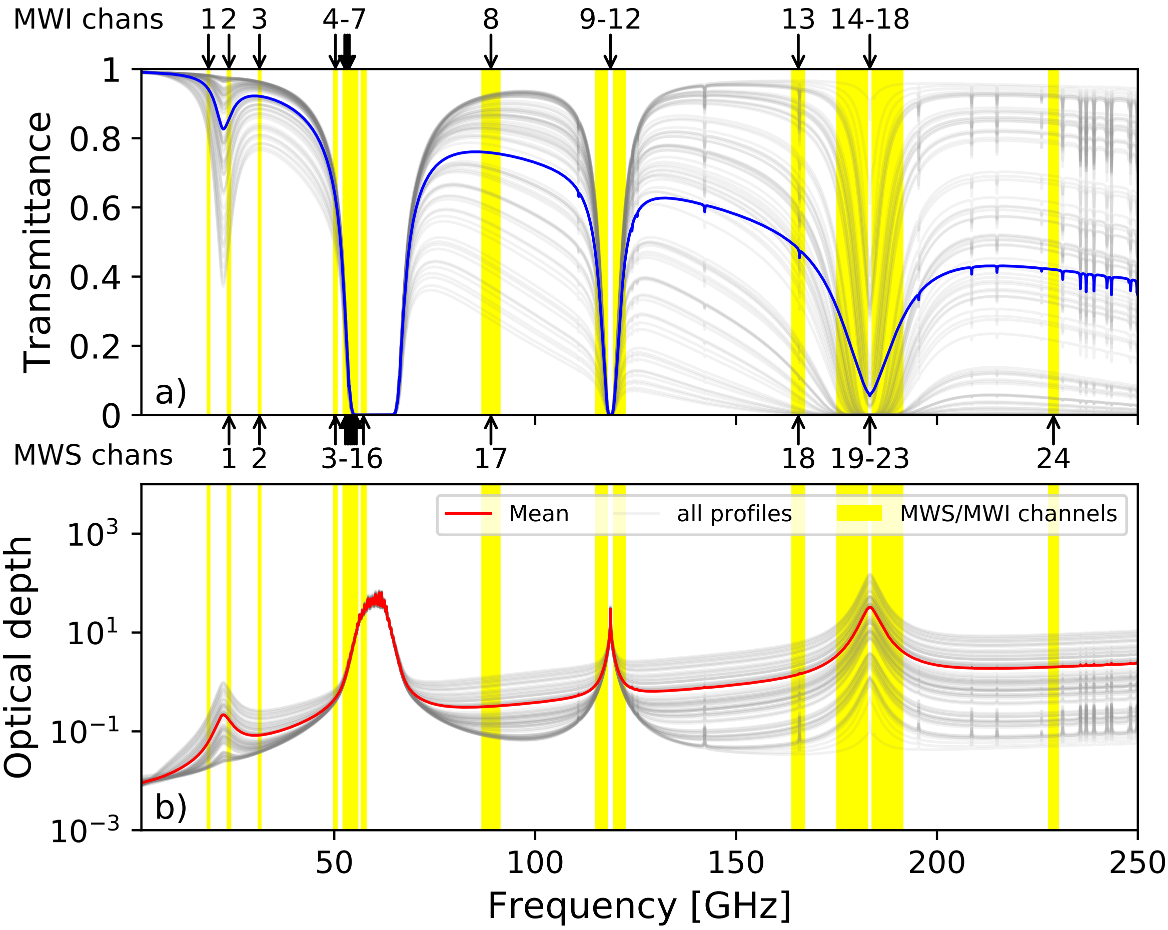

Figure 2: As Figure 1 but enhanced for the microwave part of the spectrum below 250 GHz. The coverage of MWI and MWS channels are shaded yellow.

[1] https://www.orbitalmicro.com/gems

1.3 MicroWave Sounder (MWS)

MWS will be part of the payload of the MetOp-SG A satellite, the first one to be launched. It builds on the heritage of past successful microwave radiometers such as the Advanced Technology Microwave Sounder (ATMS) (Kim et al., 2014), and the Advanced Microwave Sounding Unit (AMSU) Kidder et al. (2000), with overlapping channels chosen to provide continuation with these missions. It also has a unique channel at 229 GHz that has no legacy and which will provide measurements of ice clouds. In the clear-sky this channel will primarily be affected by the water vapour continuum in the clear-sky as it is not near any major lines. The position of MWI and MWS channels in the microwave spectrum are shown in Figure 2. As it demonstrates all of the major features are covered by both of these instruments.

2 Radiative transfer models and line databases

Assimilation of satellite measurements in numerical weather prediction (NWP) models, and retrieval of atmospheric and surface quantities requires an accurate radiative transfer model. Line-by-line (LBL) models, when operating in forward mode, calculate radiances by performing the full absorption calculation over all spectral lines (the 'line' in line-by-line), which are often numerous. Owing to this they can be very computationally and time intensive, which renders them unsuitable for use in NWP models. A 'fast' model recreates the results of the line-by-line calculation in a timely manner, within an acceptable error, by parameterising the absorption process. When simulating satellite instruments, the computational expense is further reduced by restricting the spectral range to the channels of the sensors in question. The conversion from monochromatic to broadband further introduces a loss of accuracy, which can be minimised via various techniques (i.e. band correction coefficients). Multiple separate radiative transfer models have evolved over several decades and their independence provides robustness, which can be evaluated with inter-model comparisons. This section describes some of the existing models used in microwave/sub-millimetre region; some are designed to be applicable only to this range and some have a wider spectral reach to the infrared and even visible domains.

2.1 Line-by-line models

LBL models have benefited in recent times by increases in computational power and storage. Some are created for a particular purpose, typically related to space-borne or ground-based atmospheric or astronomical measurements, and some are made publicly available to serve the research community; often the first leading to the second. A subset of these LBL models: AMSUTRAN, ARTS, ATM, MonoRTM and the Rosenkranz model, are discussed here in turn. All apart from ARTS can be thought of as complete absorption models, where the absorption routines and fixed associated spectroscopic parameters are specified. ARTS allows the spectroscopy and routines to be individually selected, including many of these models as options.

2.1.1 AMSUTRAN

AMSUTRAN is a transmittance model with TOA down-looking geometry that has been developed and maintained by the Met Office for over 20 years with the primary purpose of producing a set of satellite instrument specific channel-averaged transmittances for a standard atmospheric profile dataset. The code can also generate monochromatic output, which is primarily used for its own development. The core of the code was originally based on the complex refractivity based Millimeter Propagation Model (MPM) (Liebe and Layton, 1987), with line and continuum parameters taken from Liebe (1989) and Liebe et al. (1992). The only molecules considered in MPM89 are water vapour, oxygen and nitrogen. Full details can be found in Turner et al. (2019).

A handful of AMSUTRAN's spectroscopic parameters have undergone modification based on more recent research, such as improved values for the line coupling coefficients and broadening parameters for key lines. Spectroscopy extends to 1000 GHz yet the focus of verification has remained below 200 GHz, as this is domain of the current suite of space-borne atmospheric instruments.

The changes made to the MPM87/MPM89 configuration are:

- All oxygen line parameters have been replaced with those given in Tretyakov et al. (2005, Table 5).
- The oxygen continuum parameterisation is from Liebe et al. (1992).
- The nitrogen continuum is from Liebe et al. (1993).
- The air-broadened half-width of the 22.235 GHz water vapour line has been replaced by the HITRAN 2000 equivalent (Rothman et al., 2003), based on the endorsement by Liljegren et al. (2005).
- The air-broadened half-width and associated temperature dependence for the 183.31 GHz water vapour line have been replaced by those derived by Payne et al. (2008). The study presents two values for the first quantity, and the one adopted by AMSUTRAN is theoretically derived from the complex implementation of the Robert-Bonamy (CRB) theory (Robert and Bonamy, 1979).
- The 35 most intense ozone lines below 300 GHz have been incorporated using line parameters from HITRAN 2000. The implementation is described in Turner et al. (2019, Appendix A).

The above configuration and listed modifications constitute the spectroscopy that was 'frozen' in 2016 and remains un-changed at the time of writing, though this is likely to change in the future.

2.1.2 ARTS

The Atmospheric Radiative Transfer Simulator (ARTS) is a public domain project[2], which was initiated and developed jointly in 2000 by the University of Bremen and Chalmers University, and now the University of Hamburg (Buehler et al., 2018; Eriksson et al., 2011; Buehler et al., 2005). It was initially created for remote sensing applications (though not a fast model), and was designed for the millimetre/sub-millimetre but now also extends to the thermal infrared. In contrast to the other models discussed, it is truly flexible in design, allowing the user to select, or even add, the component parts such as absorption routines and line parameters, and therefore emphasis has been placed on a modular structure. Implemented in C++ programming language, it is the only model here not to be written in Fortran, and also provides spherical geometry up to three dimensions. It is also heavily developed in the area of ice cloud simulation in preparation for ICI retrievals (Barlakas and Eriksson, 2020; Fox et al., 2019).

2.1.3 ATM

The Atmospheric Transmittance at Microwaves (ATM) model was constructed in the years preceding 2000 primarily for use in the astrophysical community (Pardo et al., 2001a). It includes lines up to 10 THz in order to account for the far-wing opacity below 2 THz. Line intensities are derived from constituents of the rotational Hamiltonian; for water vapour this is the Watson-type (Watson, 1977). Rotational constants for the $H_2^{16}O$ molecule are from Matsushima et al. (1995). Line broadening parameters are quoted to originate from Rothman et al. (1992), and most appear to be from Liebe (1989), for all apart from the nominal air and self broadened half-widths of the 183.31 GHz line. The wet and dry continuum parameters are derived from in-situ measurements made on the summit of Mauna Kea (Hawaii) in very dry conditions (Pardo et al., 2001b).

2 https://www.radiativetransfer.org/

2.1.4 MonoRTM (AER)

The MonoRTM[3] radiative transfer model is produced by the Radiative Transfer group at Atmospheric and Environmental Research (AER); a U.S. based experimental research centre. AER is well-known for LBLRTM (Line-By-Line Radiative Transfer Model), which is widely used and utilizes the same physics as MonoRTM but is designed for more intensive use across the spectrum. See Clough et al. (2005) for an overview of all AER models. By contrast, MonoRTM is designed to process a small number of monochromatic frequencies, such as for the microwave/sub-millimetre. Wavenumbers are the spectral unit used across all domains, in contrast to frequency, which is used in AMSUTRAN, ATM and the Rosenkranz model. The associated line files and continuum codes (MT-CKD) are regularly reviewed and refined at regular intervals. These are discussed at more length in sections 2.2.2 and 3.2.2.

2.1.5 Rosenkranz models

The earlier version of the Rosenkranz family of microwave LBL models, Rosenkranz (1998), otherwise known as PWR98 or sometimes R98, is similar to the MPM model in its core structure with only a few differences including a 750 GHz line cutoff and only half (15) the number of water vapour lines. The line intensities are from the HITRAN 1992 database (Rothman et al., 1992) and the broadening parameters match those in Liebe (1989) with the exception of one or two values. The water vapour continuum is a combination of the foreign continuum from the latter, and a re-investigation of the self continuum calculated in Liebe et al. (1993), adjusted to be consistent with a line cutoff.

As with MPM some of the spectroscopic parameters have been updated over time, with too many adjustments to list here. At the time of writing the model was last updated in 2019[4], hence will be referred to as PWR19. For the molecules of interest, the main differences from the previous release are:

- The addition of a 16th $H_2^{16}O$ line centered at 658.01 GHz.
- Some broadening and shifting parameters for the 22.235 and 183.31 GHz lines are replaced by those given in Tretyakov (2016) and Koshelev et al. (2018a).
- The addition of self-induced pressure shift parameters and a limited number of pressure shift temperature dependencies.
- A routine for calculating the speed-dependent lineshape for the 22.235 GHz line is included.
- Ozone has been extended from 17 to 320 lines.
- Second order line mixing has been added to oxygen with parameters from Makarov et al. (2018)

Prior to the PWR19 version, the model was updated in 2017 and this version is described in Cimini et al. (2018). As far as can be determined, the main differences between PWR17 and PWR98 are:

- The foreign and self continuum parameters are scaled by 1.105 and 0.79, respectively, following Turner et al. (2009).

[3] http://rtweb.aer.com/monortm_frame.html [4] https://rscl-grss.org/coderecord.php?id=483

- Almost all parameters have changed based on various laboratory studies that focus on constraining key lines, the only exceptions being some of the broadening temperature dependencies.

All three versions: PWR98, PWR17 and PWR19 are compared in the following sections.

2.1.6 LBL Comparisons

As many of these LBL models are developed in isolation performing inter-comparisons are a vital tool for validating results, catching errors and assessing the uncertainty due to the range of possible parameters and procedures, for example see: Pardo and Rayer (2016); Cady-Pereira et al. (2018) and Schreier et al. (2018). Comparing model simulations with observations via radiative closure experiments, to 'close the gap' between parameters estimated and true values, are also an essential part of the evaluation process as it is impossible to decide which model is more correct without real world data (Brogniez et al., 2016; Bobryshev et al., 2018).

Focusing on sub-millimetre wavelengths; Melsheimer et al. (2005) compares clear-sky simulations from eight LBL models, including ARTS, where many of the models have variable choices of: line catalogue, partition function, line shape, continuum absorption, refraction and geometry. Differences of up to $\sim$10% near line centres are found when own choice of spectroscopy was allowed. When it is fixed to isolate model procedures, differences reached 16% at higher altitudes, depending on the lineshape applied (Van-Vleck Weisskopf (VVW) or Voigt). This corresponds to $\sim$1 K difference in upwelling brightness temperature in window regions. Deviations of up to 2% are also found to originate from the different temperature conversion schemes of the line strengths. The list of causes identified for discrepancies between models is extensive, including: line-shapes, inclusion of self-broadening and pressure shift routines, partition functions, vertical interpolation, Planck vs. Rayleigh-Jeans brightness temperature, surface emissivity routine, refraction, sensor description and bugs in the code. The authors conclude that spectroscopic assumptions are the largest source of uncertainty for the calculation of absorption coefficients.

Radiative closure experiments commonly show much larger differences between simulations and measurements than between the models themselves and this has also been attributed to insufficient knowledge of the spectroscopy (Matricardi, 2007). The absorption models compared in this review: AMSUTRAN, ATM, MonoRTM and PWR are reduced to their absorption routines to isolate spectroscopic differences. Any brightness temperature differences are performed with the same radiative transfer and profile interpolation tools, which is based on AMSUTRAN.

2.2 Line databases

In additional to the complete absorption models, an extensive compilation of spectral lines can readily be found in one of the continually evolving spectroscopic databases that are publicly available. These are lists of parameters that are maintained and incrementally refined based on a variety of evaluation techniques and new data that has emerged since the last incarnation. These databases tend to be in cgs (centimetre-gram-second) units, i.e. wavenumber, as they also cover the infrared region where units of frequency is not appropriate. They contain numerous lines totaling hundreds, if not thousands, of transitions when all isotopologues are included.

Care must be taken when running radiative transfer calculations that the line database employed complements the continuum models used. See section 3.3 for more detail on the continuum.

2.2.1 HITRAN

The most well-known example is possibly HITRAN (HIgh-resolution TRANsmission molecular absorption database), which has been released approximately every four years since the early 1970's (Gordon et al., 2017; McClatchey et al., 1973). The group are continuously updating various molecules, totaling 55 at the current time, which are available on the online database[5]. The most recent complete release is HITRAN 2016 but HITRAN 2020 is due in 2021. Both HITRAN 2016 and the previous version, HITRAN 2012, are investigated in this review.

2.2.2 AER

AER adopts an empirical philosophy for validating atmospheric spectroscopy, based on the results of atmospheric campaigns. The line database designed for use in its radiative transfer models takes HITRAN as a base and makes modifications to significant lines based on the results of dedicated atmospheric closure experiments, e.g. Turner et al. (2012). For example, ten water vapour lines in the 0–1000 GHz range were modified for the update to AER version 3.5; the intensities of the 22.23, 183.31, 325.15 and 380.19 GHz lines were reduced by 1–2% (Clough et al., 1973), and the air-broadened half-widths of the 22.23, 183.31, 556.93, 620.70, 752.03, 916.17 and 987.92 GHz lines were increased by between 2-6 % based on the RHUBC-II campaign (Mlawer et al., 2019). A subset of the database known as the 'fast' version is also available, which retains only those lines that contribute significantly to the total absorption whilst reducing computational expense. There are 338 water vapour lines between 0–1750 GHz, which is around one fifth of the original 1600 from the parent HITRAN 2012 catalogue. The current line file available is AER 3.8, which is unchanged from AER 3.5 for water vapour in the spectral region of interest.

2.2.3 GEISA

The GEISA (Gestion et Etude des Informations Spectroscopiques Atmosphériques: Management and Study of Atmospheric Spectroscopic Information) spectroscopic database has been developed at the Laboratoire de Météorologie Dynamique (LMD), France, since the early 1970's, and there have been six releases, the latest of which is GEISA 2019[6]. See Jacquinet-Husson et al. (2016) for the latest documentation. One way in which GEISA differs from HITRAN is that it considers symmetry properties of isotopologues independently, and uses radiative closure studies to evaluate data before accepting it into the database, though this technique has thus far been restricted to the infrared. Fewer lines are included compared to the HITRAN database, for example there are 827 water vapour lines in the 1–1750 GHz region, about half that of HITRAN 2016. The previous version, GEISA 2015, contains updates to the water vapour line position and intensity parameters from 321 GHz onwards based on Coudert et al. (2014) but there has been no change in these parameters between the 2015 and 2019 versions. Remaining intensities and broadening parameters take the same values as those in the HITRAN 2016 catalogue.

[5] https://hitran.org/ [6] https://geisa.aeris-data.fr/interactive-access/?db=2019&info=ftp

Following a similar philosophy to AER, the developers of the GEISA database have recently produced a Spectroscopic Parameters And Radiative Transfer Evaluation (SPARTE) tool, in order to screen candidate spectroscopy based on comparisons with a wide range of observations, such as radiosondes (Armante et al., 2016).

2.3 Fast radiative transfer models

Fast models are useful for making the large volume of data processing involved in radiative transfer manageable, and are a necessity for the assimilation of remote sensing data in NWP models (Eyre et al., 1993). RTTOV (Radiative Transfer for TOVS) is perhaps the most well-known example of a fast model for remote sensing applications, and is discussed in the next section. Additionally there is also the Community Radiative Transfer Model (CRTM) (Liu et al., 2008); developed at NOAA Center for Satellite Applications and Research (NCAR) and the Joint Center for Satellite Data Assimilation (JCSDA), which contains many similarities to RTTOV, including use of the FASTEM surface emissivity model and the capability of using MPM as the underlying LBL model, though the standard configuration is PWR98. There are several differences, however, including construction of predictors and the input requirements. Recently, a new fast model called ARMS (Advanced Radiative Transfer Modelling System) has been developed by Yang et al. (2020), which inherits many features from RTTOV and CRTM but focuses specifically on the Fengyun satellites for NWP data assimilation, requiring enhancement of routines used for simulation of aerosols and ice clouds.

2.3.1 RTTOV

RTTOV is designed to simulate the measurements of satellite instruments (Saunders et al., 2018), but has also been adapted to calculate from ground-based observing geometry by an external party (De Angelis et al., 2016; Cimini et al., 2019). In lieu of LBL absorption routines, RTTOV uses predictors; functions of the applied atmospheric profile, which are combined with pre-constructed satellite coefficients; essentially a look-up table, to compute the optical depth of each layer from which TOA radiative quantities such as brightness temperature are calculated. AMSUTRAN is the underlying LBL model used to create microwave coefficients, and LBLRTM handles the infrared. First developed at the European Centre for Medium Range Weather Forecasting (ECMWF) in the 1990's in preparation for the TIROS Operational Vertical Sounder (TOVS) radiometers (Eyre, 1991), it became a key deliverable of the EUMETSAT-funded Numerical Weather Prediction Satellite Application Facility (NWP SAF) in 1998, and can now simulate virtually any passive satellite instrument upon request. Over time there have been many extensions and improvements made and the most recent version, RTTOV 13; released in 2020, includes a significant change to the optical depth parameterisation, as described in (Hocking et al., 2021). This change involves a re-organization of the predictor structure, which allows additional gases to be easily added to the code without having to recalculate all combinations of transmittances, a measure that was previously necessary for the infrared where large data volumes require a static transmittance database.

Validation statistics; the skill of RTTOV against its underlying LBL model, AMSUTRAN, are shown for ICI channels in Figure 3. Mean differences are very low; not exceeding 0.01 and associated standard deviations are

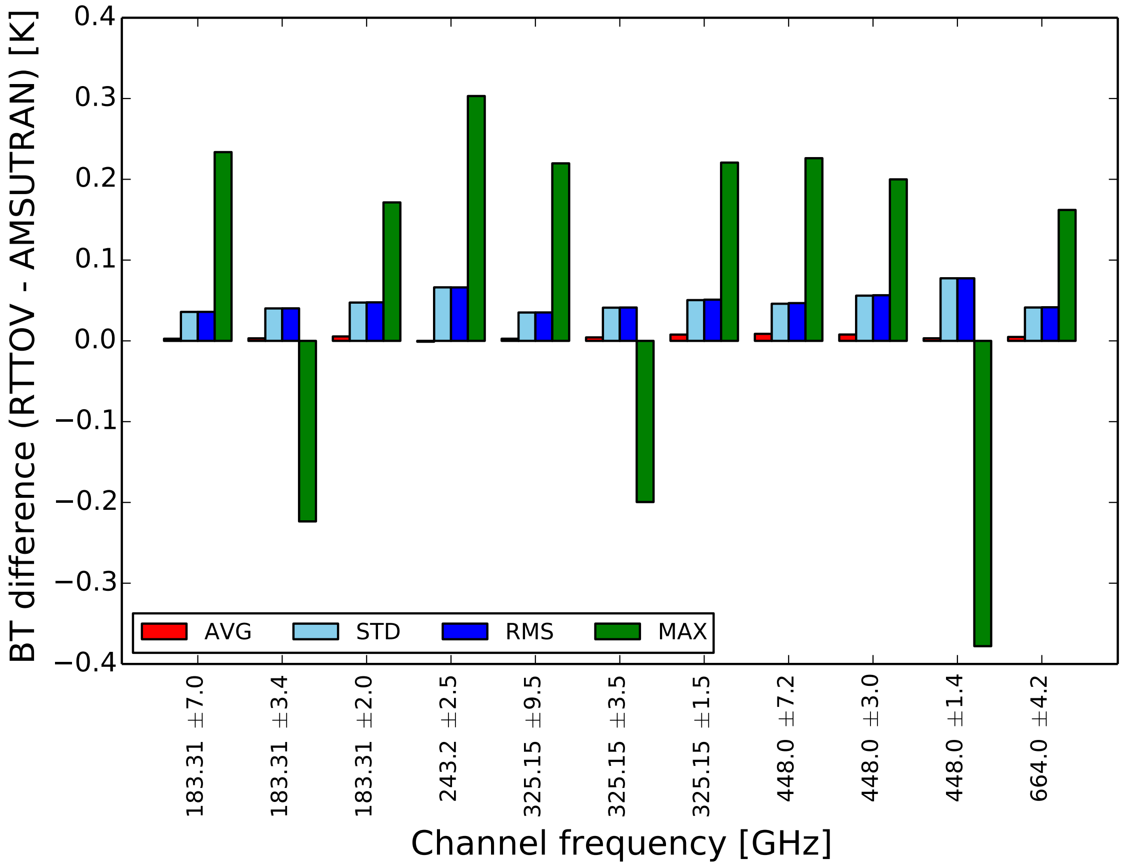

Figure 3: Clear-sky TOA brightness temperature differences in ICI channels between RTTOV 12 and channel integrated radiances from the underlying LBL model, AMSUTRAN. The spectroscopic configuration is the one from section 2.1.1, therefore ozone is only included up to 300 GHz. AVG is the mean, STD is the standard deviation, RMS is the root mean squared error, and MAX is the maximum difference between AMSUTRAN and RTTOV, over all 83 profiles and 6 viewing angles. An emissivity of 1 is assumed.

below 0.08 K. Maximum differences can be much larger for some extreme profiles though; up to a 0.4 K is seen in channel 10.

Fast models tend to show good agreement with their underlying LBL code, but can display bigger discrepancies between each other, usually resulting from the different spectroscopy in the LBL codes. For example, Garand et al. (2001) compared six fast models: RTTOV 5 and 6, OPTRAN, AER_OSS, MIT and RAYTHEON, against a LBL model, which by deduction allows comparison between them, for four of the MW channels on the Advanced Microwave Sounding Unit (AMSU). For water vapour channel 18 (183.31 ±1.0 GHz), average inter-model BT differences reached 0.4 ±0.5 K, yet the difference between RTTOV 6 and its underlying LBL are more than ten times less at 0.02 ±0.04 K, and the equivalent for AER_OSS vs. AER_LBL is 0.01 ±0.0 K. Equivalently, for temperature channel 6 (54.4 GHz), the inter-model range (excluding RAYTHEON which appears deficient in this channel) is 0.18 ±0.08 K, but the fast vs. LBL difference for RTTOV and AER are 0.08 ±0.03 K, and 0.02 ±0.04 K, respectively. Another comparison by Buehler et al. (2006) of the same AMSU water vapour channel between RTTOV 7 and the ARTS LBL model, with the same spectroscopy applied, showed that global mean differences are generally quite low; a mean of 0.01 ±0.23 K. However, the author cautions that some atmospheric profiles with extremely low water vapour content produce large differences due to the limits of the fast model parameterisation, which can fail outside of the regression range used to train the predictors, as was shown in Figure 3.

A more recent study by Moradi et al. (2020) compares the performance of RTTOV version 12 against ARTS version 2.3, CRTM version 2.3 and satellite observations from the Advanced Technology Microwave Sounder (ATMS) and the GPM Microwave Imager (GMI). Direct comparison of RTTOV and ARTS (using equivalent spectroscopy) show a mean difference of 0.24 $\pm$0.28 K in the same water vapour channel 183.31 $\pm$1.0 GHz, which is larger than the equivalent previous Buehler et al. (2006) result in the mean. However, this could be due to the fact that RTTOV incorporates real channel spectral response functions into the ATMS coefficients whereas ARTS used a boxcar function, and additionally the air-broadening parameters for the 183.31 GHz line have been adjusted in RTTOVs LBL model from the original MPM89 values. Differences between CRTM and RTTOV are largely consistent and within $\sim$0.2K difference for most channels, where all variable features are kept the same apart from spectroscopy, as CRTM uses the PWR98 model and RTTOV uses AMSUTRAN. There are bigger differences between the two fast models and the LBL model than between each other: $\sim$0.5 K for temperature channels, $\sim$1 K for water vapour channels, and $\sim$3 K in the surface sensitive/lower tropospheric channel 16 at 88.2 GHz, which cannot be explained fully by the difference in spectral response function. Comparison of the models with satellite observations yields even bigger differences and after elimination of potential in-consistencies this is attributed to the different transmittance profiles, where even a small change can be inflated by surface emissivity to produce large TB differences. The author also shows that changing spectroscopy in isolation can yield differences of several kelvin in this channel due to the aforementioned effect. For example a bias of 9 K relative to NOAA-20 ATMS measurements at 88.2 GHz is obtained when using HITRAN 2012 spectroscopy in the model, whereas the equivalent is 6.5 K with PWR98 and only 2 K with MPM. Similar large differences are seen at 23.8 and 31.4 GHz (These channels are the only ones with QV polarisation instead of QH).

2.4 Radiative Transfer Summary

- Radiative transfer models are widely used and many absorption models and line databases are very active in continuously updating parameters and procedures based on the new measurements; prompting a review of the new and old parameters.
- Parameters from: two versions of HITRAN (2012, 2016), AER, GEISA, AMSUTRAN, ATM and three versions of PWR (98, 17, 19), are specifically compared in the following sections, alongside parameters from more recent studies.
- The three complete MW absorption models considered here: AMSUTRAN, ATM and PWR, share some common features but are sufficiently different to merit meaningful comparison.
- For consistency only frequency is retained from the radio engineering units used in the microwave models. All other parameters are converted to cgs units for inter-comparison with the line database convention.

- The current skill of fast radiative transfer models, such as RTTOV, in reproducing the results of the underlying line-by-line codes is such that the difference between them is often negligible compared to the spread of results produced by alternate spectroscopic parameters and formulations, which can be up to several kelvin in some cases.

- The difference between observations and models often far exceeds inter-model spread of both LBL and fast models, reaching several kelvin particularly in surface sensitive channels. Therefore geometries that avoid the surface, such as up-looking measurements from ground based radiometers and aircrafts, is an approach that would minimise these discrepancies.

3 Water vapour

In its broadest sense water vapour can be separated into resonant (spectral lines) and non-resonant (continuum) absorption. Non-resonant absorption can be separated further into self and foreign-broadened components. Figure 4 gives an overview of the range of spectral absorption by these different components, and the percentage each aspect contributes to the total (in the self and foreign cases this is relative to the total continuum). Most of the sub-millimetre spectrum is dominated by line absorption, with the exception of frequencies around 880 GHz where in some atmospheric conditions the continuum contributes up to 55% of the absorption. The ICI channels around 664 GHz, which is considered to be a window, are still on average 75% influenced by surrounding lines: specifically those at 556.94 and 752.03 GHz. Below 300 GHz the continuum dominates by up to 85% apart from in the two regions directly surrounding the 22.235 and 183.31 GHz lines. The relative contribution of foreign and self to the total continuum is spectrally invariant with an average ratio of 3:1, however, within the possible range of atmospheric profiles it could be as much as 100% foreign in very dry conditions, or up to 53% self when it is very humid. This partition, however, is specific to the MPM89 continuum used in this analysis and will be different for other models.

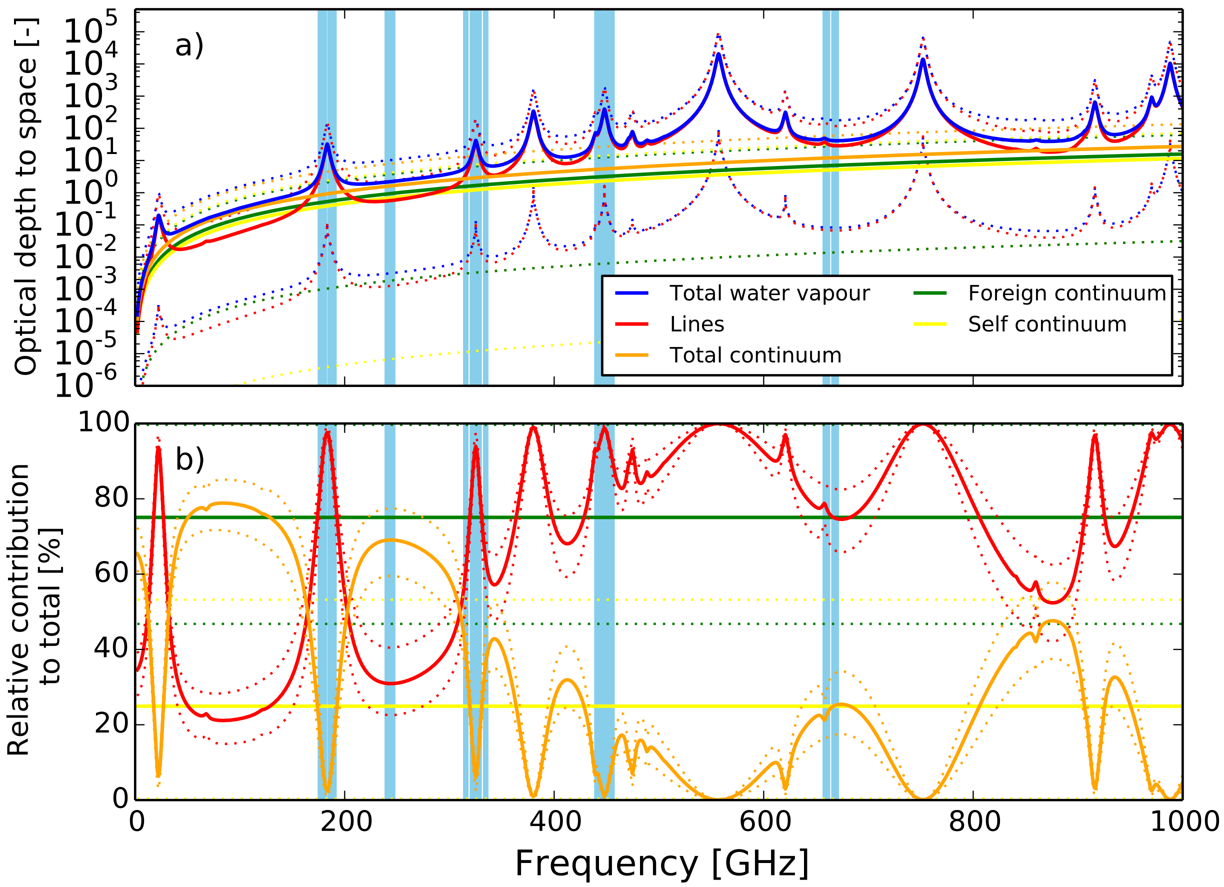

Figure 4: Resonant and non-resonant components of water vapour absorption using MPM89 parameters. a) Surface-to-space optical depths. b) Percentage contribution of each component: lines and total continuum to total water vapour, or self and foreign continuum to total continuum. Bold lines show the mean of 83 diverse profiles and dotted lines of corresponding colour are the maximum and minimum values of that component at each frequency. The passbands of ICI channels are shaded in sky blue.

3.1 Water vapour lines

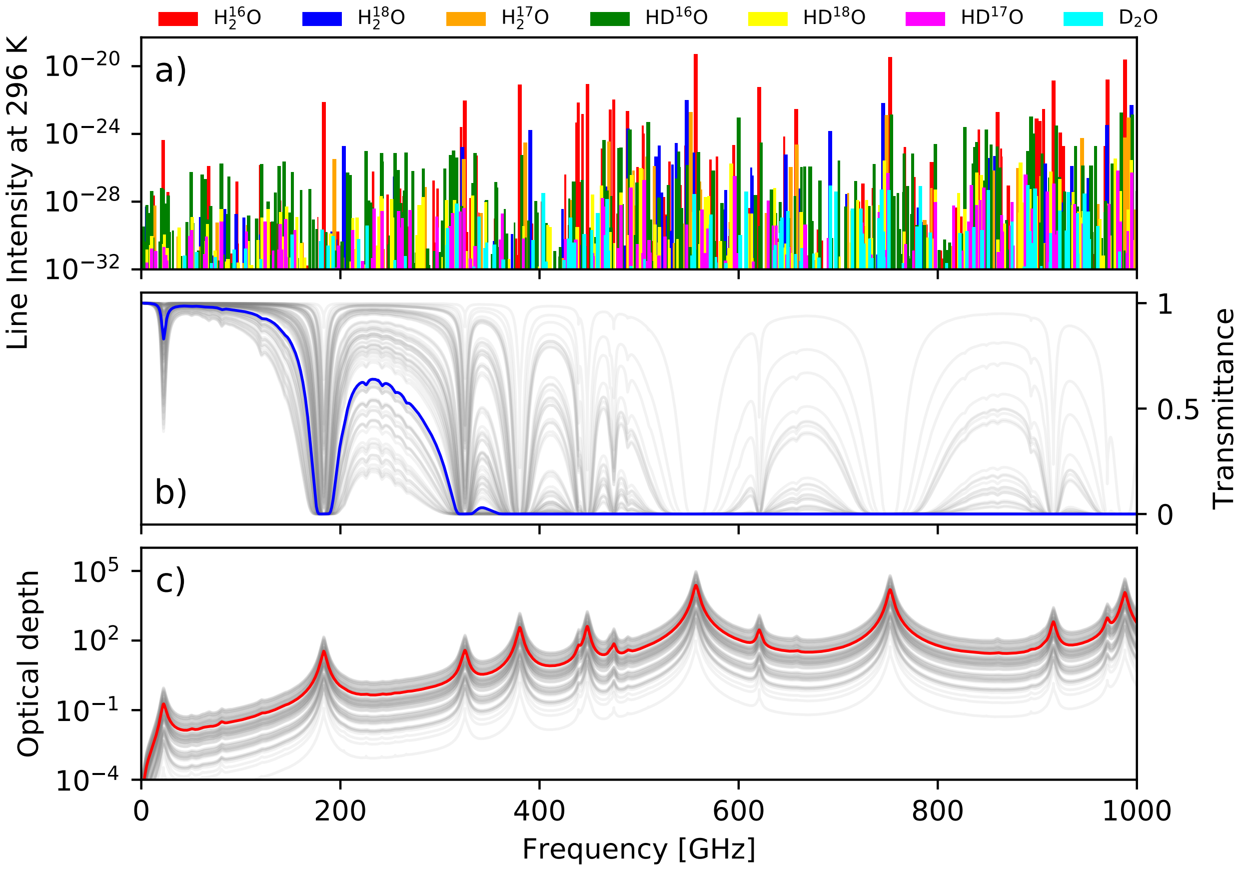

Figure 5: Water vapour lines and associated TOA radiative quantities from the HITRAN 2016 database. a) Line intensity in units of cm^{-1}/(molecules/cm^2) at 296 K for seven water vapour isotopologues (log scale). b) Surface-to-space transmittance and c) surface-to-space optical depth, for 83 diverse atmospheric profiles (grey lines) and the mean profile (blue and red lines, respectively).

Line absorption, $\alpha_l(\nu)$, is the cumulative sum over all transitions, ij, of the line intensity - also known as line strength - $S_{ij}(T)$, multiplied by the value of the respective line shape $F_{ij}(\nu)$ at a given frequency ν.

$$\alpha_l(\nu) = \sum_{ij} N(T) S_{ij}(T) F_{ij}(\nu) \tag{1}$$

where $N(T)$ is the number density of the molecule in units of cm^{-3}. The line strength is defined below in the form used by the HITRAN database in units of cm^{-1}/(molecule/cm^2), for a single molecule transition from an upper state with energy E_j to a lower state with energy E_i:

$$S_{ij}(T) = I_a \frac{A_{ij}}{8\pi c \tilde{\nu}_{ij}^2} \frac{g_j e^{-hcE_i/kT}(1 - e^{-hc\tilde{\nu}_{ij}/kT})}{Q(T)} \tag{2}$$

where I_a is the natural terrestrial isotopic abundance, A_{ij} is the Einstein-A coefficient for spontaneous emission, g_j is the upper state statistical weight, $\tilde{\nu}_{ij}$, given by $(E_j - E_i)/hc$ is the wavenumber of the transition in

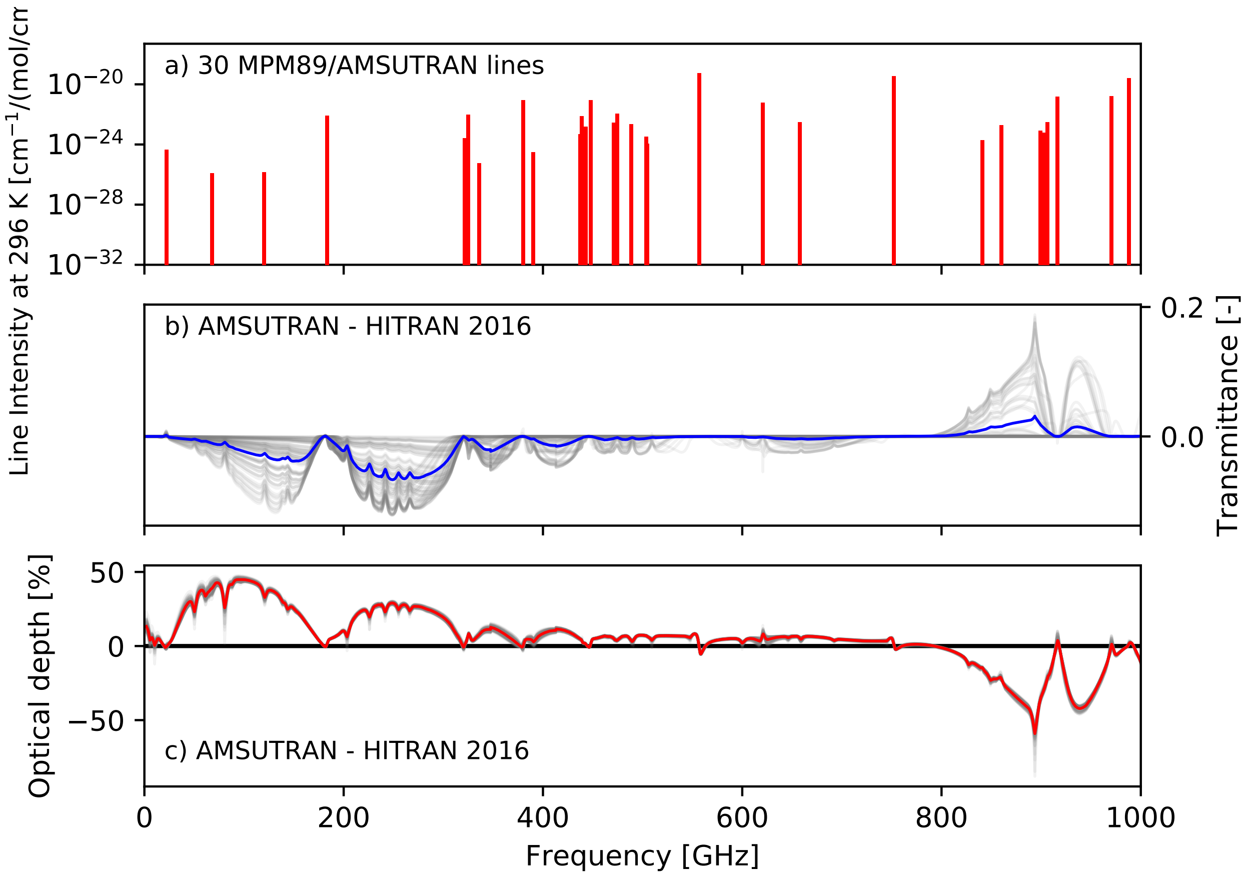

Figure 6: a) MPM89/AMSUTRAN water vapour line intensities. The TOA differences between AMSUTRAN and HITRAN 2016 database for: b) transmittance and, c) optical depths in percent for 83 diverse atmospheric profiles (grey lines) and their mean (bold lines), for water vapour lines only.

cm^{-1}, and $Q(T)$ is the Total Internal Partition Sum (TIPS). TIPS is the sum over all states, s, (i.e. rotational, vibrational, electronic, etc.) of a molecule at temperature T, given by:

$$Q(T) = d_i \sum_s d_s e^{-hcE_s/kT} \tag{3}$$

where d_i is the state-independent degeneracy factor and d_s is the state-dependent degeneracy factor. c, the speed of light; h, the Planck constant; and k, the Boltzmann constant are all in cgs units (cm/s, erg s, erg/K, respectively). In order to calculate intensity at a temperature other than the reference, which in the case of HITRAN is 296 K, $S_{ij}(T)$ must be scaled by the ratio of equation 2 with the reference and the required temperature as:

$$S_{ij}(T) = S_{ij}(296)\frac{Q(296)}{Q(T)}\frac{e^{-hcE_i/kT}(1-e^{-hc\tilde{\nu}_i/kT})}{e^{-hcE_i/296k}(1-e^{-hc\tilde{\nu}_i/296k})} \tag{4}$$

Equations 2–4 are not specific for water vapour as A_{ij} is independent of the type of transition, i.e. electric dipole, magnetic dipole etc. For water vapour at low wavenumbers Doppler-broadening can be ignored to a first approximation.

Figure 5a shows the location and intensity of the water vapour lines included in HITRAN 2016, which comprises 1668 lines between 0–1000 GHz from seven isotopologues. Values of intensity span orders of magnitude between 1.0e^{-39} and 5.0e^{-20} cm^{-1}/(molecules/cm^2) at 296 K. The troughs and peaks in the TOA transmittance (Figure 5b), and optical depth (Figure 5c), show that absorption below 1000 GHz is dominated by around 12 $H_2^{16}O$ lines. Hence, to a good approximation, it is acceptable to use only a limited number of principal isotopologue lines as they represent the vast majority of the resonant absorption, which is the case in all AMSUTRAN, ATM and the PWR models. By comparison of these quantities in Figure 5 with the equivalent due to all molecules in Figure 1, it is clear that typically most of the total absorption beyond 200 GHz is due to water vapour, producing a mean transmittance of zero in all but the driest profiles.

Panel a) of Figures 6 and 7 shows the position and intensities of the lines included in MPM89/AMSUTRAN (MPM models), and PWR98–PWR19, respectively. Radiative differences relative to HITRAN 2016 are higher for AMSUTRAN than PWR98 below 400 GHz (up to 50% i optical depth) because the MPM models do not include a line cut-off, so are subject to the far-wing influence of nine lines between 750 and 1000 GHz, yielding greater absorption. However, as is shown later in section 3.3 this is compensated somewhat by a lower continuum absorption. For 27 of 30 lines, AMSUTRAN intensities are between 0.5 and 2 % higher than HITRANs, while only 10 of AMSUTRAN's lines have a greater halfwidth than HITRAN's, which somewhat compensates for the larger intensities. As the two quantities are difficult to separate when the line is measured this is not unexpected. For most of the spectrum there are higher transmittances and lower optical depths attributed to the HITRAN lines, which counter-intuitively results in less absorption overall for the larger line database. This is not the case for PWR98, however, where the absence of some lines, i.e the one 658 GHz recently added, causes optical depth errors of up to 50% in some atmospheric profiles. There are large differences beyond 800 GHz in both models due to the absence of the 893 lines and the strong 988 GHz line omitted in PWR98 is responsible for a large local difference many scales larger than the plots.

3.1.1 Line shape

The line shape function, $F(\nu)$, typically used in the microwave region is the Van Vleck-Weisskopf (VVW) (Van Vleck and Weisskopf, 1945), as modified by Rosenkranz (1988), which is judged to be appropriate for use when Doppler broadening is not significant. This shape takes the form:

$$F(\nu) = \frac{\nu}{\nu_{ij}} \left[\frac{\gamma_{ij} + \delta_{ij}(\nu - \nu_{ij})}{(\nu - \nu_{ij})^2 + \gamma_{ij}^2} + \frac{\gamma_{ij} - \delta_{ij}(\nu + \nu_{ij})}{(\nu + \nu_{ij})^2 + \gamma_{ij}^2} \right] \tag{5}$$

where ν is the frequency, ν_{ij} is the central frequency of the line, γ_{ij} is the pressure-broadened half-width, and δ_{ij} is the pressure-induced interference, which applies to line mixing and only affects oxygen in this study (Section 5.3). For water vapour δ can be taken to be zero. The prefactor, ν/ν_{ij}, varies in form from model to model, sometimes appearing as ν^2/ν_{ij}^2 or including π in the denominator, depending on which parameters are contained in the line strength or full absorption equation, but they should evaluate equally. The VVW line-shape can be thought of as the sum of two Lorentzian lines centred at $\pm\nu_{ij}$, which reduces to the Lorentz shape in the local limit. The Voigt profile is a convolution of the Lorentzian and the Gaussian (Doppler) line shapes and is more accurate to use with very high-peaking channels such as MWS channel 16 while reducing to a Lorentzian at high pressures. The Voigt cannot be calculated analytically so approximations must be made,

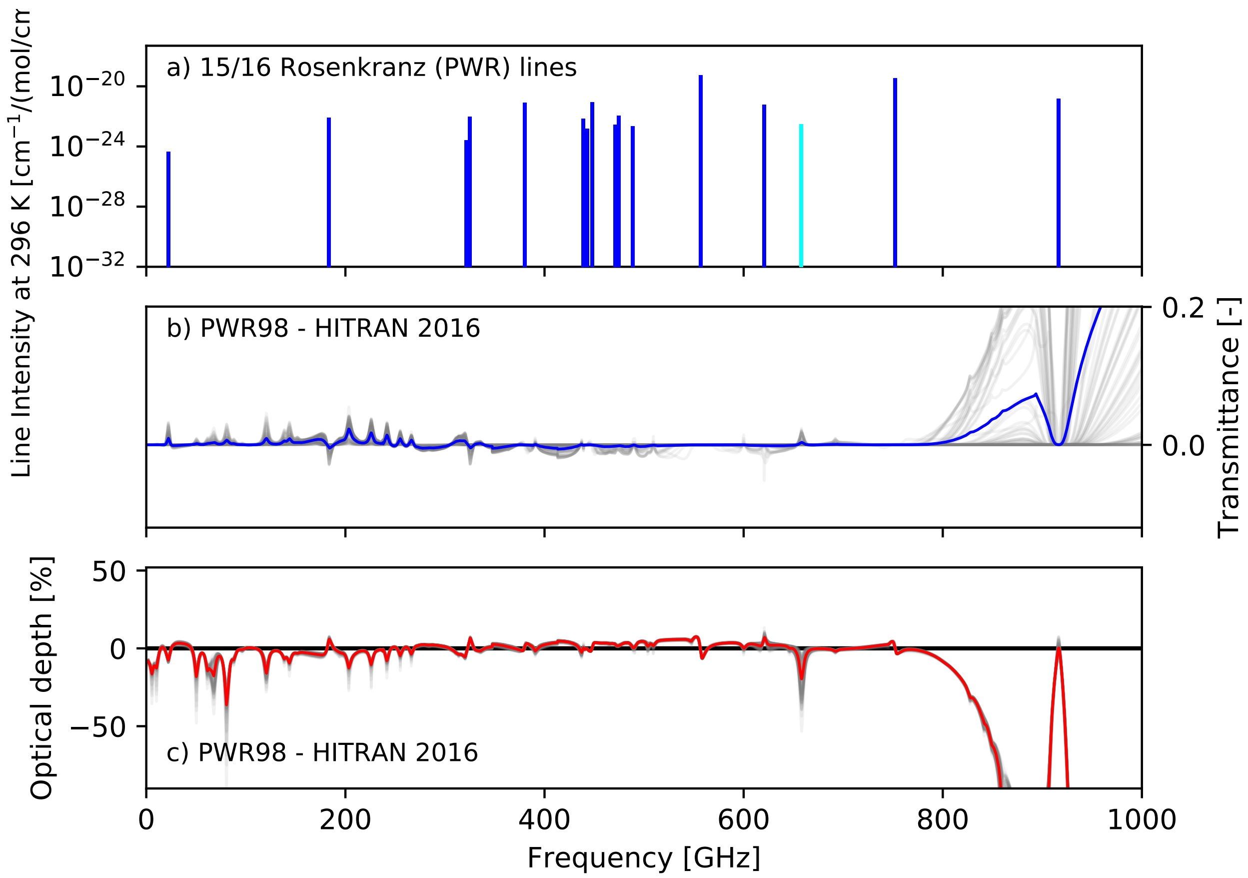

Figure 7: a) Line intensities for 15 PWR98 lines (blue) and the 16th line at 658 GHz, which is in PWR19 (cyan). TOA differences between PWR98 and HITRAN 2016 database for: b) transmittances and, c) percentage optical depths, for 83 diverse atmospheric profiles (grey lines) and their mean (bold line), for water vapour lines only.

such as the Humlicek approximation used in MonoRTM (Humlíček, 1982).

The general form of the Lorentzian (pressure broadened) half-width, $\gamma(p,T)$, is a combination of the half-width at half-maximum due to self broadening (water vapour in this case), γ_{self}, and air broadening, γ_{air}, scaled by the atmospheric temperature and pressure:

$$\gamma(p,T) = (p - p_{self})\gamma_{air}(p_{ref},T_{ref})\theta^{n_{air}} + p_{self}\gamma_{self}(p_{ref},T_{ref})\theta^{n_{self}} \tag{6}$$

where p is the total pressure, θ is the inverse reference temperature equal to T_{ref}/T, and n_{air} and n_{self} are the air-broadened and self-broadened temperature exponents, which are sometimes assumed to be the same. For water vapour, p_{self}, is the partial pressure of water vapour and $p - p_{self}$ is the partial pressure of dry air. The units of γ_{air} and γ_{self} are cm^{-1}/atm using the cgs convention and are typically provided at a reference temperature of 296 K.

There is a further perturbation found to affect the lines central frequency in the form of a pressure shift:

$$\nu_{ij}^{*} = \nu_{ij} + \delta(p_{ref}, T_{ref}) p \theta^{n_{shift}} \tag{7}$$

where the shifting parameter, $\delta(p,T)$, can refer to either air or self shifting. Including pressure shifts in absorption models is a relatively recent development and the values available, as well as the form of the temperature dependence, are quite uncertain. In the following sections the value of n_{shift} has been assumed to be the same as the associated pressure broadening exponent, n_{air} or n_{self}, however, there may be other forms. For example, the ARTS code takes n_{shift} to be $0.25 + 1.5n$.

In the last few years the line-shape has been studied and further refined to account for speed dependencies (SD) of the collisional cross section, which can be thought of as a 'fine' line shape effect. High signal-to-noise ratios have allowed evaluation of the SD parameters for the major lines at: 22.235 GHz (Koshelev et al., 2016), 118.75 GHz (Koshelev et al., 2017), 183.31 GHz (Koshelev et al., 2021b) and most recently the 60-GHz oxygen complex Koshelev et al. (2021a). The PWR19 includes this line-shape for the 22.235 and 118.75 GHz lines (Rosenkranz and Cimini, 2019). TOA differences of the speed-dependent shape relative to the VVW profile are estimated be up to 0.3 K (0.2%) around 183.31 $\pm$10 GHz (Koshelev et al., 2021a, Figure 14.). The following comparison only considers VVW line-shape parameters.

3.1.2 Line parameters

The available parameters of six key water vapour lines relevant to MetOp-SG are now discussed in turn with relation to the nine absorption models and databases (collections), which are listed in Table 4, and additionally more recent or notable studies, shown in Figures 8–14. Where necessary parameters are reprocessed to cgs units at 296 K using the associated or best available estimate of the temperature dependence. Uncertainty ranges are shown adjacent to the value where available, however, errors in the fit are rarely included because these numbers are often comparatively very small. The location of the line centre is given in frequency units (GHz), and the associated rotational quantum numbers of the transition are shown in parentheses, where the states $J_{K_aK_c}$ are the total angular momentum of the molecule, J, and the asymptotic components of J along the inertial axes, K_a and K_c.

3.1.3 22.235 GHz line ($6_{16} \leftarrow 5_{23}$)

This line features strongly in existing microwave radiometry, and there have been multiple studies dedicated to deriving its line parameters, often alongside the 183.31 GHz line. The adjacent channels 2, on MWI, and 1, on MWS, centred at 23.8 GHz will use this line for measuring total column water vapour.

22.235 GHz line intensity

Figure 8 presents seven studies that give 22.235 GHz line intensities, six of which cluster between 4.348e^{-25} and 4.454e^{-25} cm^{-1}/(molecules/cm^2), a range of 2.5%. The value included in the GEISA 2019 database, however, appears low compared to the others, at 4.19e^{-25} cm^{-1}/(molecules/cm^2). This value is derived from

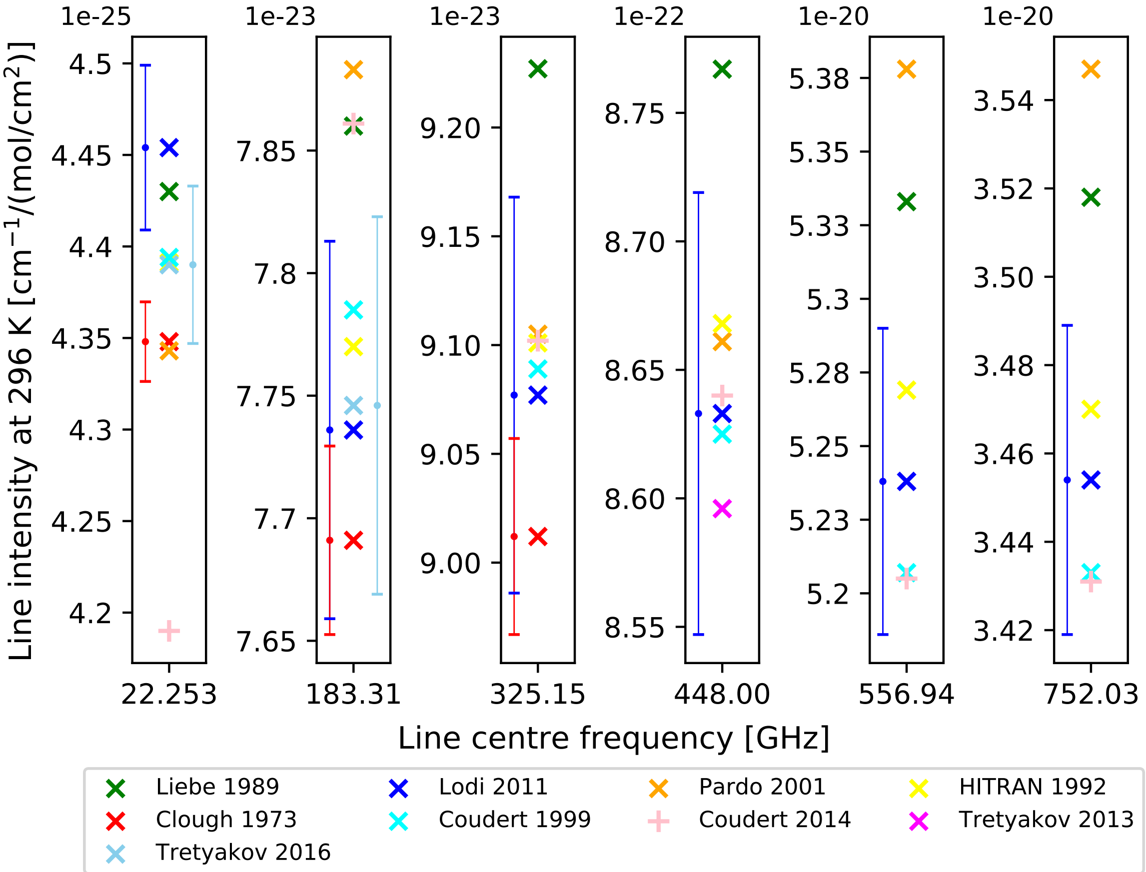

Figure 8: Line intensity for six water vapour lines given by different studies. Error bars show quoted uncertainties on the adjacent values where provided. See text for details.

high temperature far-infrared measurements for the whole microwave and infrared region, fitted using a modified version of the Bending–Rotation approach (Coudert et al., 2014). The mean of first six is 4.39e^{-25} cm^{-1}/(molecules/cm^2), which is the same as the intensity derived by the most recent study (Tretyakov, 2016), perhaps unsurprisingly as it is based on consideration of a consolidation of previous works. Clough et al. (1973) estimate an uncertainty of 0.5% on an intensity of 4.348^{-25} cm^{-1}/(molecules/cm^2, which is used in the AER 3.8 line database and is derived from measurements of the Stark effect. This range overlaps with part of the 1% uncertainty attached to the Tretyakov (2016) value, but not the 1% attached to the HITRAN 2016 value from Lodi et al. (2011), which is the highest value in the studies considered here.

22.235 GHz air-broadened half width

Similarly to the line intensity, the majority of air-broadened half-widths cluster together, with values ranging between 0.0900 and 0.0921 cm^{-1}/atm (Figure 9). The 0.0959 cm^{-1}/atm value from Liebe (1989), used by the ATM model appears high relative to this range. The AMSUTRAN model replaced this value in 2005 with the lower one included in HITRAN 2000 (0.0906 cm^{-1}/atm), after Liljegren et al. (2005) showed better agreement with model simulations using microwave radiometer retrievals of temperature and water vapor profiles. Omit-

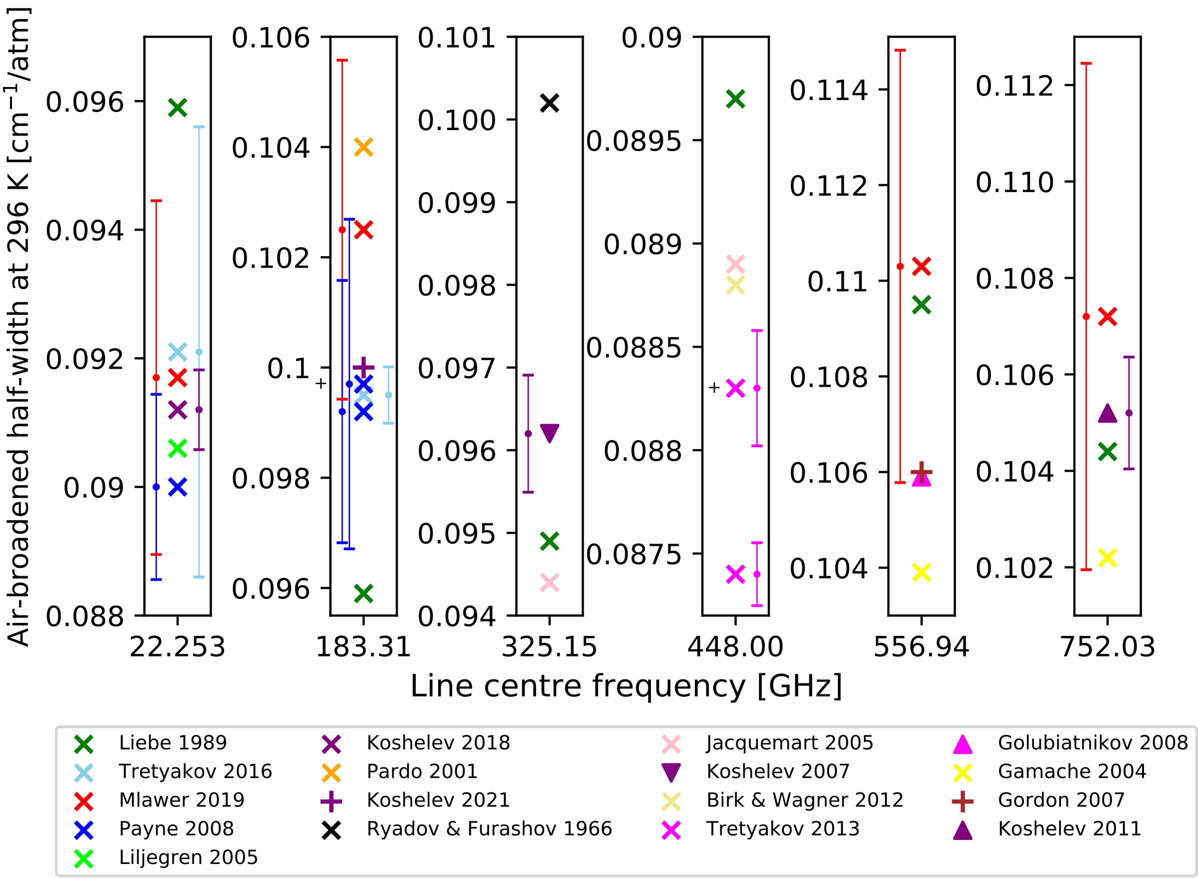

Figure 9: Air-broadened half-widths for six water vapour lines given by different studies. Error bars show quoted uncertainties on the adjacent values where provided. The Koshelev et al. (2018a) value at 22.235 GHz is the one derived from the radio-acoustic detection spectrometer in the study. A small + adjacent to a value indicates there is more than one results provided in the study which has relevance to an absorption model, see text for details.

ting Liebe (1989), the five remaining studies are within 2.3 % of each other.

The most popular air-broadened half-width adopted by all these collections is the empirically constrained value of Payne et al. (2008). The authors perform a radiative closure experiment using microwave radiometers at ARM sites and determine a value of 0.0900 cm^{-1}/atm (1.6 % uncertainty), and additionally 0.0913 cm^{-1}/atm (3 % uncertainty), the latter theoretically derived using the complex implementation of the Robert-Bonamy (CRB) method. The first value has been included in HITRAN since the 2008 release and is additionally in PWR17 and GEISA 2019. It was introduced to the AER line files at version 1.1 but at version 3.3 the parameter underwent a recalculation using the same procedure as Payne et al. (2008), but with different values of self-broadening and temperature dependencies. At AER version 3.5 this procedure was repeated once more using further updated parameters, as detailed in Mlawer et al. (2019), resulting in the value of 0.0917 cm^{-1}/atm (assuming the same 3 % uncertainty as the original analysis) included in AER 3.8.

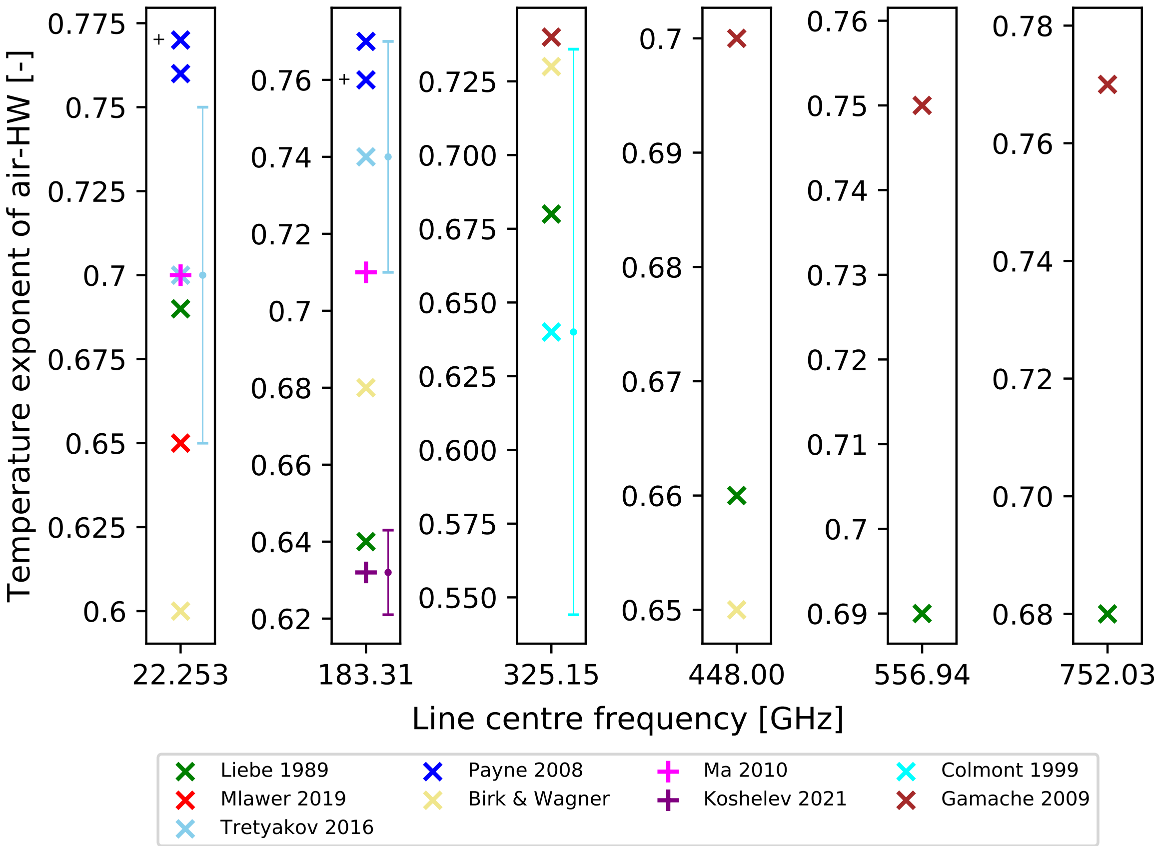

Figure 10: Temperature exponent of air-broadened half-width for six water vapour lines given by different studies. Error bars show quoted uncertainties on the adjacent values where provided. A small + adjacent to a value indicates there is more than one results provided in the study which has relevance to a model, see text for details.

A recent review of the 22.235 GHz line shape parameters by (Koshelev et al., 2018a) used two set of laboratory apparatus: a radio acoustic detection (RAD) spectrometer and a video spectrometer, to investigate the effects of systematic measurement error, as this is often the largest source of inconsistency between results. The RAD spectrometer showed the lowest uncertainty of the two methods with a derived value of 0.0912 cm^{-1}/atm, and was subsequently adopted by PWR19. The uncertainty calculated from the total error budget is 0.68%, much lower than the 3.9% uncertainty given by the nearby Tretyakov (2016) value. Two additional studies worth mentioning but not included in Figure 9 are: Cazzoli et al. (2007), who obtain a value of 0.0878 cm^{-1}/atm from laboratory measurements, and Ma et al. (2010), who theoretically derive a value of 0.0895 cm^{-1}/atm, which includes a scaling factor to adjust the broadening component from pure nitrogen to air. Both values are lower than the range included in the collections considered.

22.235 GHz temperature exponent of air-broadened half width

The temperature exponent attached to the air-broadened half-width is shown by six studies to vary between 0.6–0.76 (Figure 10) which is a large spread (24%). Note that the seventh value of 0.77 included in HITRAN

2016 and GEISA 2019 is omitted from this range, as it appears to be a mis-quotation of the original value of 0.76 quoted by Payne et al. (2008). For AER 3.5 it was determined that the latter value was too high, and it was adjusted to 0.65 (source unknown). Two separate studies: Ma et al. (2010) and Tretyakov (2016), independently determine an exponent of 0.70, which is close to the earlier value of 0.69 provided by Liebe (1989).

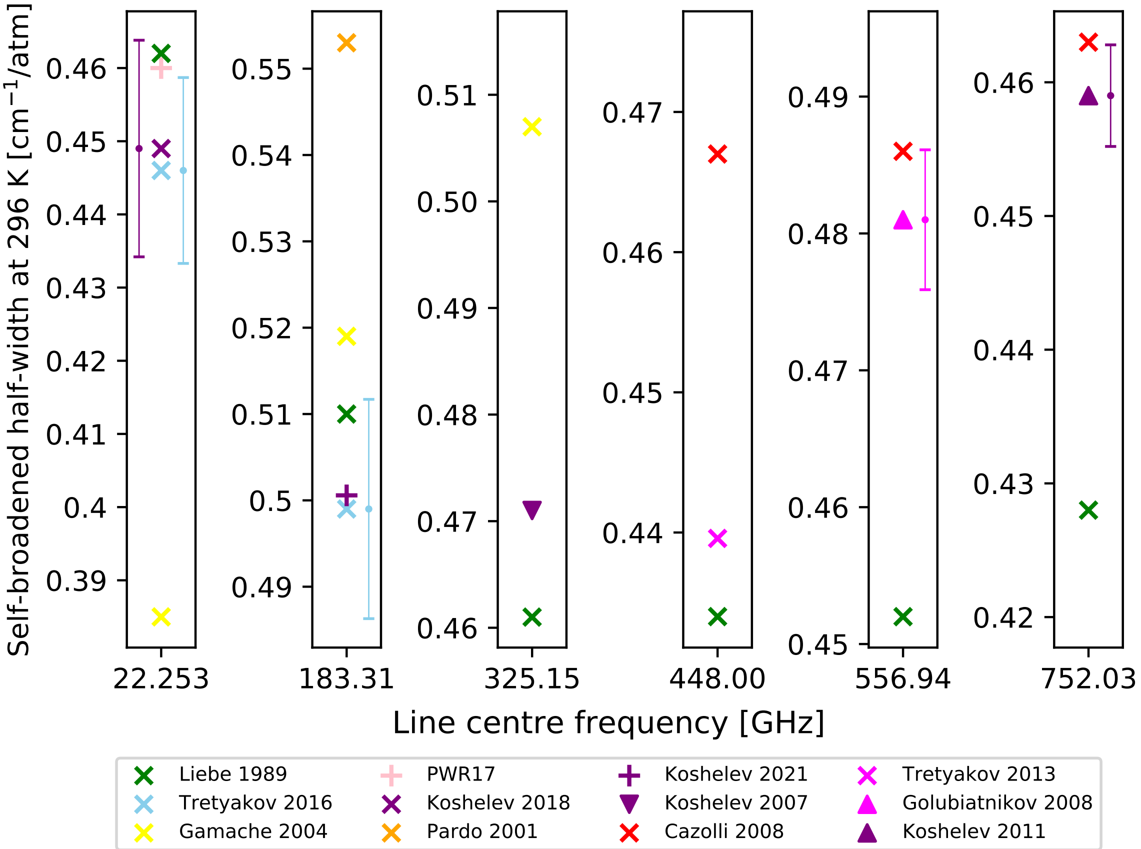

Figure 11: Self-broadened half-widths for six water vapour lines given by different studies. Error bars show quoted uncertainties on the adjacent values where provided, see text for details.

22.235 GHz self-broadened half-width

Of the five values of self-broadened half width shown in Figure 11, four cluster between 0.446–0.460 cm^{-1}/atm (3.5%), and one, Gamache and Hartmann (2004), is significantly less at 0.385 cm^{-1}/atm. The latter value, however, is used in all four of the line databases: HITRAN 2012 and 2016, GEISA 2019 and AER 3.8. The two most recent studies presented: Tretyakov (2016) and Koshelev et al. (2018a), produce very similar values of 0.446 and 0.449 cm^{-1}/atm, respectively.

22.235 GHz temperature exponent of self-broadened half-width

A separate temperature exponent for the self-broadened half-width of water vapour is not currently listed in the larger line databases, and at least for HITRAN, the corresponding exponent for air-broadened for that line is advised in its place (these values are not included in Figure 12). Only two studies provide separate values. The first is from Liebe (1989), and is 1.0 - so effectively no temperature dependence, used by AMSUTRAN, ATM and R17, but more recently Tretyakov (2016) recommend a value of 1.2, which is used by PWR19.

22.235 GHz air-induced pressure shift

Pressure shifts of the line centres, both air and self induced, have been less studied in the past (AMSUTRAN, ATM and PWR98 do not include the effects at all), but they are becoming more prevalent. HITRAN 2016 and GEISA 2019 include the value of -0.879e^{-3} cm^{-1}/atm derived by Payne et al. (2008). It should be noted that the value is quoted as -0.882e^{-3} cm^{-1}/atm in the publication so there is a slight discrepancy. AER 3.8 uses a value of -0.800e^{-3} cm^{-1}/atm (which was also in the previous version of HITRAN), which is of unknown origin but has a large uncertainty of $\pm$0.989e^{-3} cm^{-1}/atm according to Tretyakov (2016, Table 3.). More recently, Koshelev et al. (2018a) calculate a larger shift of -1.115e^{-3} cm^{-1}/atm using RAD spectrometer measurements, which has been included in PWR19. However, the slightly earlier study by Tretyakov (2016) proposes a mean shift of 0.0 with a 2.53e^{-3} cm^{-1}/atm uncertainty (not shown in Figure 13). PWR19 also begins to considerer temperature exponents for the pressure shifts but at present only one air-induced value is included for the 22.235 GHz line and is equal to 2.6 from Cazzoli et al. (2007). The earlier PWR17 model includes air shifts which appear to be two to three times smaller than PWR19, however the source for these values is unknown.

22.235 GHz self-induced pressure shift

The effects of self-induced pressure shifting of line centres is currently only included in the PWR19 model out of those considered here, which is equal to 27.51e^{-3} cm^{-1}/atm and originates from RAD spectrometer measurements (Koshelev et al., 2018a). Figure 14 shows three values for the 22.235 GHz line, where it can be seen that the aforementioned study and the 20.79e^{-3} cm^{-1}/atm value measured by Cazzoli et al. (2007) appear similar compared to the -13.52 e^{-3} cm^{-1}/atm estimated by Tretyakov (2016), which deviates significantly and also has a different sign (negative).

3.1.4 183.311 GHz line ($3_{13} \leftarrow 2_{20}$)

Arguably the most important water vapour line in satellite microwave radiometry to date. As the strongest water vapour line below 200 GHz it has channels on multiple satellite instruments, which has prompted many studies dedicated to deriving its line parameters.

183.31-GHz line intensity

Eight studies contribute to the range of line intensities for the 183.31 GHz line intensity shown in Figure 8, spanning 7.691e^{-23}–7.883e^{-23} cm^{-1}/(molecules/cm^2), which corresponds to a spread of 2.46 % and a mean value of 7.79e^{-23}. The lowest value is the one included in AER 3.8 (Clough et al., 1973) and the highest is used by the ATM model (Pardo et al., 2001a). The most recent calculation by Tretyakov (2016) is at the lower end of the range with a value of 7.746e^{-23} cm^{-1}/(molecules/cm^2), and an estimated uncertainty of 1%, which overlaps with the 0.5 % uncertainty estimated by Clough et al. (1973) .

183.31-GHz air-broadened half-width

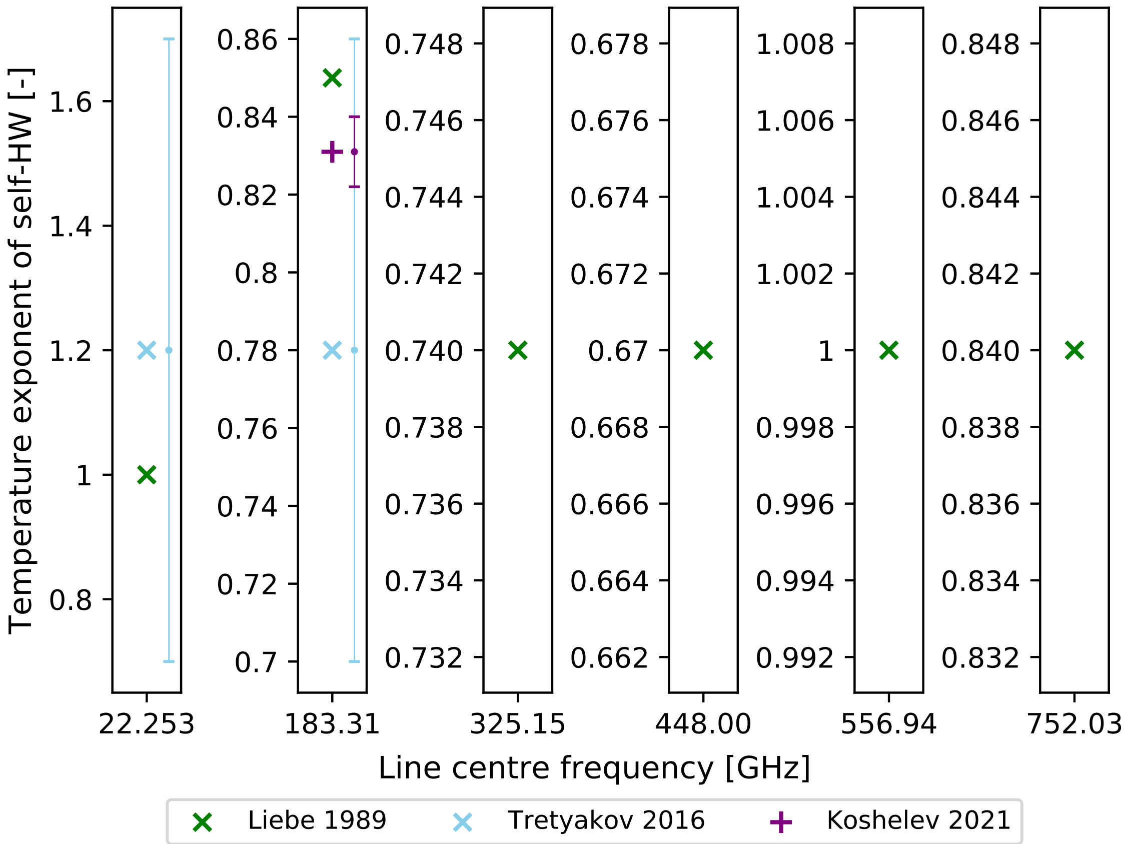

Figure 12: Temperature exponents of self-broadened half-width for six water vapour lines given by different studies. Error bars show quoted uncertainties on the adjacent values where provided, see text for details.

Air-broadened half-widths for the 183.31 GHz line from six studies are shown in Figure 9, which vary between 0.0992–0.1040 cm^{-1}/atm, a range of 4.75%. Like the line intensity, the highest value originates from ATM (Pardo et al., 2001a). Similarly to the 22.235 GHz line, the most popular value for air-broadened half-width, used by HITRAN 2016, HITRAN 2012, PWR17 and GEISA 2019, is from Payne et al. (2008) and equals 0.0992 cm^{-1}/atm (2.4 % uncertainty). AMSUTRAN, however, uses the supplementary value of 0.0997 cm^{-1}/atm (3 % uncertainty)provided in the same study, but derived using the theoretical complex implementation of the Robert-Bonamy (CRB) method, which is only slightly higher. Tretyakov (2016) calculate a value of 0.0995 cm^{-1}/atm, which sits between both Payne et al. (2008) values and has a modest 0.5% uncertainty range, encompassing four closely set half-width estimates. The fourth is the most recent study by Koshelev et al. (2021b), who derive the temperature dependencies of the broadening, shifting an speed dependent parameters for the 183.31 GHz line, and provide an updated measured value of the air-broadened half-width of 0.1000 cm^{-1}/atm. The associated uncertainty range refers to quality of the experimental fit.

Following the same procedure as the 22.235 GHz line, the AER parameter underwent a recalculation with updated values of self-broadening and temperature dependencies, as detailed in Mlawer et al. (2019), produc-

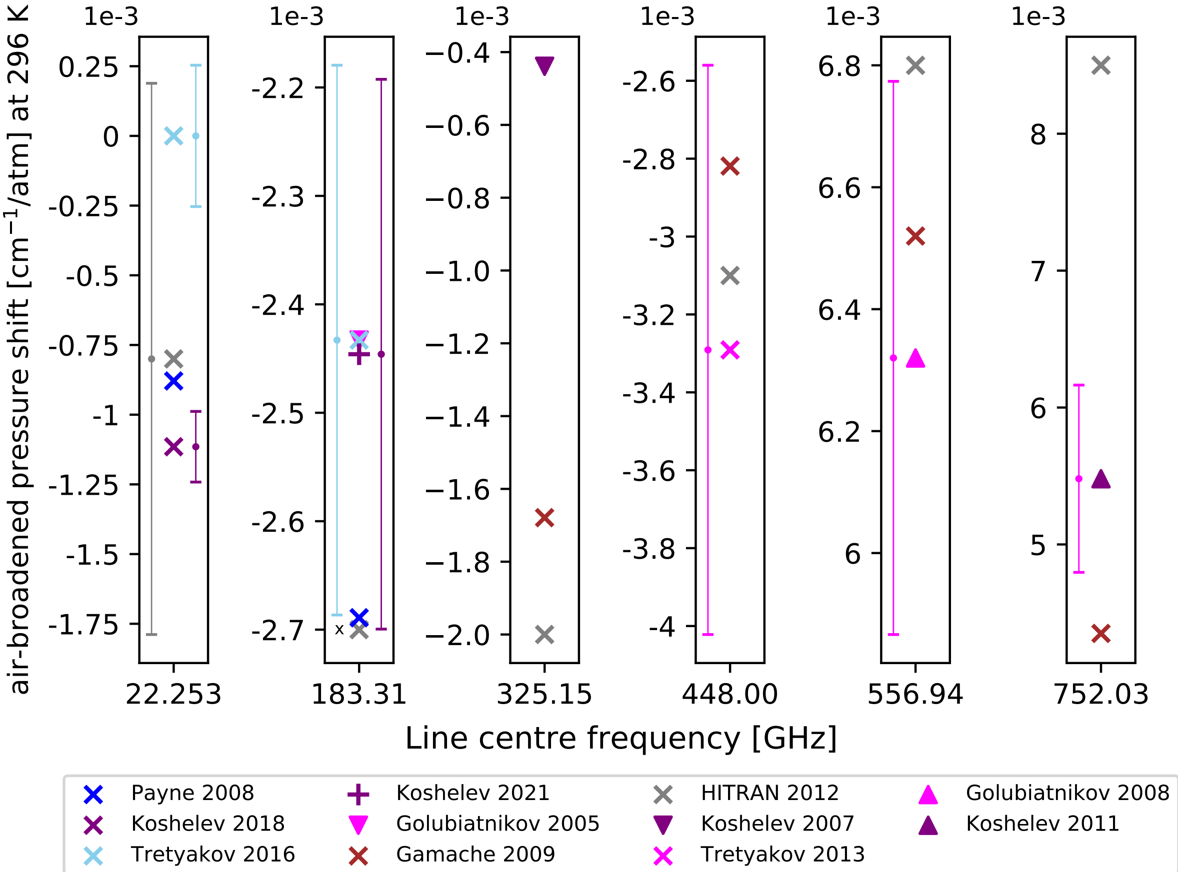

Figure 13: Air-induced pressure shifts for six water vapour lines given by different studies. Error bars show quoted uncertainties on the adjacent values where provided, see text for details. The sources for values labeled HITRAN 2012 are either unknown or unsure.

ing a higher value of 0.1025 cm^{-1}/atm (assuming the same 3 % uncertainty as the original analysis), which entered the AER line database at version 3.5 and is at the upper end of the range.

183.31-GHz temperature exponent of air-broadened half-width

The temperature exponent of the air-broadened half-width is shown by six studies to vary between 0.63–0.77 (Figure 10). Again, as in the 22.235 GHz line, the value of 0.76 which is used by HITRAN 2016 and GEISA 2019 is thought to be a mis-quotation of the original 0.77 value quoted in (Payne et al., 2008) (but this has been corrected in the HITRAN online for the next release). This value was adopted in PWR17, PWR19 and AM-SUTRAN. AER 3.8 determined in more recent analysis that this value was too high, and it was subsequently adjusted to 0.71 based on the theoretical work of Ma et al. (2010). The recent Koshelev et al. (2021b) study gives a measured value of 0.632 with a 1.74% uncertainty, the lowest exponent considered here, however, this is for a Voigt line-shape.

183.31-GHz self-broadened half-width

There are five values of self-broadened half-width for the 183 GHz line shown in Figure 11, ranging between

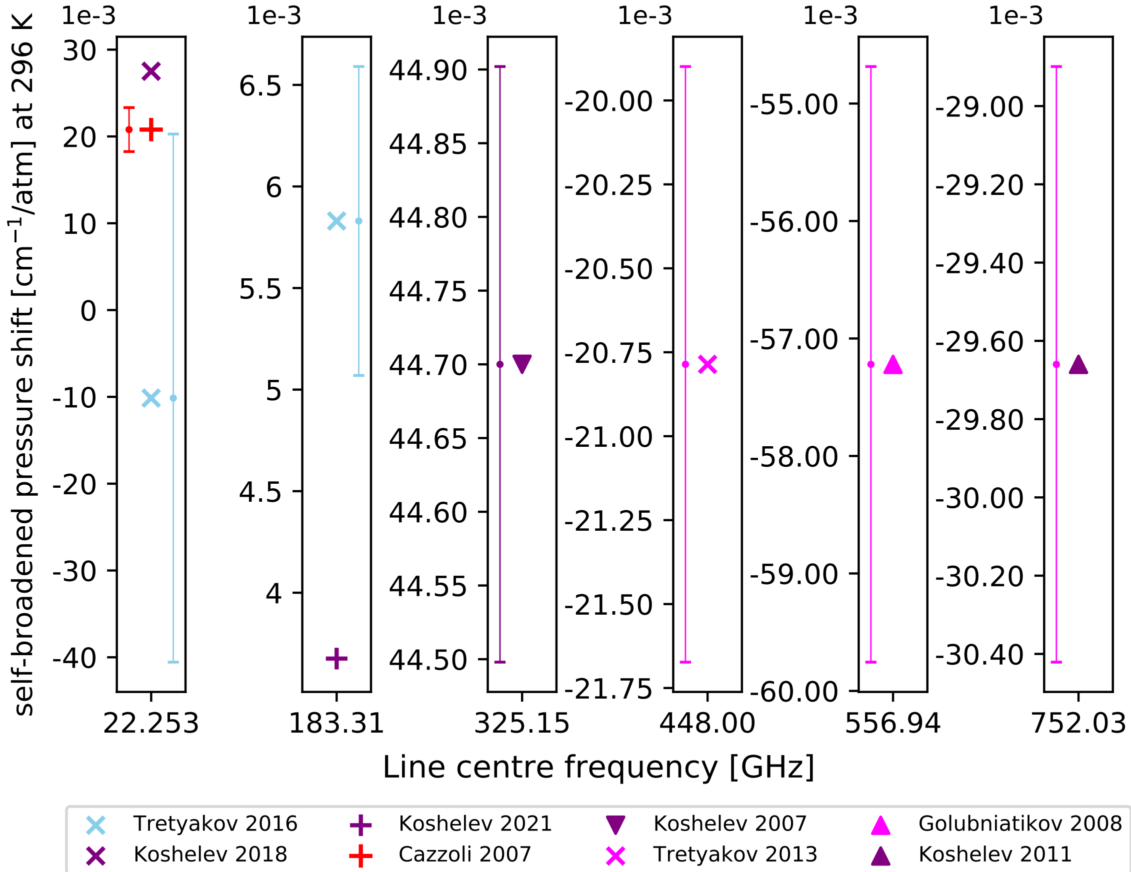

Figure 14: Self-induced pressure shift for six water vapour lines given by different studies. Error bars show quoted uncertainties on the adjacent values where provided, see text for details. The 22.235 GHz line used by R19 is the one derived by radio-acoustic detection in Koshelev et al. (2018a).

0.499–0.553 cm^{-1}/atm. This range is about 10% of the value, double that of the air-broadened half-width, but the upper Pardo et al. (2001a) value used by ATM could be considered an outlier as it is significantly higher, reducing the range to just under 4%. The Gamache and Hartmann (2004) value of 0.519 is used in all of the larger line databases (HITRAN, GEISA, AER). The more recent studies by Koshelev et al. (2021b) and (Tretyakov, 2016) predict lower values.

183.31-GHz temperature exponent of self-broadened halfwidth

There are three relevant studies that provide values for the self-broadened temperature exponent of the 183.31 GHz line (Figure 12). The Liebe (1989) value of 0.85 used by AMSUTRAN, ATM and PWR17 is 8.6% higher than the more recently calculated value of 0.78 adopted by PWR19 Tretyakov (2016). The Koshelev et al. (2021b) value of 0.831 leans towards the upper end of the range, however.

183.31-GHz air-induced pressure shift

Similar to the pattern observed with the 22.235 GHz line, HITRAN 2016 and GEISA 2019 include an air-induced pressure shift of -2.69e^{-3} cm^{-1}/atm derived by Payne et al. (2008), whereas AER 3.8 uses a value of

-2.70e^{-3} cm^{-1}/atm (which was also in the previous version of HITRAN) and is possibly the value of Payne et al. (2008) rounded to one significant figure. More recently, Tretyakov (2016) make a best estimate of -2.43e^{-3} cm^{-1}/atm, which appears to originate from the dedicated study of the 183.31 GHz line by Golubiatnikov (2005), and is adopted in PWR19. A very similar result is obtained by Koshelev et al. (2021b), of -2.446e^{-3} cm^{-1}/atm, suggesting the earlier values are underestimated.

183.31-GHz self-induced pressure shift
There are only two values of the self-induced pressure shift shown in Figure 14 for the 183.31 GHz line, one of which is 5.847e^{-3} cm^{-1}/atm (Tretyakov, 2016), used in PWR19, and the other is from Koshelev et al. (2021b) provides a middling value of 3.68e^{-3} cm^{-1}/atm.

3.1.5 325.15 GHz line ($5_{15} \leftarrow 4_{24}$)

The following four sub-millimetre lines have not been subject to the same focus as the first two, as there have been very few applications using the frequencies. However, the 325.15 GHz line was considered as a potential channel in the proposed MASTER (Millimeter Wave Acquisitions for Stratosphere/Troposphere Exchange Research) instrument and thus the available parameters were investigated by Perrin et al. (2005), resulting in the creation of a bespoke linelist to best meet the needs of the instrument. The review considers previous versions of the HITRAN and JPL catalogues, which have been superseded in the interim period.

325.15-GHz line intensity
Line intensities from seven studies are shown in Figure 8 for the 325.15 GHz line, ranging between 9.012–9.227e^{-23} cm^{-1}/(molecules/cm^2), corresponding to a spread of 2.36 % and a mean of 9.10e^{-23} cm^{-1}/(molecules/cm^2), which co-incidentally is the same as the most recent study presented and included in GEISA 2019 (Coudert et al., 2014). Five of the studies, (Lodi et al., 2011; Pardo et al., 2001a; Coudert, 1999; Coudert et al., 2014), are within 0.31 % of each other. The AER 3.8 value from Clough et al. (1973) is below this range and its uncertainty estimate of 0.5 % does not overlap with the other studies. The Liebe (1989) value used in AMSUTRAN is far higher than the rest.

325.15-GHz air-broadened half-width
Air-broadened half-widths from four studies, which vary between 0.0944–0.1002 cm^{-1}/atm (a 6% range), are shown in Figure 9. Two of the studies: Liebe (1989), used by AMSUTRAN and ATM, and Koshelev et al. (2007), used by PWR17 and PWR19, are very close in value: 0.0959 and 0.0962 cm^{-1}/atm, respectively. The Ryadov and Furashov (1966) value of 0.1002 cm^{-1}/atm included in HITRAN 2016 appears to be quite high, however, was carefully chosen based on criteria specified by the new 'diet' implemented for water vapour half-widths (Gordon 2007). The AER 3.8 database contains the lowest value in the range calculated by Jacquemart et al. (2005), which is also used by the 2012 version of HITRAN.

325.15-GHz temperature exponent of air-broadened half-width
The temperature exponent associated with the air-broadened half-width given by four studies shown in Figure 10, varies between 0.64–0.74. HITRAN 2012 and AER 3.8 use the value of 0.73 given by Birk and Wagner

(2012), which was only slightly modified for the 2016 version of HITRAN to 0.74 based on Gamache and Laraia (2009). Two iterations of the Rosenkranz model, PWR17 and PWR19 choose to adopt a value of 0.64 based on Colmont et al. (1999).

325.15-GHz self-broadened half-width

Three values of self-broadened half-width for the 325.15 GHz line are shown in Figure 11, ranging between 0.461–0.507 cm^{-1}/atm (9.5%). All three were derived prior to 2007, with the most recent value of 0.471 cm^{-1}/atm adopted by two latest iterations of the Rosenkranz model being based on Koshelev et al. (2007), a study that focuses specifically on three water vapour lines between 321–380 GHz.

325.15-GHz temperature exponent of self-broadened half-width

Liebe (1989) is the sole resource for a separate value for the self-broadened temperature exponent considered here (0.74), and is used in all five absorption model line lists (Figure 12).

325.15-GHz air-induced pressure shift

The more recent version of HITRAN (2016) includes a pressure shift of -1.679e^{-3} cm^{-1}/atm taken from Gamache and Laraia (2009), see Figure 13. This is a slight reduction from value given in the previous release (2012), which was -2.000e^{-3} cm^{-1}/atm from an unknown source. PWR19 adopts a smaller shift of -0.439e^{-3} cm^{-1}/atm which is taken from the RAD spectrometer experiments described in Koshelev et al. (2007), where the individual shifts for N_2 and O_2 have been combined as 0.79N_2 + 0.21O_2 to approximate the shift due to air. The uncertainty due to fit on this parameter is too small to display in Figure 13 given the scale, but it evaluates to less that 0.5%.

325.15-GHz self-induced pressure shift

Figure 14 shows only one value of 44.78e^{-3} cm^{-1}/atm, which is used in PWR19 and is also sourced from the RAD spectrometer results in Koshelev et al. (2007). Note the uncertainty range attached, which arises from the fit is smaller than the ranges associated with other sub-millimetre lines and is less than 0.5%.

3.1.6 448.00 GHz line ($4_{23} \leftarrow 3_{20}$)

Apart from a handful of studies, this sub-millimetre line has rarely been studied in isolation. Even so, it seems like there is good agreement between the independent studies shown here, and the least spread for all parameters.

448.00-GHz line intensity

The sources and distribution of the line intensities at 448.00 GHz are similar to the 325.15 GHz (Figure 8), apart from AER 3.8 adopts the HITRAN 2012 values from Coudert (1999), instead of Clough et al. (1973), for this, and the remaining sub-millimetre lines. There is only one dedicated study that focuses on key lines in the 350-500 GHz range, which yields the lowest value of 8.596e^{-22} cm^{-1}/(molecules/cm^2) (Tretyakov et al., 2013a). Six of the seven line intensities are within 0.85 % of each other, between 8.596e^{-22} – 8.668e^{-22} cm^{-1}/(molecules/cm^2). The seventh value, from Liebe (1989), has a higher value of 8.767e^{-22}

cm^{-1}/(molecules/cm^2), however, the full range is still the lowest of all six lines considered here (2%).

448.00-GHz air-broadened half-width

Air-broadened half-widths from five studies, between 0.0874–0.0897 cm^{-1}/atm, have the smallest spread of all six lines considered with only 2.6 % difference between lowest and highest, see Figure 9. Values from the two consecutive versions of HITRAN, 0.0889 and 0.0888, cm^{-1}/atm, respectively are minimally different. The two latest Rosenkranz models draw their respective values from Tretyakov et al. (2013a, Table 1.), where R17 uses the experimental value derived from a radio-acoustic detection spectrometer, and PWR19 uses the calculated value. The latter is larger and closer in value to the HITRAN parameters.

448.00-GHz temperature exponent of air-broadened half-width

The temperature exponent attached to the air-broadened half-width given by the three studies relevant here are 0.65, 0.66 and 0.70 (Figure 10). HITRAN 2012 and AER v3.8 use the lower value provided by Birk and Wagner (2012), which is similar to the earlier Liebe (1989) value of 0.66, adopted by AMSUTRAN, ATM and R17. The upper Gamache and Laraia (2009) value of 0.70 is included in the latest collections: HITRAN 2016, GEISA 2019 and R19. Again, the 448.00 GHz range for this parameter is the smallest of all lines considered (7.4%).

448.00-GHz self-broadened half-width

Similar to the 325.15 GHz line behavior, there are three values of self-broadened half-width for the 448.0 GHz line (Figure 11), spanning a range of 7.4% between 0.434–0.467 cm^{-1}/atm. The upper value is based on the semi-classical calculations of Cazzoli et al. (2008), a study which focuses on five lines above 1 Thz, and is included in all the larger line databases. Both Rosenkranz models use the experimental value of 0.440 cm^{-1}/atm of Tretyakov et al. (2013a) derived using a RAD spectrometer.

448.00-GHz temperature exponent of self-broadened half-width

Like the other four sub-millimetre lines, only Liebe (1989) provides a separate value for the self-broadened temperature exponent of 0.67 (Figure 12), which is used in all five absorption models.

448.0-GHz air-induced pressure shift

The more recent version of HITRAN includes a negative shift of -2.819e^{-3} cm^{-1}/atm taken from Gamache and Laraia (2009), a slight reduction from the previous value of -3.100e^{-3} cm^{-1}/atm from HITRAN 2012. The PWR19 model adopts a value of -3.921e^{-3} cm^{-1}/atm calculated from the RAD spectrometer N_2 and O_2 data in Tretyakov et al. (2013a) assuming a 0.79N_2 + 0.21O_2 combination. The other two values given in the study, one from a resonator spectrometer and one calculated from externally sourced parameters, sit on opposite edges of the error estimate attached to the chosen shift.

448.00-GHz self-induced pressure shift

The single self-broadened shift for the 448.00 GHz line shown in Figure 14 is -20.79e^{-3} cm^{-1}/atm, which is from a RAD spectrometer experiment detailed in Tretyakov et al. (2013a) and is believed to be the first ever measurement of the parameter for this line. This value is included in the PWR19 model.

3.1.7 556.94 GHz line ($1_{10} \leftarrow 1_{01}$)

Even though it is the strongest line below 1000 GHz, studies dedicated to the rotational transition at 556.94 GHz remain few. However, the inclusion of a channel covering the 541–580.4 GHz range on the Submillimeter wave Radiometer (SMR) instrument, launched on the Odin satellite in 2001, provided some incentive for reliable measurements of the spectroscopic parameters of the encompassing lines, such as Golubiatnikov et al. (2008).

556.94-GHz line intensity

The same six sources as the other sub-millimetre lines, applied to the same respective models, are responsible for the range of 556.94 GHz line intensities shown in Figure 8, with values between 5.205e^{-20} – 5.378e^{-20} cm^{-1}/(molecules/cm^2) (3.28% range). For this line both the Liebe (1989) and Pardo et al. (2001a) values are at the upper end of the range.

556.94-GHz air-broadened half-width

Only two of the five studies that provide values for the air-broadened half-width for the 556.94 GHz line use dedicated experimental measurements. Golubiatnikov et al. (2008) employ a backward wave oscillator (BWO) based spectrometer to constrain the value to 0.1059 cm^{-1}/atm, which has been adopted in the two latest Rosenkranz models (though believed to be un-adjusted for temperature). On the basis of data for the different isotopologues given in the same study, the value of 0.1080 $\pm$0.002 cm^{-1}/atm is suggested until new measurements are available (M. Tretyakov, personal communication, 2021). AER 3.8 includes a modified width derived from the radiative closure procedure detailed in Mlawer et al. (2019), to produce the highest value of 0.1103 cm^{-1}/atm. These values are within the range of earlier studies, see Figure 9.

556.94-GHz temperature exponent of air-broadened half-width

Two values for the temperature exponent attached to the air-broadened half-width are used in all nine collections. These are 0.69 (Liebe, 1989), and 0.75 (Gamache and Laraia, 2009).

556.94-GHz self-broadened half-width

As with all four sub-millimetre lines, there are three values of self-broadened half-width for the 556.94 GHz line (Figure 11), spanning a range of 7.2% between 0.452–0.486 cm^{-1}/atm. The upper value is based on the semi-classical calculations of Cazzoli et al. (2008) and is included in all the larger line databases. Both Rosenkranz models use the experimental value of 0.481 cm^{-1}/atm from Golubiatnikov et al. (2008), derived using a BWO spectrometer.

556.94-GHz temperature exponent of self-broadened half-width

Again, only Liebe (1989) provides a separate value for the self-broadened temperature exponent, equal to 1.0 (i.e. no temperature dependency), which is used in all five absorption models.

556.94-GHz air-induced pressure shift
Values are between 6.32^{-3} and 6.80 $^{-3}$ cm^{-1}/atm (Figure 13). All of the larger line database use one of the two higher values and PWR19 includes the lower value, which is from Golubiatnikov et al. (2008).

556.94-GHz self-induced pressure shift
The single value of self-broadened shift for the models considered, is -57.22e^{-3} cm^{-1}/atm from (Golubiatnikov et al., 2008), which is included in PWR19 and is the largest self shift of all the six lines .

3.1.8 752.03 GHz line ($2_{11} \leftarrow 2_{01}$)

Even though it is the second strongest line below 1000 GHz, there are still very limited studies of the 752.03 GHz line. The only notable publication available is the short dedicated work by Koshelev (2011) that derives broadening and shifting parameters.

752.03-GHz line intensity
The same sources as the other sub-millimetre lines are used with almost exactly the same distribution of intensity values as the 556.94 GHz line seen for the 752.03 GHz line (Figure 8). Six intensity values range between 3.431e^{-20} – 3.547e^{-20} cm^{-1}/(molecules/cm^2), a range of 3.33%.

752.03-GHz air-broadened half-width
As with the 556.94 GHz line, AER 3.5 includes a modified air-broadened half-width derived from the radiative closure procedure detailed in Mlawer et al. (2019), which is the highest value in the range between 0.1022 – 0.1072 cm^{-1}/atm (Figure 9). Koshelev (2011) employs a RAD spectrometer to constrain the value to 0.1052 cm^{-1}/atm, which has been adopted in the two latest Rosenkranz models. These values are larger than the two earlier studies by Liebe (1989) and Gamache and Hartmann (2004).

752.03-GHz temperature exponent of air-broadened half-width
A similar story to the 556.94 GHz line is told, two values for the temperature exponent associated with the air-broadened half-width are included in the nine collections. These are 0.68 (Liebe, 1989), and 0.77 (Gamache and Laraia, 2009).

752.03-GHz self-broadened half-width
The same pattern as the two previous lines, there are three values of self-broadened half-width spanning a range of 7.8% between 0.428–0.463 cm^{-1}/atm (Figure 11). The upper value is based on the semi-classical calculations of Cazzoli et al. (2008) and is included in all of the larger line databases. Both Rosenkranz models use a value of 0.459 cm^{-1}/atm provided by Koshelev (2011) and derived using a RAD spectrometer.

752.03-GHz temperature exponent of self-broadened half-width
The Liebe (1989) study yields a value of 0.84 for the self-broadened temperature exponent, which is used in all five absorption models.

752.03-GHz air-induced pressure shift

Three values between 4.35e^{-3} and 8.5 e^{-3} cm^{-1}/atm are shown in Figure 13. For this line the upper value of unknown origin included in HITRAN 2012 and AER 3.8 appears large compared the other two values, which are within 1.2e^{-3} cm^{-1}/atm of each other. PWR19 includes the value of 5.48e^{-3} cm^{-1}/atm provided in Koshelev (2011) whose uncertainty range does not encompass either of the other values.

752.03-GHz self-induced pressure shift

A value of self-broadened pressure shift of -29.66e^{-3} cm^{-1}/atm is included in PWR19, which originates from Koshelev (2011) and is thought to be the first self shift ever measured for this line.

3.1.9 HITRAN 2020

At the time of finalising this report HITRAN has just updated its full H_2O line catalogue online for the first time since HITRAN 2016 with new line positions and intensities based on Conway et al. (2020), and a revised broadening and shift algorithm Vispoel et al. (2019). For all six of the lines discussed here the new line intensities are very similar to the previous values. New broadening and shift parameters are included for the three higher frequency lines, whereas the three lower frequency lines retain the previous values. The 556.94 and 752.03 GHz air-broadened half-widths are adopted from Mlawer et al. (2019), and the other new parameters result from modified complex Robert-Bonamy calculations by R.R. Gamache.

3.1.10 Line absorption

Considering now how these parameters perform when taken together, Figure 15 presents the difference in absorption in the vicinity of each of the six water vapour lines between MPM89 and the other nine models/databases, using each models respective absorption routines. An entry for AMSUTRAN is only shown separately for 22.235 GHz and 183.31 GHz because for all other lines its parameters are equal to MPM89. The absorption from each line is calculated on its own to isolate the effects of the individual parameters without any influence from other lines in the vicinity, and differing far wing procedures such as a cutoff. The lower panels show the equivalent results with all pressure-induced shifts removed. The percentage differences (dashed lines) are also shown for the shifted absorptions to inform the comparison. It is possible to deduce the dominant parameters for each line by looking at the differences between models, rather than focusing on the relative difference to the reference model, which is an arbitrary choice. Higher values equate to weaker absorption and lower means stronger. As the true absorption will be affected by the wings of other lines this is only part of the picture, and the full examination is left until section 3.3, which also includes continuum absorption to give meaningful results.

For the 22.235 GHz line (Figure 15a), absorption from HITRAN 2016 is strongest at the line centre (more negative) but becomes one of the weaker models beyond around $\pm$4 GHz (more positive). Conversely, ATM is the weakest model at the line centre but stronger in the wings. There is a 9% difference between the two models at the centre, which reduces to $\sim$2.5% at $\pm$7 GHz. Absorption at the line centre is dominated by the pressure-broadened half-width parameters and bigger values act to decrease absorption here while increasing

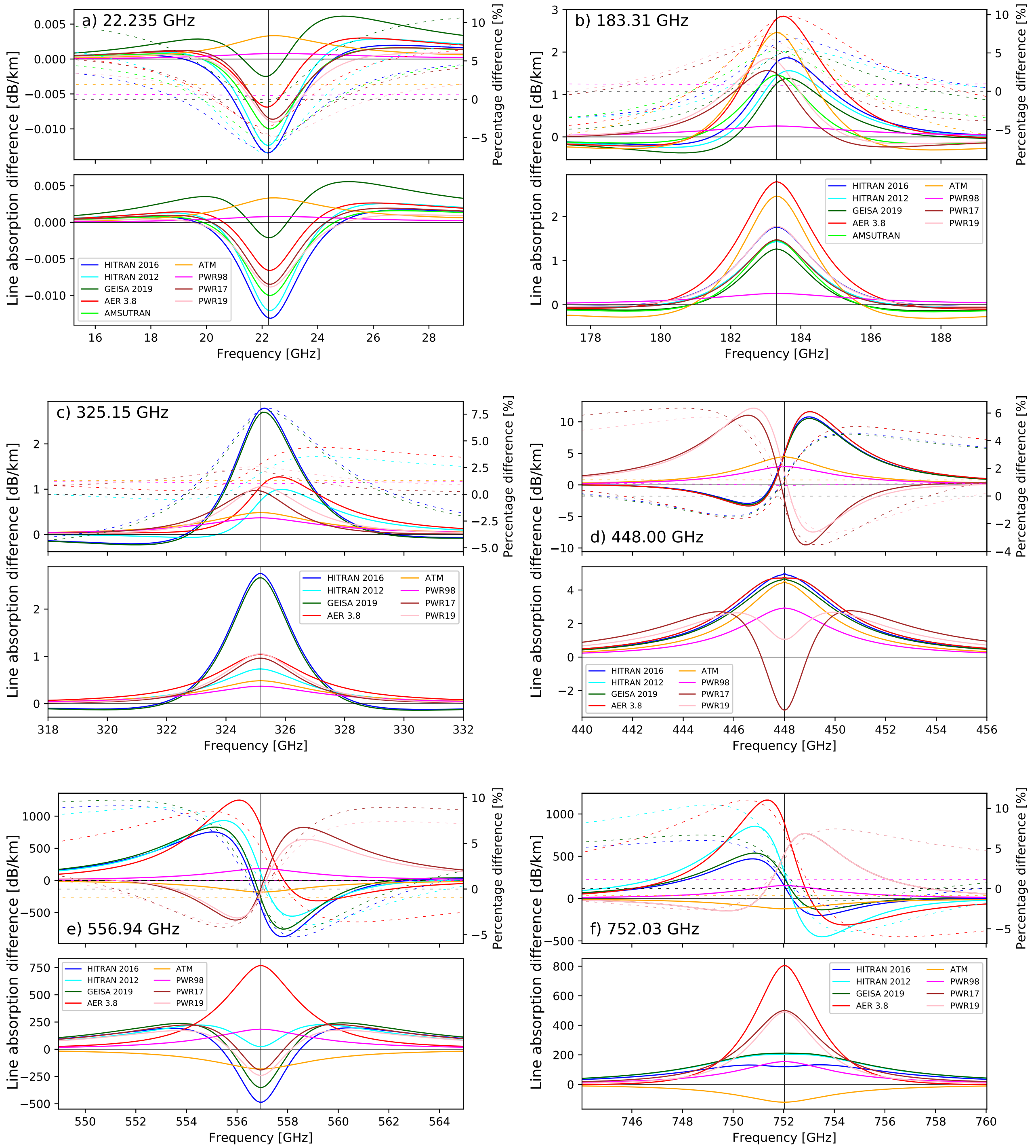

Figure 15: Line absorption for each model relative to MPM89 for each of the key water vapour lines calculated in isolation, i.e. no influence from other lines. Top panels are the difference between the sum of absorption on all levels to the top of atmosphere with pressure shifts if they are included (solid lines). Bottom panels are the equivalent with all pressure shifts set to zero. The top panels right hand axes also show the percentage differences calculated as 100(X-Y)/mean(X,Y) (dashed lines). Data are the mean of the diverse set of 83 profiles used throughout this review.

it at the wings, due to the way the line-shape is formulated. This effect is isolated for MPM89 and AMSUTRAN as the only difference between them is AMSUTRAN's air-broadened half-width is 5% less than MPM89's, which shows up as a 5% difference at the line centre, reducing to 0% at ±2 GHz, then decreasing absorption by nearly 5% at ±7 GHz. This is why the GEISA database, which has an unusually weak line intensity and among the lowest broadening half-width values, is still slightly stronger til around ±1 GHz than MPM89, ATM and PWR98, which all have larger half-widths. GEISA reaches 10% lower absorption than MPM89 at 22.235 ±7 GHz, however. Line intensity acts as a simple scaling factor, which can be observed by the constant 2% difference between ATM and MPM89, where only the line intensity differs between the two sets of parameters. There are minimal pressure-induced shifts visible for this line, with PWR19 showing the biggest effect with a shift of 0.3 GHz to higher frequencies.

For the 183.31 GHz line, MPM89 is the strongest at the line centre and weaker in the wings, which is common feature of the model for most of the water vapour lines but the absence of line cutoff makes up for the lack of wing absorption, somewhat. AER 3.8 has the weakest absorption at the centre (nearly ∼10% less than MPM89) due to a very weak line strength and second highest air-broadened half width of 0.1025 cm^{-1}/atm. The highest air-broadened half-width is 0.1040 cm^{-1}/atm from ATM but the associated line strength is also the highest, which compensates for the weak absorption at the centre. ATM absorbs around 5% more strongly than MPM89 at ±7 GHz, but the pressure shift included in AER 3.8 means more absorption is only seen at 183.31-7 GHz. One interesting point is that HITRAN 2016 and PWR19; and HITRAN 2012 and PWR17, look almost identical if not for the shift of around 0.3 GHz in opposite directions. For PWR19 this originates in part from the self-shifting parameter that has been added to the PWR19 models but not HITRAN as yet.

For 325.15 GHz, the large air-broadened half-width of 0.1002 cm^{-1}/atm from Ryadov and Furashov (1966) applied in HITRAN 2016 and GEISA 2019 has a dominant effect on the absorption compared to the other models. They are up to 7.5 % weaker at the line centre and 5% stronger at ±7 GHz, with a cross-over point beginning at around ±2 GHz. Most other models are within 2% of each other, with relatively constant offsets set largely by line strength, apart from HITRAN 2012 and AER 3.8 at 325.15+1 GHz due to the pressure shift to higher frequencies.

Pressure-induced shift also has a strong asymmetric effect on the last three lines. For 448.00 GHz, all the larger line databases shift about 1 GHz towards higher frequencies due to the air-shift parameters included, and both PWR17 and PWR19 shift around 1.5 GHz towards lower frequencies due to the addition of the self-induced shift component. The lowest air-broadened half-width present is 0.0874 cm^{-1}/atm in PWR17 and is based on resonator spectrometer measurements from Tretyakov et al. (2013a). This pushes PWR17 line absorption outside of the range of the other models; about 1% stronger than PWR19 at 448.00+1 GHz and 1% weaker at 448.00-7 GHz. The PWR19 model updated this value to 0.0883 cm^{-1}/atm, which is the equivalent calculated result from the same study. Without the pressure shifting parameters the spread between remaining models is less than 2%; the smallest of all the six lines, though this is not necessarily due to good knowledge of the parameters but rather a lack of focused studies. The inclusion of pressure shifts results in a divergence of up to 8% between models.

The large empirically constrained values of AER 3.8 air-broadened half-widths, as described in Mlawer et al.

(2019), have a noticeable effect on the 556.94 and 752.03 GHz lines, which is more easily seen in the non-shifted panels. With pressure shifts there is a minimum around 1 GHz below line centres, and a maximum beyond 2 GHz above them. The ATM model shows consistently strong absorption for these lines across the frequency range. There are large pressure shifts towards higher frequencies for the PWR17 and PWR19 models between 1–2 GHz, and similar size shifts in the opposite direction for the four larger line databases. Interestingly, PWR17 and PWR19 show practically the same absorption and shift (they overlap in Figure 15f) despite having different pressure shift parameters, which must evaluate to similar results.

Table 4: Spectroscopic parameters of key water vapour lines from databases and LBL models. Where applicable, values of line intensity (S), air-broadened half-width (γ_{air}) and self-broadened half-width (γ_{self}) have been adjusted from their reference temperature of 300 K to 296 K for consistency. A separate temperature dependence for self-broadened half-width (n_{self}) is not specified in HITRAN, GEISA or AER so is set to the same value as the temperature dependence of air-broadened half-width (n_{air}). Sources for the data are given in the footnotes. Unless otherwise stated, values for AMSUTRAN, ATM and PWR98 are from MPM89.

Parameter	ν	S	γ_{air}	n_{air}	γ_{self}	n_{self}	δ_{air}
units	GHz	$\frac{cm^{-1}}{molecules \times cm^2}$	$\frac{cm^{-1}}{atm}$	-	$\frac{cm^{-1}}{atm}$	-	$\frac{cm^{-1}}{atm}$
22.235 GHz							
HITRAN 2016	22.235337[a]	4.454e-25[b]	0.0900[c]	0.77[c*]	0.385[d]	0.77[c*]	-0.879e-3[c]
HITRAN 2012	22.235337[a]	4.394e-25[e]	0.0900[c]	0.60[f]	0.385[d]	[f]	-0.800e-3[c*]
GEISA 2019	22.235007[?]	4.190e-25[g]	0.0900[c]	0.77[d]	0.385[d]	0.77[d]	-0.879e-3[c]
AER 3.8	22.235067[?]	4.348e-25[h]	0.0917[i]	0.65[?]	0.385[d]	0.65[?]	-0.800e-3[c*]
AMSUTRAN	22.235080	4.430e-25	0.0906[j]	0.77[c*]	0.462	1.00	-
ATM	22.234617	4.343e-25[k]	0.0959	0.69	0.462	1.00	-
PWR98	22.235080	4.390e-25[l]	0.0959	0.69	0.460	0.61[m]	-
PWR17	22.235080	4.394e-25[e]	0.0900[c]	0.76[c]	0.460	1.00	-0.297e-3[?]
PWR19	22.235080	4.454e-25[b]	0.0912[n]	0.76[c]	0.449[o]	1.20[o]	-1.115e-3[n]
183.31 GHz							
HITRAN 2016	183.310107[a]	7.736e-23[b]	0.0992[c]	0.76[c*]	0.519[d]	0.76	-2.689e-3[c]
HITRAN 2012	183.310107[a]	7.785e-23[e]	0.0992[c]	0.68[f]	0.519[d]	0.68	-2.700e-3[c*]
GEISA 2019	183.310197[g]	7.860e-23[g]	0.0992[c]	0.76[c*]	0.519[d]	0.76	-2.689e-3[c]
AER 3.8	183.310107[a]	7.691e-23[h]	0.1025[i]	0.71[p]	0.519[d]	0.71	-2.700e-3[c*]
AMSUTRAN	183.310074	7.861e-23	0.0997[c*]	0.77[c*]	0.510	0.85	-
ATM	183.310074	7.883e-23[k]	0.1040[?]	0.64	0.553[?]	0.85	-
PWR98	183.310107	7.770e-23[l]	0.0958	0.64	0.510	0.85	-
PWR17	183.310074	7.785e-23[e]	0.0992[c]	0.77[c]	0.500[?]	0.85	-0.811e-3[?]
PWR19	183.310074	7.736e-23[b]	0.0995[o]	0.77[c]	0.499[o]	0.78[o]	-2.446e-3[o]
325.15 GHz							
HITRAN 2016	325.153101[a]	9.077e-23[b]	0.1002[q]	0.74[r]	0.507[d]	0.74	-1.679e-3[q]
HITRAN 2012	325.153101[a]	9.089e-23[s]	0.0944[t]	0.73	0.507[d]	0.73	-2.000e-3[?]
GEISA 2019	325.153161[g]	9.102e-23[g]	0.1002[p]	0.74[r]	0.508[d]	0.74	-1.679e-3[q]
AER 3.8	325.153101[a]	9.012e-23[h]	0.0944[t]	0.73	0.507[d]	0.73	-2.000e-3[?]
AMSUTRAN	325.152919	9.227e-23	0.0949	0.68	0.461	0.74	-
ATM	325.159822	9.105e-23[k]	0.0949	0.68	0.461	0.74	-
PWR98	325.152919	9.101e-23[l]	0.0948	0.68	0.461	0.74	-

[a] Lanquetin et al. (2001) [b] Lodi et al. (2011) [c] Payne et al. (2008) [d] Gamache and Hartmann (2004) [e] Coudert (1999) [f] Birk and Wagner (2012) [g] Coudert et al. (2014) [h] Clough et al. (1973) [i] Mlawer et al. (2019) [j] Liljegren et al. (2005) [k] Pardo et al. (2001a) [l] Rothman et al. (1992) [m] Liebe and Dillon (1969) [n] Koshelev et al. (2018a) [o] Tretyakov (2016) [p] Ma et al. (2010) [q] Ryadov and Furashov (1966) [r] Gamache and Laraia (2009) [s] Martin et al. (2016) in Rothman et al. (2013) [t] Jacquemart et al. (2005)

Table 4: continued.

Parameter	ν	S	γ_{air}	n_{air}	γ_{self}	n_{self}	δ_{air}
units	GHz	$\frac{cm^{-1}}{molecules \times cm^2}$	$\frac{cm^{-1}}{atm}$	-	$\frac{cm^{-1}}{atm}$	-	$\frac{cm^{-1}}{atm}$
PWR17	325.152888	9.089e-23[s]	0.0962[u]	0.64[v]	0.471[v]	0.74	-0.152e-3[?]
PWR19	325.152888	9.077e-23[b]	0.0962[u]	0.64[v]	0.471[u]	0.74	-0.439e-3[u]
448.00 GHz							
HITRAN 2016	448.001185[a]	8.633e-22[b]	0.0888[f]	0.70[r]	0.467[w]	0.70	-2.819e-3[r]
HITRAN 2012	448.001185[a]	8.625e-22[s]	0.0889[t]	0.65[f]	0.467[w]	0.65	-3.100e-3[?]
GEISA 2019	448.001215[g]	8.640e-22[g]	0.0888[f]	0.70[r]	0.467[w]	0.70	-2.819e-3[r]
AER 3.8	448.001185[a]	8.625e-22[s]	0.0889[t]	0.65[f]	0.467[w]	0.65	-3.100e-3[?]
MPM89	448.001075	8.767e-22	0.0897	0.66	0.434	0.67	-
ATM	448.001261	8.661e-22[k]	0.0897	0.66	0.434	0.67	-
PWR98	448.001075	8.668e-22[l]	0.0899	0.66	0.435	0.67	-
PWR17	448.001085	8.625e-22[s]	0.0874[x]	0.66	0.440[x]	0.67	-1.568e-3[?]
PWR19	448.001085	8.633e-22[b]	0.0883[x*]	0.70[r]	0.440[x]	0.67	-3.291e-3[p]
556.94 GHz							
HITRAN 2016	556.935991[a]	5.238e-20[b]	0.1039[d]	0.75[r]	0.486[w]	0.75	6.520e-3[r]
HITRAN 2012	556.935991[a]	5.207e-20[b]	0.1039[d]	0.75[r]	0.486[w]	0.75	6.520e-3[r]
GEISA 2015	556.936021[g]	5.205e-20[j]	0.1039[d]	0.75[r]	0.487[w]	0.75	6.520e-3[r]
AER 3.8	556.935991[a]	5.207e-20[i]	0.1103[i]	0.75[r]	0.487[w]	0.75	6.800e-3[?]
MPM89	556.936002	5.333e-20	0.1095	0.69	0.452	1.00	-
ATM	556.936071	5.378e-20[k]	0.1095	0.69	0.452	1.00	-
PWR98	556.936002	5.269e-20[l]	0.1095	0.69	0.452	1.00	-
PWR17	556.935985	5.238e-20[b]	0.1053[y]	0.69	0.481[y]	1.00	2.028e-3[?]
PWR19	556.935985	5.238e-20[b]	0.1053[y]	0.75[r]	0.481[y]	1.00	6.320e-3[y]
752.03 GHz							
HITRAN 2016	752.033098[a]	3.454e-20[b]	0.1022[d]	0.77[r]	0.463[w]	0.77	4.350e-3[r]
HITRAN 2012	752.033098[a]	3.433e-20[s]	0.1022[d]	0.77[r]	0.463[w]	0.77	4.350e-3[r]
GEISA 2019	752.033098[g]	3.431e-20[j]	0.1022[d]	0.77[r]	0.463[w]	0.77	4.350e-3[r]
AER 3.8	752.033098[a]	3.433e-20[s]	0.1072[i]	0.77[r]	0.463[w]	0.77	8.500e-3[?]
MPM89	752.033227	3.518e-20	0.1044	0.68	0.428	0.84	-
ATM	752.033047	3.547e-20[k]	0.1044	0.68	0.428	0.84	-
PWR98	752.033227	3.470e-20[l]	0.1044	0.68	0.428	0.84	-
PWR17	752.033113	3.433e-20[s]	0.1052[z]	0.68	0.459[z]	0.84	1.758e-3[?]
PWR19	752.033113	3.454e-20[b]	0.1052[z]	0.77[r]	0.459[z]	0.84	5.48e-3[z]

[u] Koshelev et al. (2007) [v] Colmont et al. (1999) [w] Cazzoli et al. (2008) [x] Tretyakov et al. (2013a) [y] Golubiatnikov et al. (2008)
[z] Koshelev (2011)

Table 4: continued.

Parameter	ν	S	γ_{air}	n_{air}	γ_{self}	n_{self}	δ_{air}
units	GHz	$\frac{cm^{-1}}{molecules \times cm^2}$	$\frac{cm^{-1}}{atm}$	-	$\frac{cm^{-1}}{atm}$	-	$\frac{cm^{-1}}{atm}$

* Values originating from the same study may differ, check sections on individual line parameters for details.
? Source unknown.

3.1.11 Water vapour lines summary

For these six lines the following conclusions can be drawn:

- In general, there is more certainty about line intensities than all other parameters, which are known to within 1.5–3.5 %, based on the range observed, however, there are outliers for each line and often the quoted uncertainty does not cover all of the other values.
- Earlier studies such as Liebe (1989) and Pardo et al. (2001a) are sometimes outside of the range given by more recent studies but for some parameters, such as the temperature dependence of self-broadened half-width, the former is still the only source available for the current line-shape used.
- There are more studies dedicated to the 22.235 and 183.31 GHz lines, and values appear to converge for these based on more recent results. There are far fewer studies dedicated to the four sub-millimetre lines.
- The HITRAN 2016 air-broadened half-width for the 325.15 GHz line was modified from the previous value to that of Ryadov and Furashov (1966) even though the value is significantly higher than more recent studies, as a result of a recently prescribed 'Diet' applied to HITRAN, where a theoretical value is accepted when there is no experimental one available (Gordon et al., 2007).
- Despite many studies in some cases, there is no convergence and a wide range of estimates for the temperature dependence of the air-broadened half-width, which spans 0.6 and 0.77.
- There are few estimates for temperature exponents of self-broadened half-width, but a wide spread with values between 0.67 and 1.2. Two of the lines, however: 22.235 and 556.94 GHz, include estimates of no temperature dependence at all.
- Pressure-induced shifts show large differences between lines and studies, some even changing sign. The most constrained parameter is the 183.31 GHz air-induced pressure shift with five studies within 12% of each other.
- In general, the 448 GHz line has the lowest spread of values relative to the other lines, which suggests it is either more well known or too little measured.
- Uncertainties attached to individual studies, when present, often do not encompass the full range of parameters in a single comparison, suggesting experimental set-up is the dominant source of parameter difference.

- Care must be taken in interpreting uncertainties as they may vary in meaning, i.e. some represent the goodness of fit, one standard deviation or the total error budget of all components involved. Only the latter can be compared directly to other experiments.
- Studies that use different apparatus and methods to obtain the same parameter, e.g. Koshelev et al. (2018a) and Tretyakov et al. (2013b), can provide insights into the experimental error and increase the robustness of results.
- Line absorption is up to 9% different between the nine collections of parameters when isolated from the influence of other lines.
- Air-broadened half-widths appear to dominate absorption, a larger value acts to reduce it in the line centre and increase it the wings. A crossover occurs at around 2–3 GHz where differences between models are low.

3.2 Water vapour continuum

Water vapour continuum is a spectrally smooth absorption characterized by a quadratic pressure and a negative temperature dependence, which was first observed in atmospheric windows in the early 1900's (Rubens and Aschkinass, 1898). Though it can be the dominant component in window regions near the surface or lower troposphere, its source is still under debate (Serov et al., 2017; Shine et al., 2012), essentially concerning the relative importance of collision-induced absorption, water vapour dimers (Serov et al., 2014; Tretyakov et al., 2013b), and the contribution of far-wings of spectral lines (Serov et al., 2017; Clough et al., 1989). Despite various theories, as there is still no complete physical based description for the continuum, models rely on parameters determined empirically with a focus on particular spectral regions, such as part of the microwave or infrared. These tend to be either laboratory-based experiments or atmospheric campaigns that make in-situ measurements to quantify (or modify) all, or some of, the self and foreign continuum coefficients, C_s^T and C_f^T, and their temperature dependencies, n_s and n_f. In the microwave region, the continuum has been verified to follow a quadratic function of frequency (Koshelev et al., 2011), because of dominating contribution from the 'radiation term' to the frequency dependence of the continuum though this is not the case at higher frequencies (Odintsova et al., 2017; Scribano and Leforestier, 2007). The common form of the continuum equation is:

$$\alpha_c(\nu) = \nu^2\theta^3(C_s(T)p_{wv}^2 + C_f(T)p_{dry}p_{wv}) \tag{8}$$

where $C_s(T)$ and $C_f(T)$ are each comprised of a coefficient at a reference temperature and an exponential scaling factor n_s or n_f as:

$$C_{s,f}(T) = C_{s,f}^T\theta^{n_{s,f}} \tag{9}$$

T is commonly 296 or 300 K, and n_f is often taken as zero, ie. no foreign temperature dependence.

3.2.1 Dimers

The body of work dedicated to resolving the water vapour dimers role in atmospheric conditions has made advances in the last decade with the first un-ambiguous measurement made in 2012 (Tretyakov et al., 2013b). The authors confirm that the largest fraction of continuum absorption at millimetre wavelengths and room temperatures can be attributed to stable dimers. The stable dimer is a bimolecular state associated with a pair of weakly hydrogen bound molecules, in this case water vapour monomers, $(H_2O)_2$. Other bimolecular states include quasi-bound (metastable) or free-pairs, though the contribution of the latter is known to be negligible at atmospheric conditions (Serov et al., 2017). These two states require evaluation of the pair lifetime but the stable dimer does not differ from any other polar molecule and produces a characteristic line spectrum. Serov et al. (2014) present resolved spectra for measured and ab-initio derived dimers at warm temperatures between 280 – 322 K in the 188 – 258 GHz range, to which six almost equally spaced peaks every 12 GHz are attributed. The bound dimer has been evaluated to account for $\sim$100% of all dimer absorption around 200 K decreasing to $\sim$50% around 300 K. Koshelev et al. (2018b) subsequently reported 13 sequential dimer peaks in the range between 100 – 240 GHz. Odintsova et al. (2019, Figure 4.) presents results that imply the stable dimer is the dominant contribution to the self continuum at millimetre wavelengths, when comparing measurements from Koshelev et al. (2018b); Podobedov et al. (2008) and Koshelev (2011) with the ab initio dimer model from

Scribano and Leforestier (2007). The model suggests that the quadratic function of frequency is approximately acceptable between around 120–300 GHz, but strongly deviates between 75–120 GHz and beyond 300 GHz.

3.2.2 MT-CKD

MT-CKD (Mlawer-Tobin-Clough-Kneizys-Davies) is a far-wing based continuum model developed at AER alongside its line databases (Mlawer et al., 2012), whose form differs to the traditional description given in Equation 8. It covers the entire atmospheric spectrum with a different set of continuum coefficients specified every 10 cm^{-1} (300 GHz), which are interpolated to the required frequency. The temperature dependence of the self continuum is also not in the form of a scalar exponent, but is largely contained within the coefficients themselves, which are specified at 260 K and 296 K. The left hand panel of Figure 16 shows the basic principle behind the far-wing model applied to a water vapour line. A cut-off, commonly 25 cm^{-1} from the line centre, is specified and all absorption below where the cut-off intersects the lineshape is designated as continuum, which is the sum of the plinth and the far wings. The right hand panel shows a schematic of the adjustments made in the original derivation of the earlier CKD model based on discrepancies between the traditional description and what was observed (Clough et al., 1989). The CKD continuum, first released in 1989, applied a 'χ-term' to the Van-Vleck Huber lineshape (nearly identical to the Van-Vleck Weisskopf in the microwave) to account for excess absorption within water vapour bands (super Lorentzian) and reduced absorption between bands (sub Lorentzian). All shaded regions not part of the lineshape were considered to be continuum.

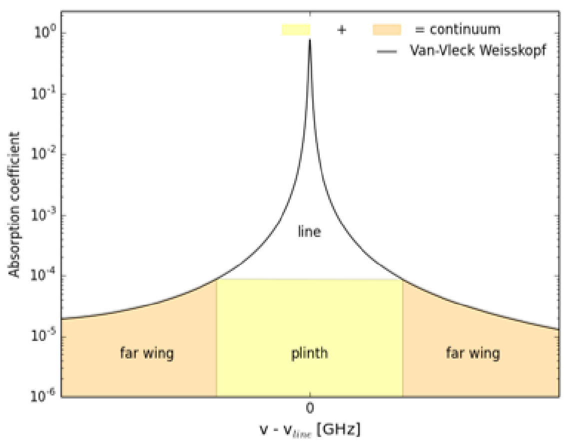

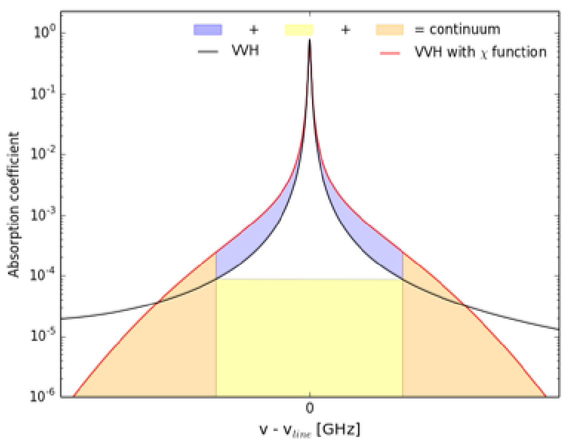

Figure 16: Left - Schematic of the far-wing theory of the continuum. A cutoff specifies the position of the far wings either side of the line centre, and the shaded area comprising far-wings and the plinth which are designated as continuum. Right - Schematic of the origin of the MT-CKD continuum specified by a pseudo-lineshape which is modified by the 'χ-function'. All of the shaded absorption outside of the original line shape is designated the continuum.

The MT-CKD model has evolved incrementally since its initial release in 2003 in response to various atmospheric campaigns targeting different parts of the spectrum. Initially the function was scaled to fit the data and by version 2.4 it no longer represented the functional form and it was clear it needed to be reformulated. MT-CKD 2.4, released June 2009, was constrained in the microwave and sub-millimetre based on data from ARM ground-based radiometers that took measurements at 23.8, 31.4, 150 and 170 GHz (Payne et al., 2011), but most of the weight was given to results from the 31.4 GHz channel. MT-CKD 3.0 was released in December 2016 with further adjustments made based on the RHUBC-II campaign (Mlawer et al., 2019). The update combined results of radiative closure studies from six different instruments, including the SAO FTS (Smithsonian Astrophysical Observatory submillimeter Fourier Transform Spectrometer) that measures in the interval between 450–1800 GHz, resulting in a reduction of the foreign continuum, and a slight increase in the self continuum in this region. Foreign coefficients at even lower frequencies were also lowered to allow a smooth continuation of the function, and the self continuum was increased slightly to maintain consistency with Payne et al. (2011).

Table 5: Water vapour continuum studies: Experimental configuration.

Model	**Frequency** (GHz)	**Temperature** (K)	**Foreign component**	**Lines**	**Line cutoff** (750 GHz)
MPM89	137.8	281–316	air	MPM89	no
PWR98	137.8,40–800	281–316,296–336	air	PWR98	yes
Turner 09	150	atmosphere	atmosphere	MPM89/PWR98	no/yes
Pardo 01	350–1100	atmosphere	atmosphere	ATM	no
Kuhn 02	153–350	306–356	N_2	PWR98	yes (no)
Podobedov 08	300-2700	293–333	N_2	HITRAN 2004	yes (no)
Koshelev 11	107.7–143.3	261–328	N_2	PWR98 (adj)	yes
Slocum 13	300–1500	296	air	HITRAN 2008	no
Wentz 16	19–89	atmosphere	atmosphere	PWR98	yes
MT-CKD 3.0	0.0–infrared	atmosphere	atmosphere	AER 3.5	yes
MT-CKD 3.5	0.0–infrared	atmosphere	atmosphere	AER 3.8	yes

Table 6: Water vapour continuum studies: Parameter values. All C_s and C_f are quoted at a temperature of 296 K. Round brackets refer to results from using different spectral lines. Square brackets contain the range of values produced by frequency dependent formulations (and temperature dependent in the case of n_s).

Model	$\mathbf{C}_s^T$ (dB/km)/(GHz^{2}hPa^2) [x10^{-8}]	$\mathbf{C}_f^T$	$\mathbf{n}_s$ –	$\mathbf{n}_f$ –
MPM89	7.48†	0.214†	7.50	0.0
Turner 09 for MPM89	5.99†	0.233†	7.50	0.0
PWR98	8.63†	0.246†	4.50	0.0
Turner 09 for PWR98	6.81† (6.82^d)	0.271† (0.269^d)	4.50	0.0
Pardo 01	-	0.274†	-	-
Kuhn 02	10.16† (9.63–10.23)	0.284*† (0.257-0.313)	5.10 (4.78–5.29)	1.34
Podobedov 08	4.48† (4.14)	0.220*† (0.169)	5.50 (5.8)	1.80
Koshelev 11	8.89†	0.271*†	5.24	0.91
Slocum 13	-	0.283	-	-
Wentz 16	3.66$^\dagger\nu^{0.1}$ [4.46-5.51]	0.270†	4.50	0.0
MT-CKD 3.0	7.84^c [6.75–8.76]	0.257^c [0.231–0.290]	3.50^c [2.89-4.21]	0.0
MT-CKD 3.5	6.46^c [6.23–6.62]	0.269^c [0.262–0.297]	5.84^c [4.66–7.12]	0.0

† adjusted from 300 K to 296 K using the corresponding value of n_s or n_f

* foreign component adjusted from N_2 to air using a dividing factor of $G_{N_2}/G_{air} \simeq 1.12$

d PWR19 and PWR17 use a slightly adjusted C_f to account for line modifications

c mean value over all frequencies between 2–1000 GHz, and all profile temperatures for n_s

MT-CKD 3.5 was released in 2021 containing adjustments to bring the self-continuum temperature dependence, n$_s$, in line with data from Koshelev et al. (2011), presented in Figure 19. of Tretyakov (2016). An exponent value of 5.6 was estimated at around 295 K and used as the basis for increasing of the 260 K self coefficients by 40%, leading to a scaling of 296 K self coefficients by 1.25 and a corresponding reduction in the foreign coefficients of 0.925. These changes further enhance the direction of adjustments made between MT-CKD versions 2.4 and 3.0. Both models are included in the following comparison to show the evolution. Figure 17 shows the temperature variation for the range of possible temperature exponent values extracted by regression of the calculated MT-CKD self continuum against relative inverse temperature (Equation 9), where each point is an atmospheric level from the diverse 83 profile dataset, for all frequencies between 2–1000 GHz at 1 GHz resolution. There is a positive correlation between n$_s$ and temperature, which is almost, but not quite, linear, and a negative correlation between n$_s$ and frequency. This is clear departure from the traditional scalar value applied in other continuum models.

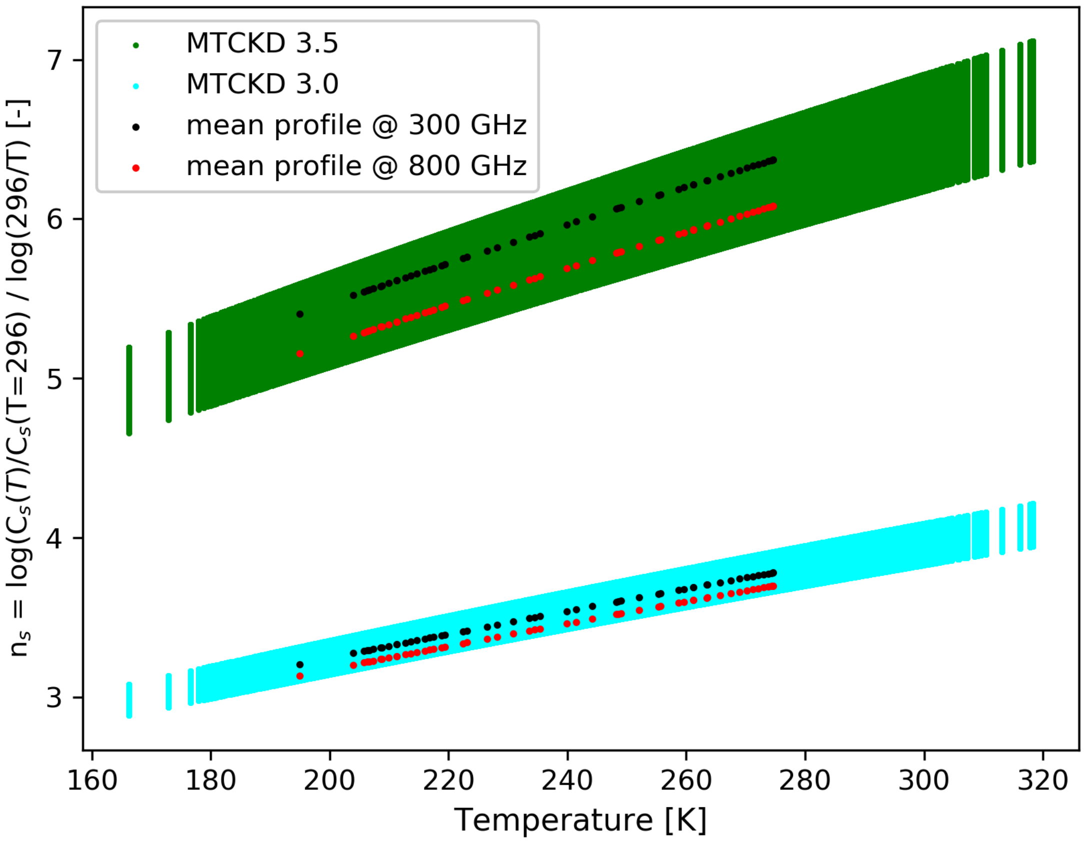

Figure 17: Temperature exponents of the self continuum backed out of the MT-CKD continuum by regressing the logarithm of C$_s$ / C$_s$(296 K) against the logarithm of the relative inverse temperature at 296 K. The 83 diverse profile dataset on 54 levels and frequencies every 1 GHz from 2-1000 GHz are used to approximate the full range of values. Black dots are temperature exponents on each level of the 83rd (mean) profile at a frequency of 300 GHz, and red dots are the same at 800 GHz.

3.2.3 Continuum models

Recent studies and well-known models that provide continuum parameters in the microwave/sub-millimetre region are listed in Table 5, alongside their experimental conditions. The associated coefficient values are given in Table 6. Frequency refers to either the single frequency that the experiment was performed at, or a range from which continuum parameters are determined from a fit to the data. In the case of Rosenkranz (1998) (PWR98) both of conditions are true, as the foreign continuum is determined from a single frequency based on Liebe (1989), but the self is calculated from a fit to multiple frequencies based on Liebe et al. (1993), which itself is based on fitting the results of multiple studies across different frequency ranges. The PWR98 values were then adjusted to be consistent with the PWR98 lines used with a line cutoff, resulting in an increase of the continuum. MPM93 (Liebe et al., 1993) itself is omitted due to the differing formulation based on the assumption of a 'pseudo-line' around 1780 GHz, and it is also often considered to be an outlier as some studies have found it to be in-consistent with various atmospheric observations (Turner et al., 2009; Hewison et al., 2006). Turner et al. (2009) itself applies empirical constraints from ground based radiometer measurements at 150 GHz to modify existing absorption models including MPM89 and PWR98 by providing respective scaling factors of 1.090 and 1.105 to C_f, and 0.80 and 0.79 to C_s. Following a similar methodology Wentz and Meissner (2016) refine the PWR98 continuum model based on measurements taken by the Global Precipitation Measurement Microwave Imager (GMI) satellite instrument at five frequencies between 10.7 and 89.0 GHz, which is an ideal vantage point for the present purpose albeit only measured at low frequencies.

For the foreign broadening component column, air denotes a laboratory experiment, whereas atmosphere means the measurements were made outside in the real atmosphere. Kuhn et al. (2002) , Podobedov et al. (2008) and Koshelev et al. (2011) use pure nitrogen (N_2) instead of air requiring a manual adjustment to the foreign coefficient to bring it in line with the other studies. The scaling factor G_{N_2}/G_{air} is commonly taken to be 0.627/0.558 $\simeq$ 1.12, from the work of Liebe and Layton (1987), which was measured at 303 K and 138 GHz. This results in a $\sim$11% change to the coefficient, which is significant given the over-simplification of the relationship. The studies of Slocum et al. (2013) and Pardo et al. (2001a) provide only a foreign continuum coefficient, the former due to the resolution of the spectrometer being too large to resolve any self-broadened peak of water vapour, and the latter due to the high, dry measurement site, 4207 metres above sea level, where the foreign component dominates. It is clear that the differing experimental conditions make objective comparisons of values difficult, particularly when the choice of underlying lines is directly related to the definition of the continuum and the inclusion or absence of a cut-off makes a large difference to the total absorption (see Figure 6).

Foreign continuum coefficient (C_f)

Figure 18 shows the foreign continuum components at 296 K from the various studies against the measurement frequency or fitted frequency range where applicable. There is a 55% difference between the lowest and highest C_f, however, the lower Podobedov et al. (2008) value, where the only difference to the higher one is a 3000 GHz line cutoff instead of the standard 750 GHz, seems anomalously low, so omitting this brings

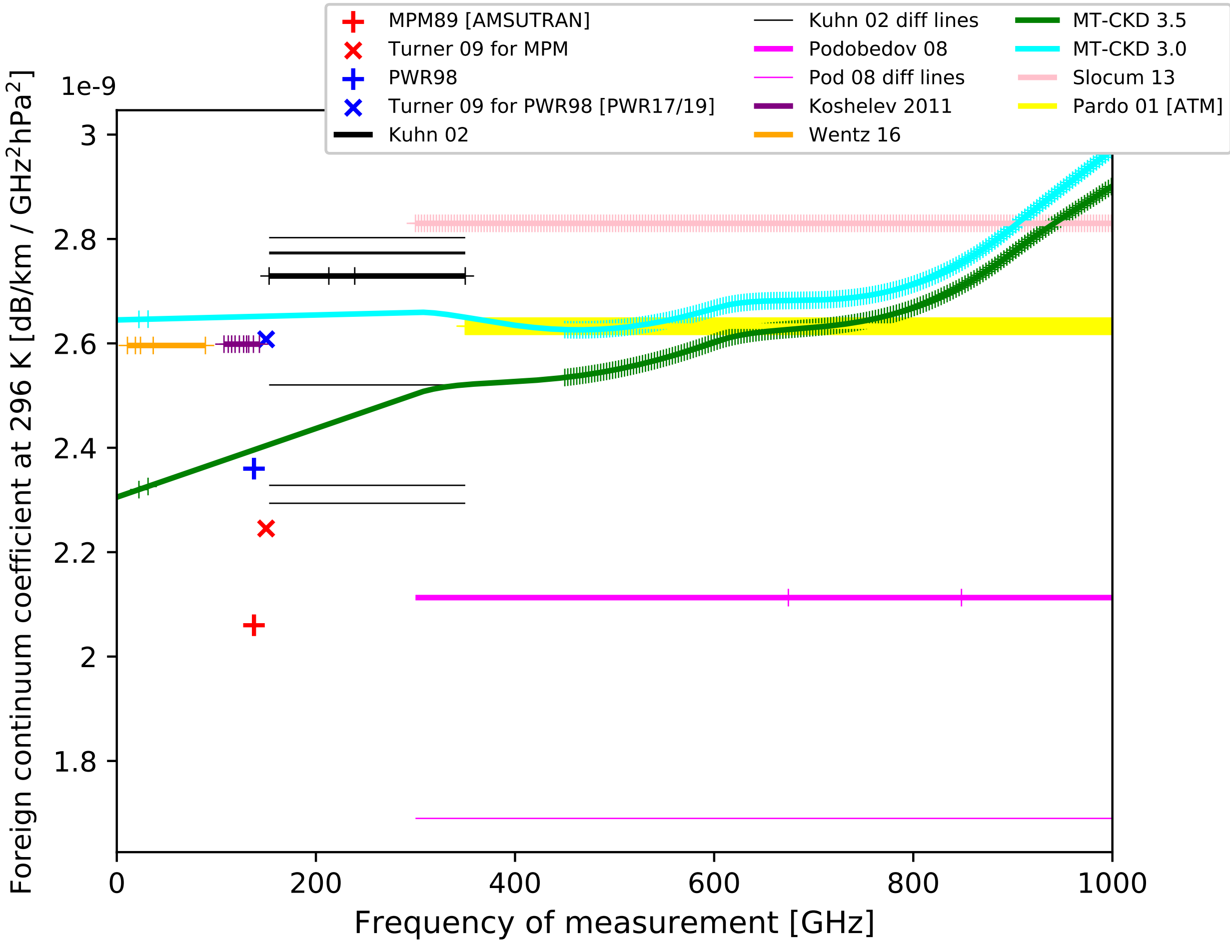

Figure 18: Foreign (air) continuum coefficients normalized to a temperature of 296 K. Crosses indicate the frequency or frequencies of the experimental measurements. Where the coefficient is derived through regression of multiple frequencies a line indicates the frequency range applicable. Where the study re-calculates the coefficient using different underlying spectral lines a thinner line indicates the alternate value.

the range to 34%. A similar magnitude difference, of ∼20%, is seen between Kuhn et al. (2002) results with and without a cutoff, and possibly between PWR98 and MPM89 where the cutoff is also the most significant difference. Hence, there is more difference between sets of experiments than there is between different lines used within one set of experiments, and there is no identifiable relationship between studies that use the same lines, experimental temperature range or foreign component. There also does not appear to a substantial correlation between frequency and coefficient value when all studies are considered, even though the most recent version of MT-CKD does appear to suggest this if taken in isolation. Even so, the Podobedov et al. (2008) value is derived from frequencies up to 2700 GHz and is the second lowest value, while Wentz and Meissner (2016) does not include any frequencies above 89 GHz and is among the highest. The former study also derives individual results for each of the eight windows between 674–2,521 GHz and no trend was observed. The more recent studies do suggest, however, that the value is closer to the upper end of the range, at 0.260 x10^{-8} (dB/km)/(GHz^{2}hPa^2) and above, particularly at sub-millimetre frequencies.

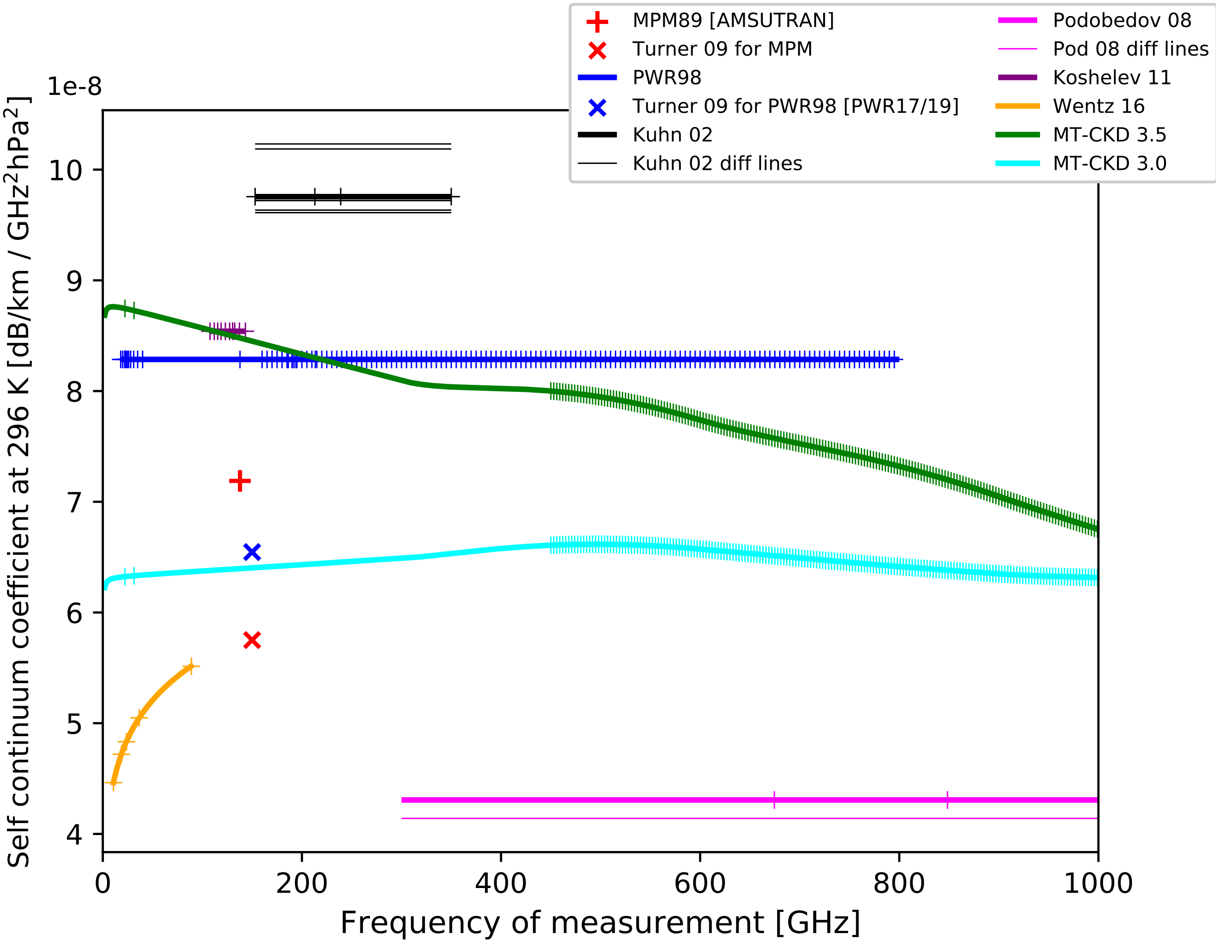

Figure 19: Same as Figure 18 but for the self continuum coefficient C$_s$ at 296 K.

Self continuum coefficient, (C$_s$)

Figure 19 shows the equivalent comparison for the self continuum at 296 K. There is an 85 % difference between the highest and lowest values, however in this case the Kuhn et al. (2002) values appear to be outliers for all of their underlying lines. Omitting these gives a range of 73 %. When considering all models there appears to be little correlation between C$_s$ and frequency even though the values in the latest version of MT-CKD show a negative trend (which compensates for the positive trend in the foreign coefficients). A similar comparison of models is presented in Odintsova et al. (2019, Figure 4.) alongside ab initio calculations of the dimer from Scribano and Leforestier (2007), and is more suggestive of a negative trend, particularly beyond 400 GHz, which can be interpreted as a failure of the quadratic approximation function. The formulation developed by Wentz and Meissner (2016) is positive over the 19–89 GHz frequency range due to the incorporation of an additional $\nu^{0.1}$ term. There is some compensation with corresponding values of the foreign continuum, i.e. the C$_s$ for MPM89 and PWR98 are among the higher values whereas they were among the lower for C$_f$. Turner et al. (2009) modified values act to move them towards the middle of the range for both models.

Temperature exponent of self coefficient (n$_s$)

The temperature dependence is very important for the self continuum as it is a strongly negative relationship, i.e. C$_s$ diminishes significantly with increasing temperature. n$_s$ varies between 2.89 and 7.50 over all studies, an 89% difference. The left panel of Figure 20 appears to show the whole range of values provided by the earlier MT-CKD model (3.0) are too low but the newer version (3.5) corrects this, placing the updated range centrally amongst the values from other studies. Omitting MT-CKD 3.0 from the comparison leaves only 50 % difference between the lowest value, 4.5 for PWR98, and the highest, 7.5 for MPM89.

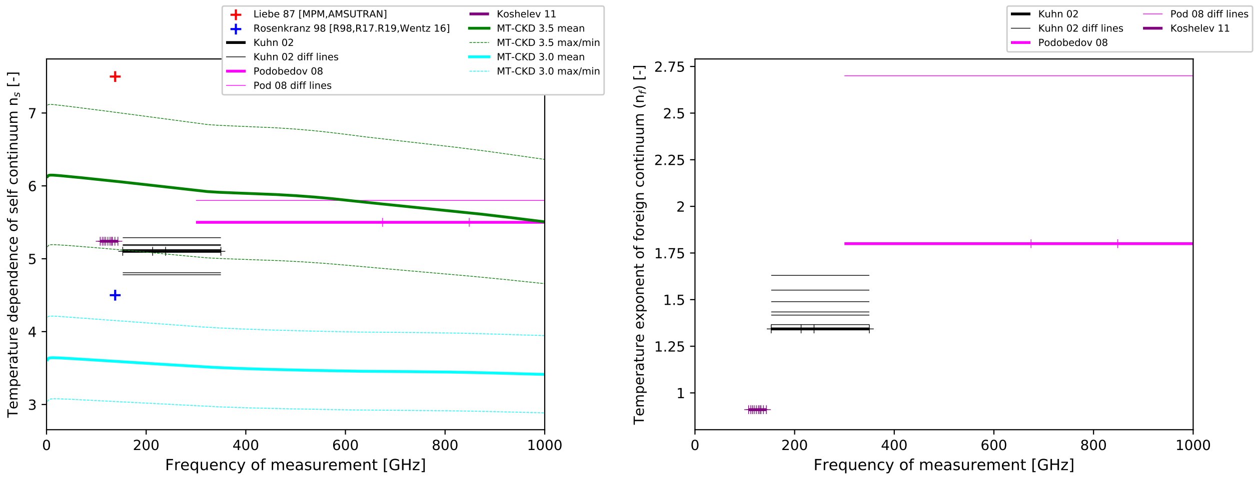

Figure 20: The temperature exponents for the self continuum coefficient (left panel), and the foreign continuum coefficient (right panel). Crosses indicate the frequency or frequencies of the experimental measurements. Where the coefficient is derived through regression of multiple frequencies a line indicates the frequency range applicable. Where the study re-calculates the coefficient using different underlying spectral lines a thinner line indicates the alternate value. The dashed lines indicate the boundaries for the range of values in the MT-CKD models.

Temperature exponent of foreign coefficient (n$_f$)

Only three of studies considered here; Kuhn et al. (2002), Podobedov et al. (2008) and Koshelev et al. (2011), provide a non-zero value for the temperature dependence of the foreign continuum. These are also the only studies to use nitrogen for the foreign component instead of air but it is not thought these two factors are related, as all three are also the only ones to fit C$_f$ against temperature. Within this limited range of studies it appears that the dependence increases with frequency (right panel of Figure 20), however, a larger range of results are needed to confirm this.

Total continuum absorption

The total and self and foreign component continuum absorption for the models is shown in Figure 21. Despite the large differences in the foreign and self coefficients, and their temperature exponents, when the total is considered, half of the models cluster together within ~7% (though the full range is around 60%). These six are the two versions of MT-CKD, although version 3.0 follows more of a curved line and is lower at intermediate frequencies, all the Rosenkranz models: PWR98, the Turner et al. (2009) modification of PWR98 and PWR19 (which uses updated lines and slightly modified the Turner et al. (2009) continuum to account for this), and Wentz and Meissner (2016), which uses PWR98 lines and modifies the original associated continuum. The continuum with the strongest absorption overall is Kuhn et al. (2002), which is expected given the coefficient values, followed by Koshelev et al. (2011), both of which use PWR98 lines and N_2 as the broadening component. Continua with the lowest absorption are the two MPM89 based models, Podobedov et al. (2008), and finally ATM, which is perhaps unsurprising given it only comprises the foreign component. A deviation in shape due to the frequency dependence of the formulation is evident in both MT-CKD model components, however for MT-CKD 3.5 the deviation of the self compensates for that of the foreign in the total absorption. Of the Rosenkranz based models the original PWR98 has a noticeably lower foreign component, and higher self component than the rest, which are corrected by the modifications of Turner et al. (2009) and Wentz and Meissner (2016).

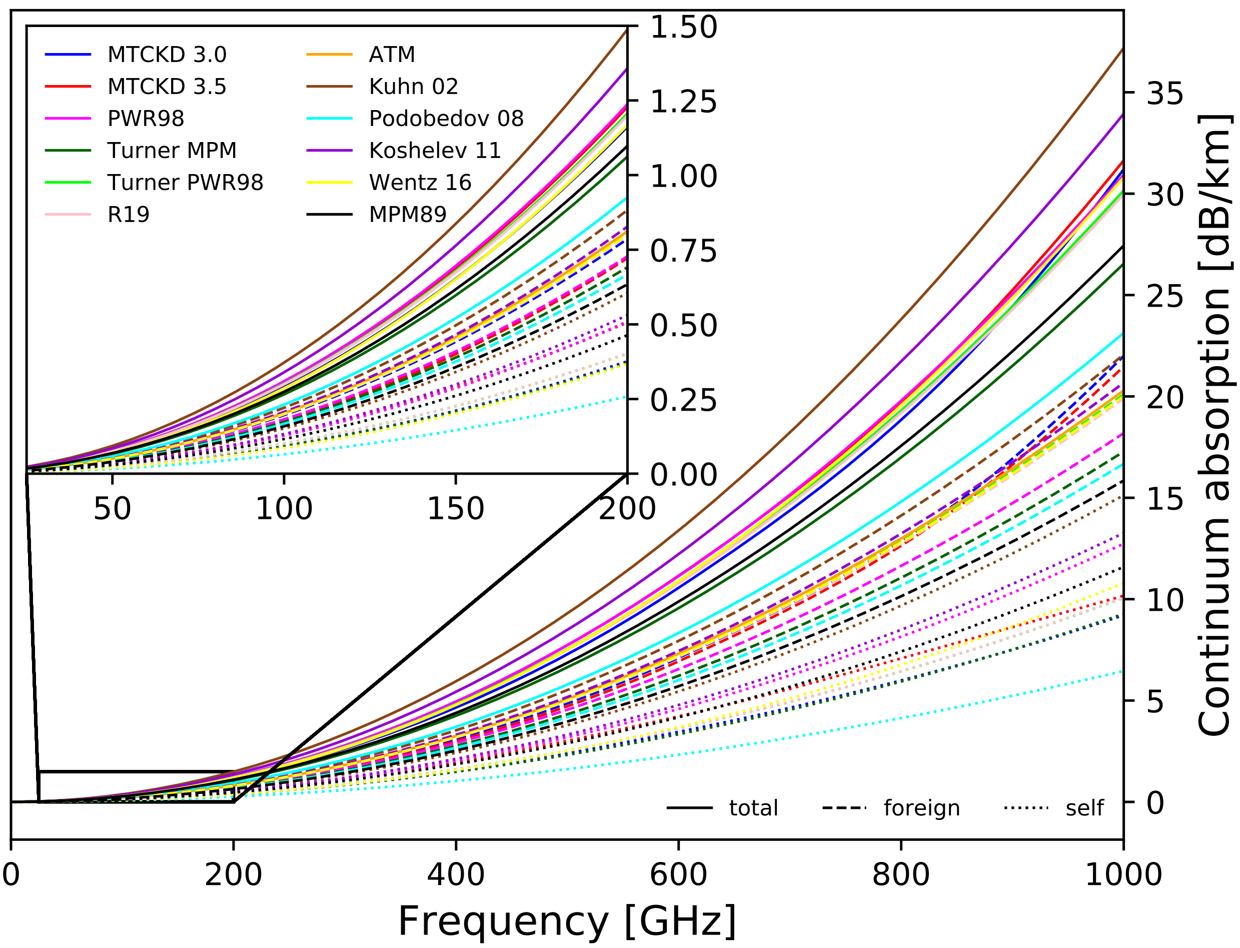

Figure 21: Total (solid lines), foreign (dashed lines) and self (dotted lines) continuum absorption for all continuum models listed in Tables 5 and 6. Lines are the sum of dB/km absorption on levels to the top of atmosphere, and are the mean of the diverse set of 83 profiles used throughout this review.

3.2.4 Water vapour continuum summary

- The first un-ambiguous detection of the water vapour dimer absorption at atmospheric conditions occurred in 2012 and subsequent experiments have revealed its unique spectra. It is determined that only part of the continuum can originate from dimers.
- The latest version of MT-CKD (3.5) was constructed on the basis of increasing the temperature dependence of the self-component to match recent results (Koshelev, 2011). The range of values increases from around 2.9–4.2 (MT-CKD 3.0) to 4.7–7.1 (MT-CKD 3.5) where the range depends on temperature and frequency. The change is manifested by an increase of 1.25 in self coefficients and 0.925 reduction in foreign coefficients.
- A comparison of 11 sets of continuum parameters shows the study-to-study difference tends to dominate over intra-experiment variations.
- There is no one continuum parameterisation that satisfies all of the requirements for MetOp-SG from a theoretical point of view, in terms of corresponding experimental conditions.
- There does not appear to be a strong correlation between frequency and strength for either self or foreign continuum.
- There is a $\sim$34% spread in foreign component coefficient, $\sim$73% spread in self component coefficient, $\sim$50% spread in temperature of self component and over 100% for temperature of foreign component, however, the latter doesn't apply in the same way as it's so close to zero anyway.
- There is a 60% spread between continuum models in total absorption, but six are within 7%. These are: the two versions of MT-CKD, particularly the latest version; all of the Rosenkranz models: PWR98, the Turner et al. (2009) modification of PWR98 and PWR19; and Wentz and Meissner (2016). The latter four all use PWR98 lines apart from the updates applied to PWR19, which is reflected in slightly modified continuum coefficients.
- Kuhn et al. (2002) and Koshelev et al. (2011) show very high, and Podobedov et al. (2008) and Pardo et al. (2001a) show very low, continuum absorption relative to the other models. For Podobedov et al. (2008) this is because it was measured at higher frequencies where the quadratic approximation is not appropriate, at least for the self continuum (Odintsova et al., 2019). For Pardo et al. (2001a) only a foreign component is included.

3.3 Continuum and line comparison

As the continuum is defined as a residual between the total absorption and the lines, there is an inextricable link between the two, and it is possible that continuum differences between models could be canceled out by a compensating choice of line parameters. In an ideal world experiment this would be the case. For example a weak continuum can be balanced by bigger line widths, or a larger or no line cutoff, which is somewhat the case for MPM89. There is a great deal of variation in the lines used in each of the studies in Table 5, with seven using a 'reduced' set (either 30 MPM or 15 PWR lines) and four using the HITRAN databases or derivatives thereof (AER). All apply a VVW lineshape apart from AER which uses a Van Vleck Huber (VVH) prefactor with a Voigt approximation, which in the low frequency limit reduces to the VVW.

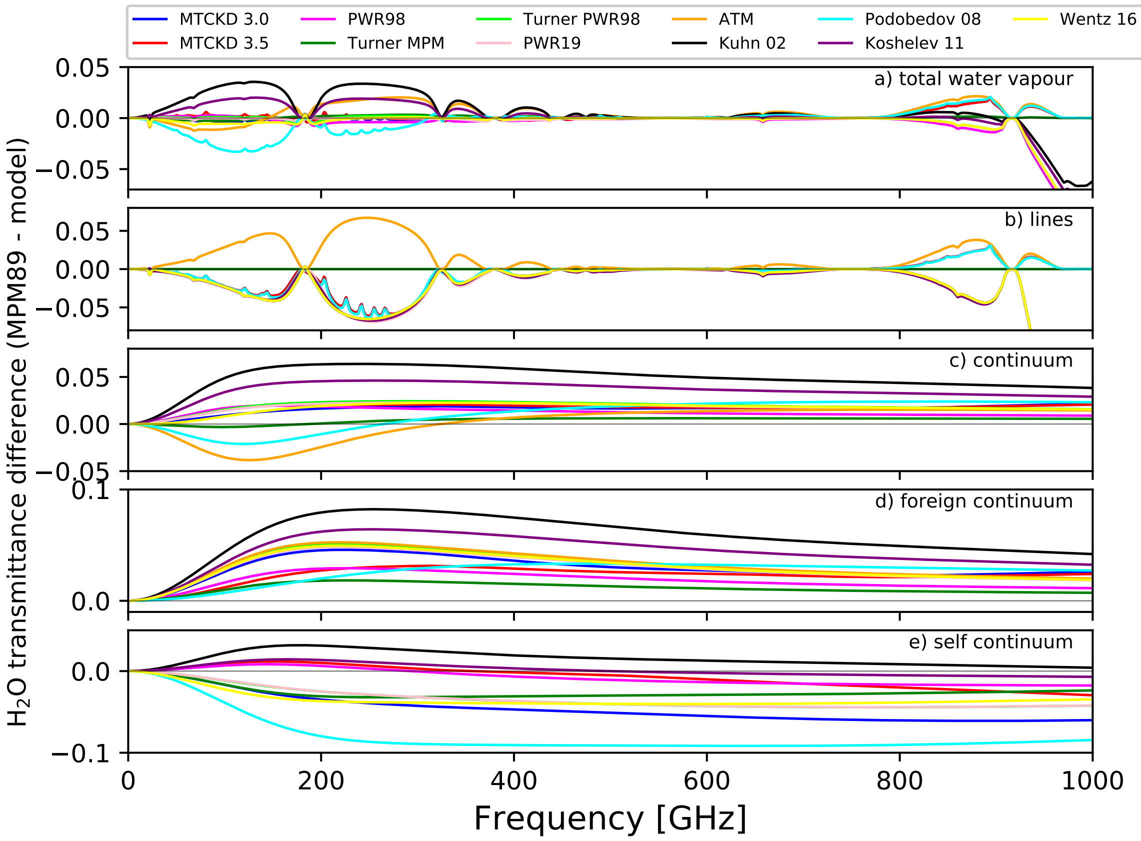

Figure 22: TOA transmittance differences between AMSUTRAN/MPM89 and other water vapour absorption models a) total water vapour, b) water vapour lines, c) water vapour continuum, d) foreign continuum and e) self continuum. The mean of 83 diverse atmospheric profiles is shown.

All models use the customary line cut-off of ~750 GHz, apart from ATM, MPM89 and the associated Turner et al. (2009). The differences in derived coefficients due to applying a line cutoff can be quite significant, and as ATM includes water vapour lines up to 4 THz the absorption from far wings could be expected to compensate for the low continuum absorption seen in Figure 21. As expected there is far less transmittance variation visible in window regions between different line databases than between those with or without a cutoff (Figure 22b). The lower transmittance from ATM lines is balanced by the higher continuum transmittance to bring the total transmittance within the range of models. In the case of Wentz and Meissner (2016), not only do the lines and continuum compensate but so do the self and the foreign continuum, to bring the overall differences with respect to MPM89 near zero (Figure 22a). In the case of Kuhn et al. (2002), however, there is a clear bias in all components.

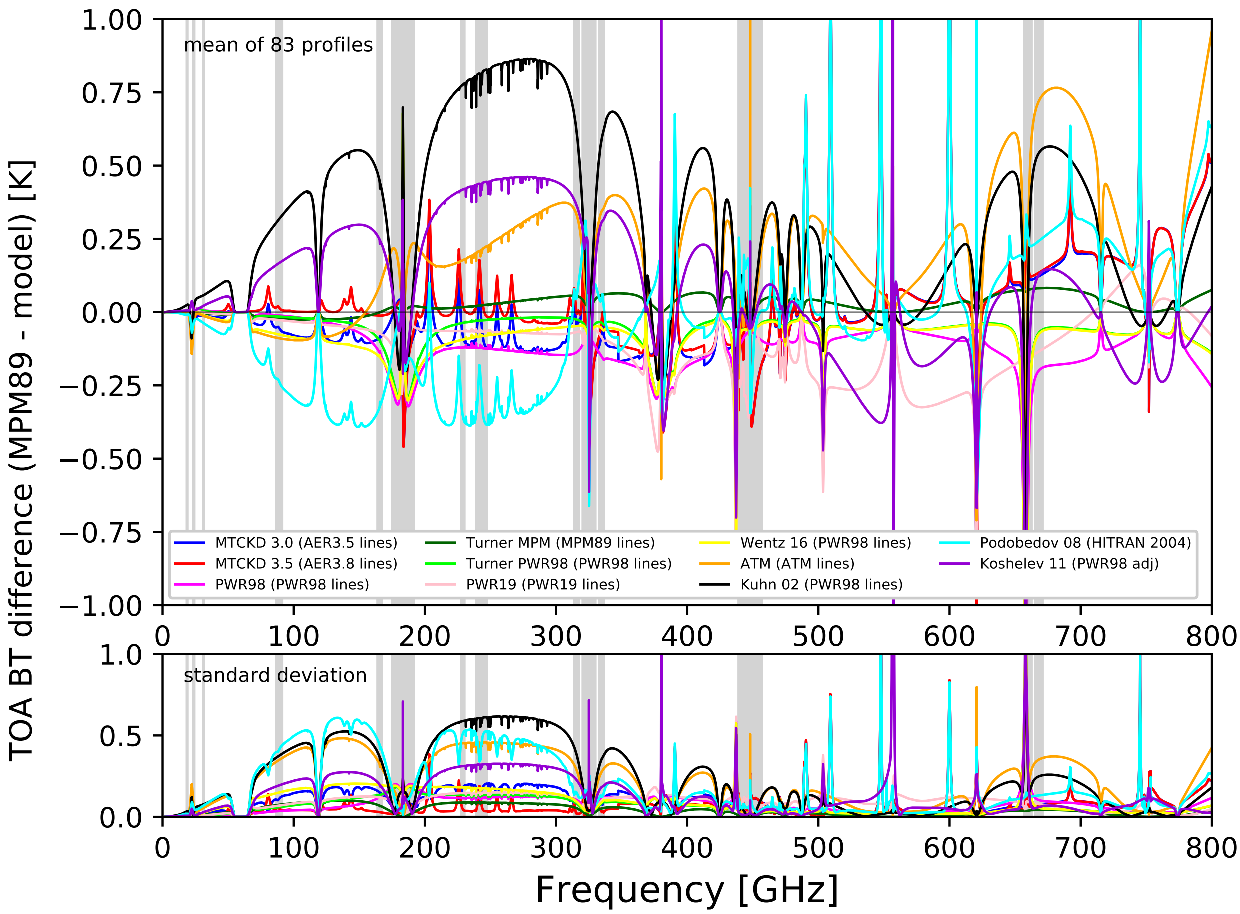

Figure 23: TOA brightness temperature differences between AMSUTRAN/MPM89 and other water vapour absorption models for the mean (upper panel) and the standard deviation (lower panel) of the 83 diverse atmospheric profile set. Simulations are at nadir with an emissivity of 1. The coverage of relevant MetOp-SG channels are shaded grey.

The range of TOA brightness temperatures is shown in Figure 23 with respect to the MPM89 model as configured in AMSUTRAN. The figure is quite complicated, but focusing on the smooth differences away from line centres which are primarily affected by the continuum (the small peaks are due to the lines omitted by the MPM89 model), differences are up to 1.25 $\pm$ 0.7 K in the 200–300 GHz partial window. However, if the four most extreme models; Kuhn et al. (2002), Koshelev et al. (2011), Pardo et al. (2001a) and Podobedov et al. (2008) are excluded, the range is only 0.2 $\pm$ 0.2 K. Differences between the two versions of MT-CKD (blue and red lines) reach 0.15 K.

Figure 23 is enhanced for MetOp-SG channels affected by water vapour; for the channels below 200 GHz

(Figure 24), and those above (Figure 25). The simulations resolution is 0.1 GHz. Channels that straddle major lines often avoid the large differences at the line centre. There are some large differences around certain Koshelev et al. (2011) line centres, where the authors applied a pressure shift based on earlier measurements that wasn't included in the original line PWR98 parameters. Maximum brightness temperature differences in each channel are listed in Table 7. The most affected are the continuum channels centred at: 165.5, 229.0, 243.2 and 664.0 GHz, though the latter difference of 1.077 K is mostly due to the absence of the 658 GHz line in ATM and PWR98 (subsequently added in PWR19), as four of the continuum models use the latter. If this line were included in the models the range would reduce to ∼0.9 K.

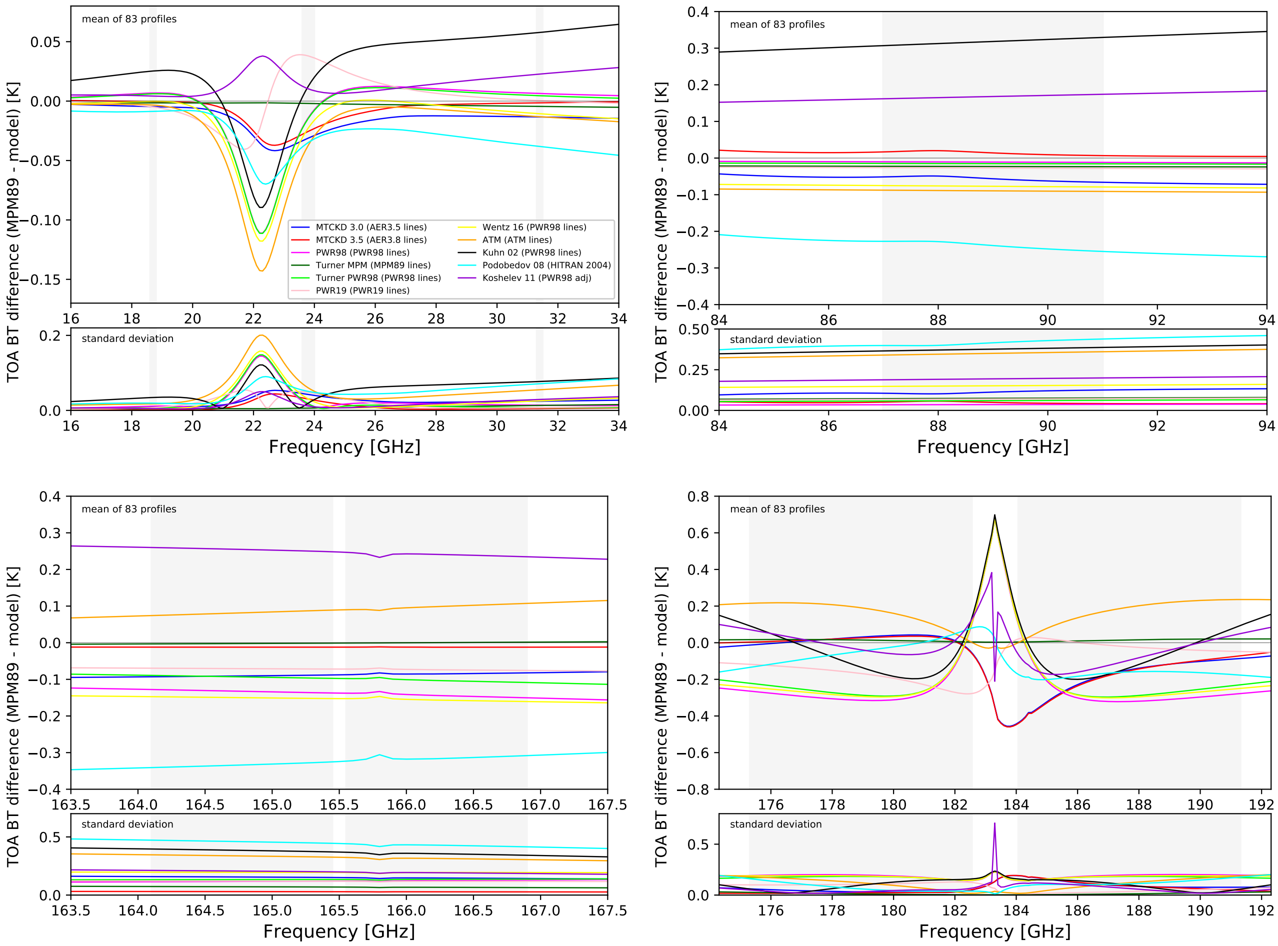

Figure 24: Figure 23 enhanced for frequencies around MetOp-SG channels below 200 GHz. Channels are shaded grey.

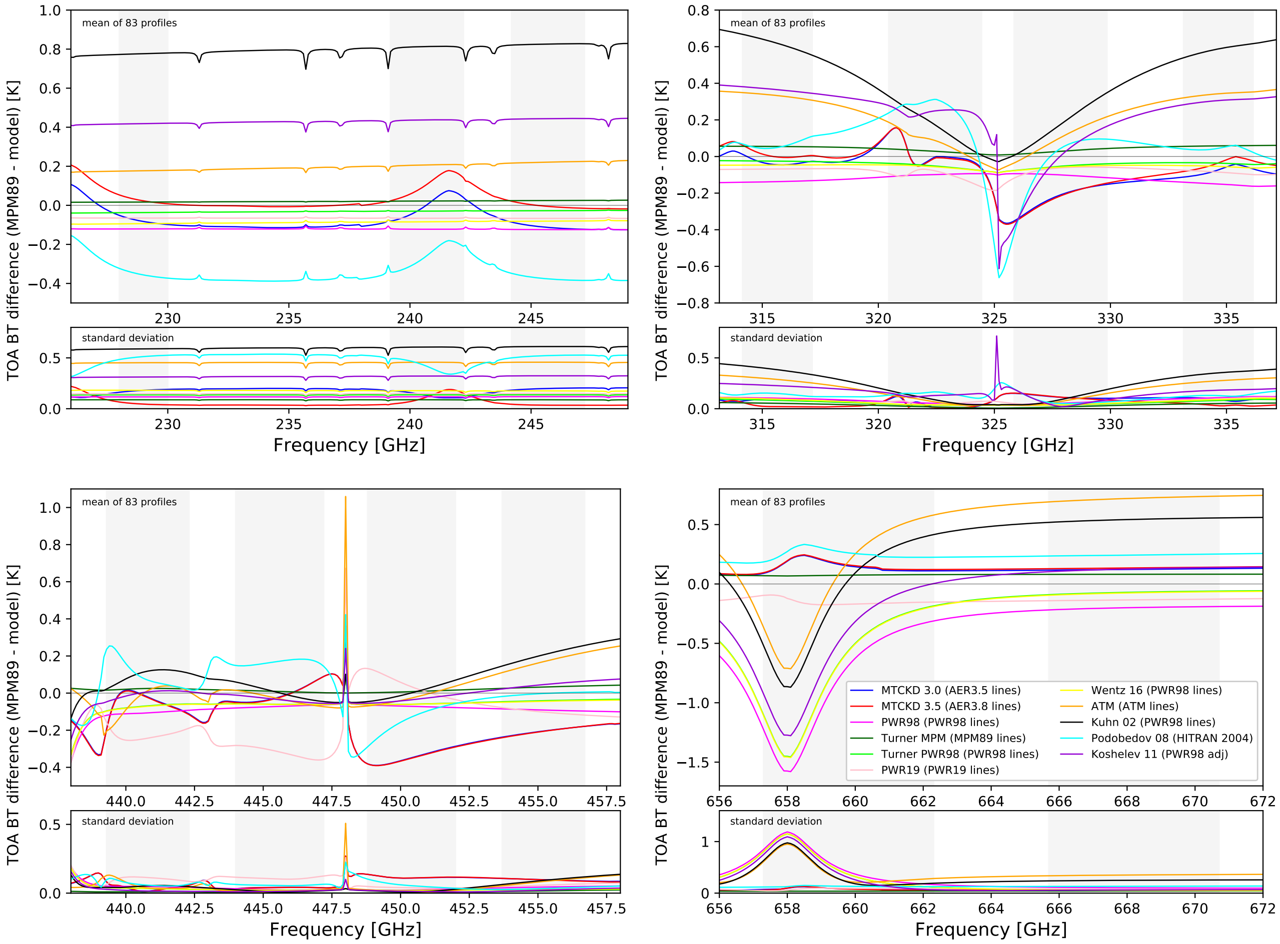

Figure 25: Figure 23 enhanced for frequencies around MetOp-SG channels above 200 GHz. Channels are shaded grey.

Table 7: Maximum TOA brightness temperature differences in MetOp-SG channels between 11 water vapour continuum models and their associated lines. Values are the mean of the maximum differences across all passbands of a channel. Simulations are calculated at nadir with an emissivity of 1.

Instrument	**Channel number**	**Centre frequency (GHz)**	**Frequency offset (GHz)**	**Bandwidth (GHz)**	**Max diff (K)**
MWI	1	18.7		0.2	0.035
MWI	2	23.8		0.4	0.079
MWS	1	23.8		0.27	0.079
MWI	3	31.4		0.2	0.097
MWS	2	31.4		0.18	0.097
MWI/MWS	8/17	89.0		4.0	0.565
MWI	13	165.5	0.75	1.35	0.806
MWS	18	165.5	0.725	1.35	0.809
MWI/MWS/ICI	14/19/1	183.31	7.0	2	0.525
MWI	15	183.31	6.1	1.5	0.532
MWI	16	183.31	4.9	1.5	0.537
MWS	20	183.31	4.5	2.0	0.542
MWI/ICI	17/2	183.31	3.4	1.5	0.568
MWS	21	183.31	3.0	1.0	0.586
MWI/ICI	18/3	183.31	2.0	1.5	0.673
MWS	22	183.31	1.8	1.0	0.692
MWS	23	183.31	1.0	0.5	0.800
MWS	24	229.0		2.0	1.190
ICI	4	243.2	2.5	3.0	1.203
ICI	5	325.15	9.5	3.0	0.763
ICI	6	325.15	3.5	2.4	0.441
ICI	7	325.15	1.5	1.6	0.412
ICI	8	448.0	7.2	3.0	0.463
ICI	9	448.0	3.0	2.0	0.723
ICI	10	448.0	1.4	1.2	0.999
ICI	11	664.0	4.2	5.0	1.077

4 Ozone

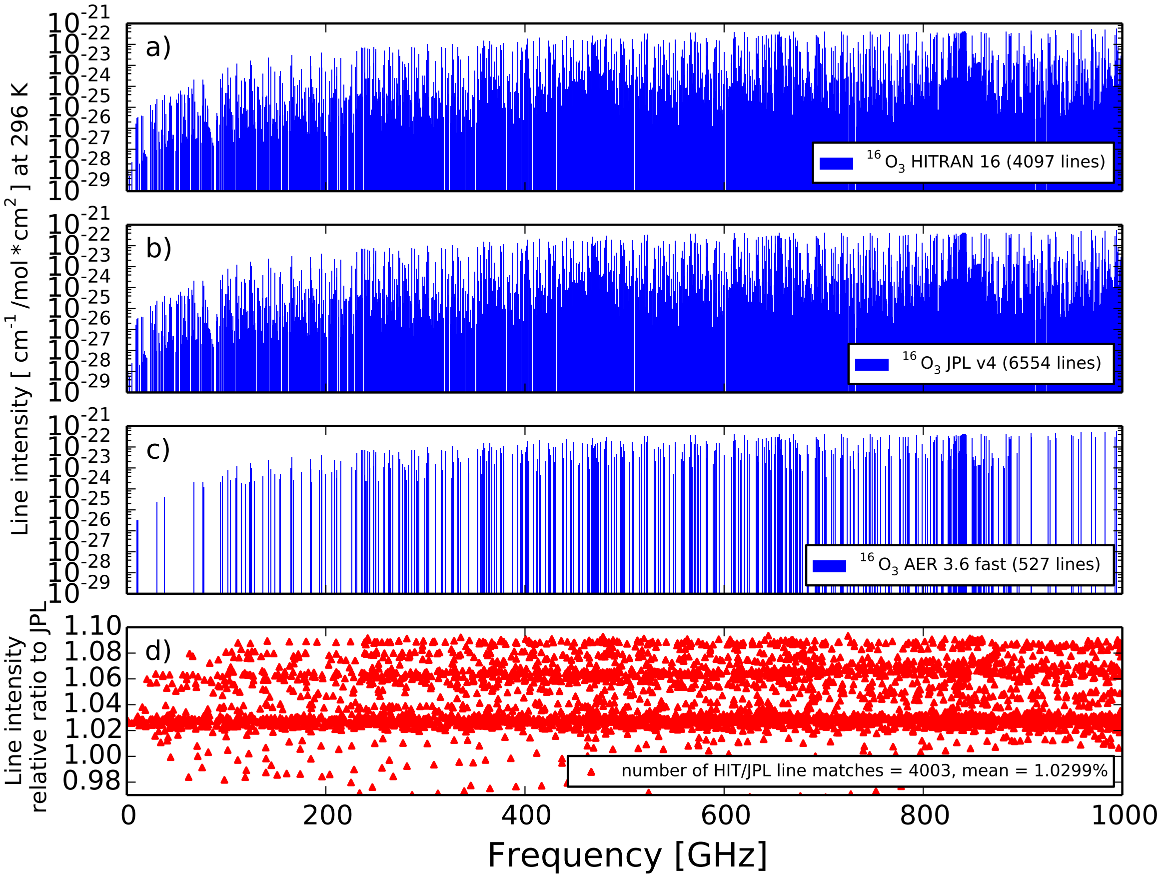

Figure 26: Line intensities for the principal isotopologue of ozone, $^{16}\mathrm{O}_3$, provided in: a) HITRAN 2016, b) JPL version 4 (converted to HITRAN units and adjusted for partition function and temperature) and c) AER 'fast' lines. d) The relative intensity difference between HITRAN 2016 and JPL intensities for corresponding lines.

Ozone is a slightly asymmetric top molecule with the dipole moment at right angles to the top axis. This makes assigning the spectra to bond lengths and angles complicated as it is based on an assumed molecular structure. It is well known for its three fundamental vibration bands in the infrared at 9.066 (ν_1), 9.597 (ν_3) and 14.27 (ν_2) microns for the $^{16}\mathrm{O}_3$ isotopologue, and ultraviolet absorption in the Harley, Huggins, Chappuis and Wulf bands (200 – $>$700 nm), which are utilised by satellite instruments to monitor ozone levels. The band of strong rotational transitions in the microwave and sub-millimetre has received less attention but it becomes more important with increasing frequency as transitions rise in intensity. Below 200 GHz the maximum impact on a satellite channel is around 0.3 K for certain 183.31 GHz channels (John and Buehler, 2004), however, greater contamination is likely at sub-mm frequencies. Ozone lines are sharp as they peak in the stratosphere so intensity is a more important parameter than those that describe broadening. There are not as many sources for ozone line parameters as for water vapour or oxygen, and it tends to be the only differences come from the different versions of HITRAN that are in circulation within LBL models.

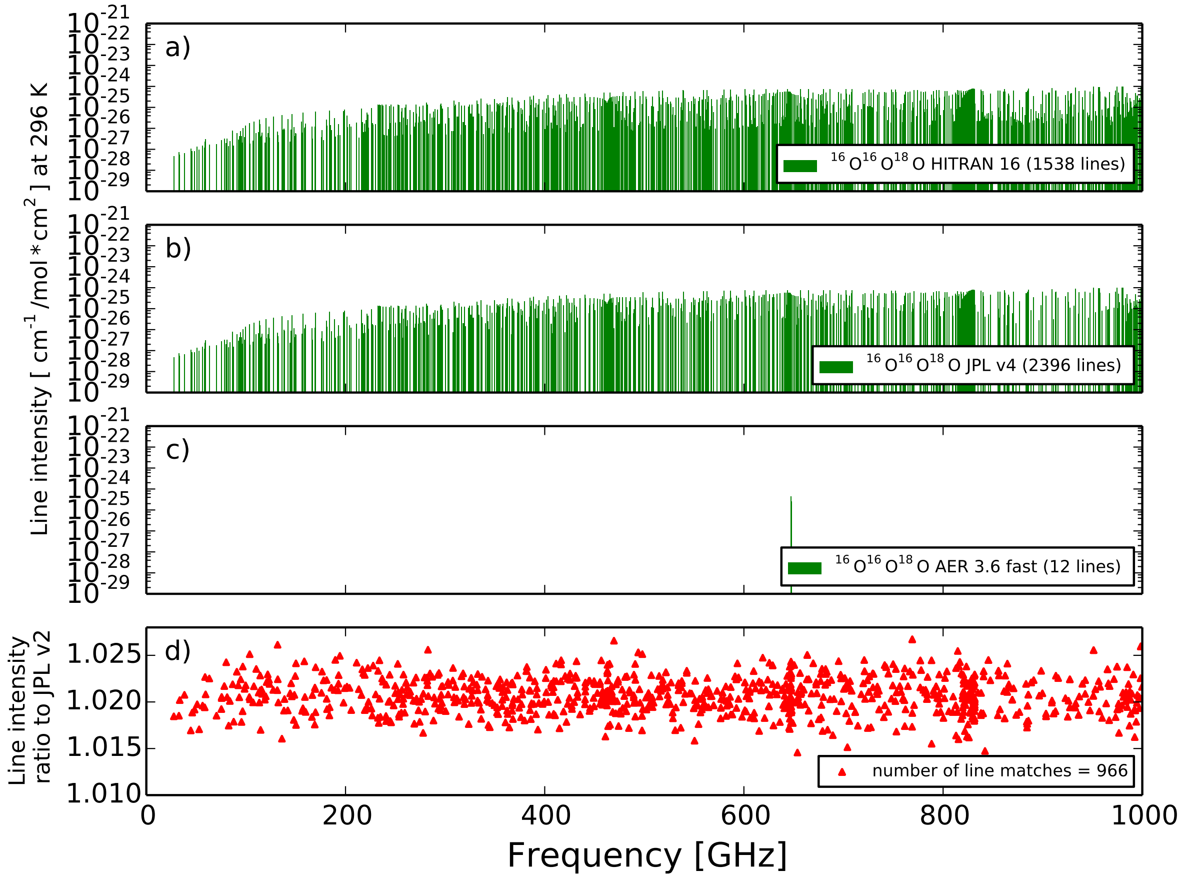

Figure 27: Line intensities for the second most abundant isotopomer of ozone ($^{16}O^{16}O^{18}O$) provided in: a) HITRAN 2016, b) JPL version 2 (converted to HITRAN units and adjusted for partition function and temperature), and c) AER 'fast' lines. d) The relative intensity difference between HITRAN 2016 and JPL intensities for corresponding lines.

4.1 HITRAN 2016

The HITRAN ozone line intensities were last modified in the microwave at the 2004 revision (Rothman et al., 2005). Values for the principal isotopologue $^{16}O_3$ (99.2901 % abundance) and both isotopomers of the second most abundent isotopologue, $^{16}O^{16}O^{18}O$ (0.3982 % abundance) and $^{16}O^{18}O^{16}O$ (0.1991 % abundance), in the earlier 1996 revision were taken from Flaud et al. (1990b) but were scaled downwards in the 2004 version by dividing values by 1.04 in line with the findings of Flaud et al. (2003). The validity of this scaling has recently been called into question by Birk et al. (2019) as the initial study centred on the infrared but the scaling was applied to all wavelengths. Intensities for the less abundant remaining isotopologue $^{16}O^{16}O^{17}O$/$^{16}O^{17}O^{16}O$ are unchanged from the values given by Pickett et al. (1998).

The majority of air-broadened half-widths (γ_{air}) for rotational ozone in HITRAN 2016 are derived, either from Flaud et al. (1990a) with polynomial expressions for J" scaled by 1.05 (2008, I.E. Gordon, private communication), or from Wagner et al. (2002) using values originally obtained for the ν_1/ν_2 or ν_3 bands. The temperature dependences of γ_{air} are either also from Wagner et al. (2002) or take the mean value of Gamache (1985). All values for self-broadened half width (γ_{self}) are based on the method of Smith (2001) described in Rothman et al. (2005) which have been subsequently modified (M.A.H. Smith, NASA Langley Research Center, private communication 2004).

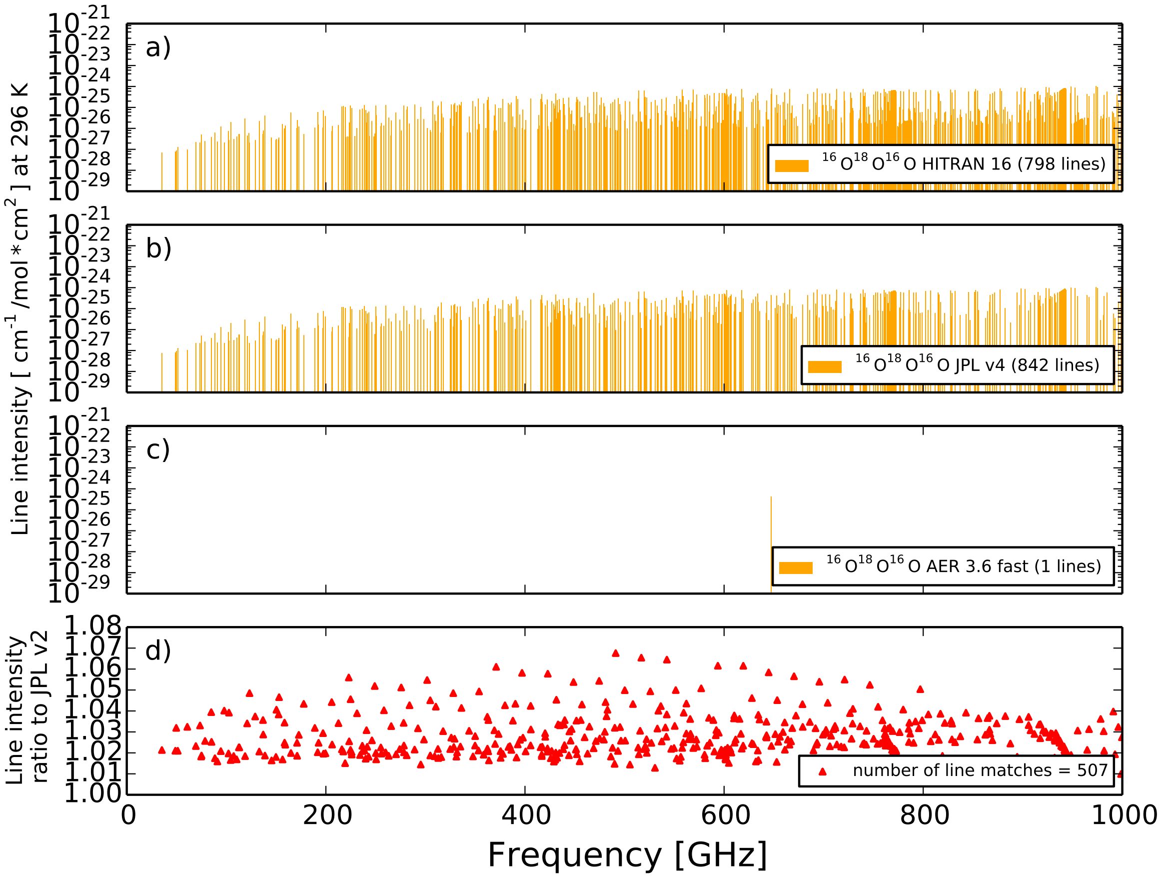

Figure 28: Line intensities for the third most abundent isotopomer of ozone ($^{16}O^{18}O^{16}O$) provided in: a) HITRAN 2016, b) JPL version 2 (converted to HITRAN units and adjusted for partition function and temperature), and c) AER 'fast' lines. d) The relative intensity difference between HITRAN 2016 and JPL intensities for corresponding lines.

4.2 JPL 2005 v4

Figure 26 shows the intensities and number of $^{16}O_3$ lines available up to 1000 GHz in HITRAN 2016, JPL version 4 and the AER 3.8 fast database, where line parameters follow those in HITRAN 2012 but are much reduced in number. Rotational $^{16}O_3$ line intensities in the Jet Propulsion Laboratory (JPL) database[a] (Pickett et al., 1998), were updated in November 2005 (JPL version 4) via the predictive calculation described in Birk et al. (2019). JPL values are converted to HITRAN units using the full temperature and partition function adjustment from Rothman and Gordon (2006). Relative ratios of HITRAN 2016 intensities to each corresponding JPL v4 line, where 4003 of the 6554 JPL lines are present in the HITRAN database, have a mean difference

[a] https://spec.jpl.nasa.gov/

of 2.99% (The thicker band at ∼1.03 in Figure 26d). The same procedure for AER lines is superfluous as its intensities are taken from HITRAN. Figure 26d essentially reproduces the HIT16 set of points in Birk et al. (2019, Figure 1) where the authors obtain an average relative difference of 4.0% which is 1% higher than the present analysis.

The value of the Total Internal Partition Sum (TIPS) used for HITRAN at 296 K is 3483.71, from Gamache et al. (2017), however, Birk et al. (2019) use a slightly different TIPS value of 3473.0 which is taken from the Spectroscopy and Molecular Properties of Ozone (S&MPO) database (Babikov et al., 2014) and deviates from the Gamache et al. (2017) value by 0.3 %. When the analysis is repeated using the S&MPO TIPS value an average relative difference of 3.3% is obtained. It is surprising that Birk et al. (2019) achieve such a precise 4.0% difference as the version 4 intensities have been modified from the original Flaud et al. (1990b) values, upon which the HITRAN pre-scaled values are based.

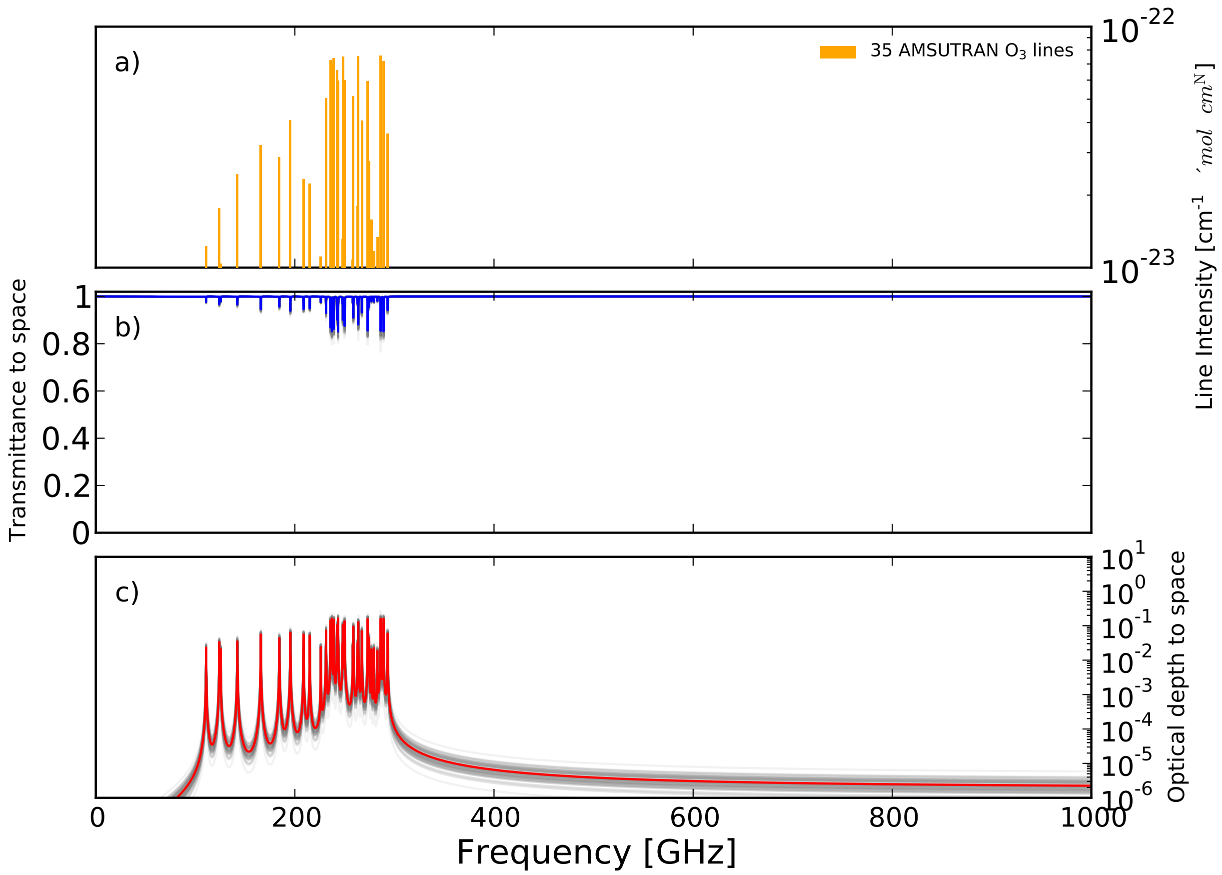

Figure 29: a) Line intensity at 296 K of the 35 ozone lines included AMSUTRAN b) Surface-to-space transmittance for 83 diverse atmospheric profiles (grey lines) and their mean (blue line) for these ozone lines only. c) Surface-to-space optical depth, for 83 diverse atmospheric profiles (grey lines) and their mean (red line) for these ozone lines only.

Figures 27 and 28 show the same information as Figure 26 but for the lesser abundant isotopomers: $^{16}\mathrm{O}^{16}\mathrm{O}^{18}\mathrm{O}$

and $^{16}O^{18}O^{16}O$. This isotopologue has a less significant contribution as line intensities do not exceed magnitudes of 10^{-25} $\mathrm{cm^{-1}/(mol\ cm^2)}$ in this region (whereas some $^{16}O_3$ lines can reach 10^{-21} $\mathrm{cm^{-1}/(mol/cm^2)}$). Only 13 lines are included in the AER 'fast' database which all centre at 647 GHz. Average relative differences between HITRAN 2016 and JPL version 2 are 2.1 % and 2.2 % respectively, using the Gamache et al. (2017) TIPS values of 7465.7 and 3647.1 which are 0.11 % and 0.13 % higher than those given in S&MPO. When the latter values are used the differences are 3.1 % and 3.5 % respectively.

4.3 Absorption models

PWR17 includes 17 ozone lines between 149–429 GHz, which were selected based on their proximity to certain satellite instruments. PWR19 increases this number to 320 between 102–799 GHz, but restricts their influence to within 1 GHz of a given frequency, as most ozone is in the stratosphere where lines are relatively narrow. The half-width calculation combines pressure and Doppler broadening and a Lorentz line shape is used. PWR17 and PWR19 take all parameter values from HITRAN 2012 and HITRAN 2016, respectively. ATM includes 1291 lines of ozone between 0.8–1987 GHz and also accounts for Doppler broadening. The rotational constants for the principle isotopologue are from Pickett 1988 and Flaud 1987, and broadening parameters are from HITRAN 2000.

AMSUTRAN includes the 35 strongest ozone lines below 300 GHz, see Figure 29, which were added to AMSUTRAN in 2005 as an option to be included with the mixed gases in response to the potential bias in 183.31 GHz channels. The line parameters are from the HITRAN 2000 catalogue (Rothman et al., 2003). Figure 31 shows the differences between these 35 lines and HITRAN 2016, so frequencies above 300 GHz display the effect of adding ozone where previously there was none. As the HITRAN 2000 lines predate the aforementioned line intensity scaling the $\sim$4% reduction is apparent between versions (31a), whereas halfwidths have mostly increased in the later HITRAN, by up to 11%, with contributions from both foreign and self-broadening components (31b). It is obvious that without ozone beyond 300 GHz, errors of up to 40 K at individual frequencies, and in particular the 664 GHz channels of ICI would be subject to significant error (31e).

4.4 JPL 2005 with broadening parameters

Clearly, the inadvertently scaled HITRAN (and subsequently AER) line intensities should not be used in their present state, but as the scaling method does not appear to be straight-forward it is not advisable to simply reverse the error by multiplying intensities by 1.04. The JPL catalogue includes a more recently derived line list with updated intensities, however, JPL does not provide broadening parameters. A line list provided directly (Iouli Gordon, Harvard & Smithsonian, personal communication, 2019) includes broadening parameters calculated following the standard HITRAN procedure from Wagner et al. (2002) with some adjustments made for J=K values. The algorithm does not cover all possible lines therefore γ_{air} = 0.07 and γ_{self} = 0.085 are introduced in these cases. 518 out of the 527 $^{16}O_3$ lines below 1000 GHz in the AER 'fast' database are present in the new line list, which accounts for 98.5% of the total sum of AER line intensities but only around 90% of HITRAN or JPL. As discussed previously, the TIPS values given in Gamache et al. (2017) could be in error,

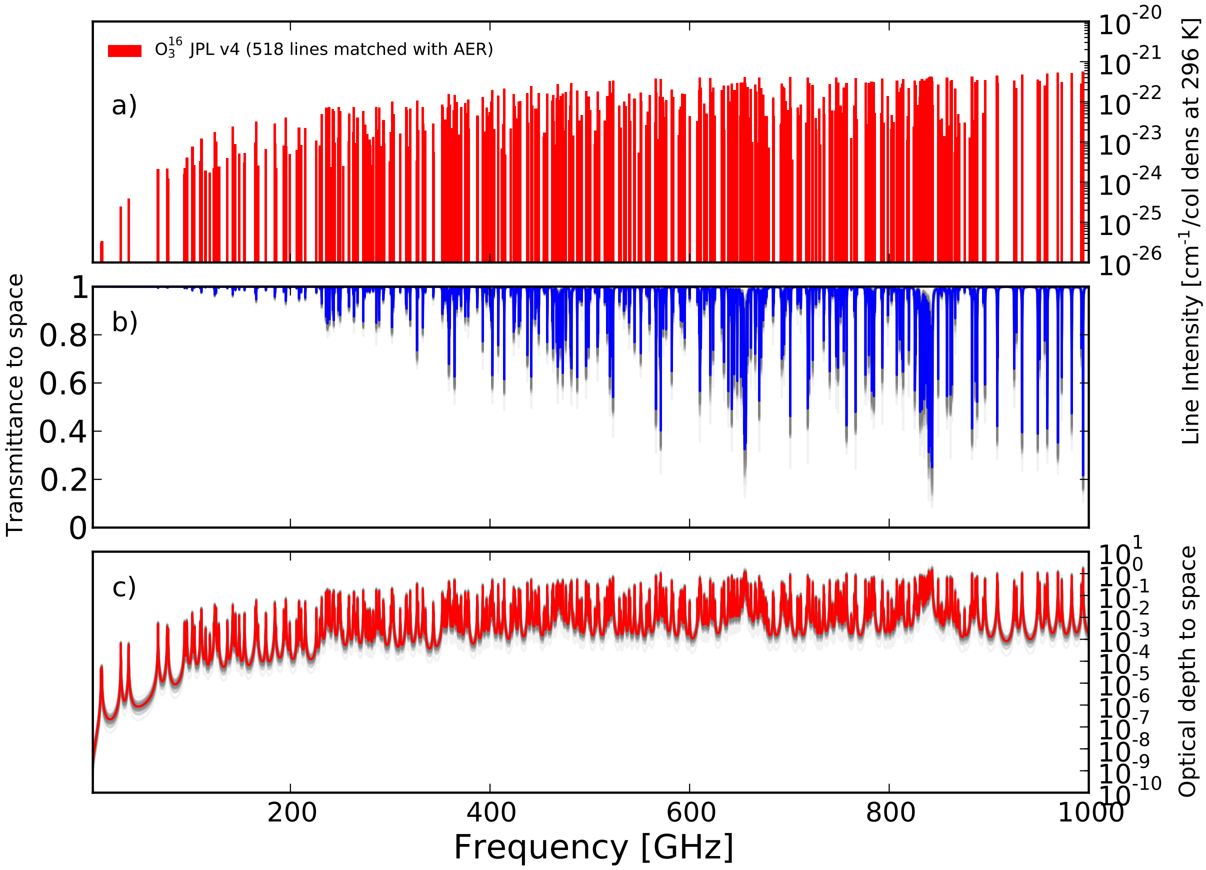

Figure 30: a) Line intensity of 518 ozone lines below 1000 GHz from JPL v4 sub-selected to those present in the AER 3.8 fast database. b) Surface-to-space transmittance and c) surface-to-space optical depth.

the S&MPO value of 3473.0 is recommended.

The resulting lines and transmittance and optical depth from this combination is shown in Figure 30. 653 lines are included in the calculation up to 1750 GHz to allow for the far wings of lines beneath the cut off threshold, however, as the half-width of ozone is so small there will be very little influence from these higher frequencies. There is also relatively little variation between profiles. The difference between this modified JPL catalogue and the original AER/HITRAN lines intensities centres at 3% (Figure 32). Brightness temperatures in ICI channels for the most part are no more than 0.2 K different apart from at 664 GHz where there is a difference of up to 2 K on the lower frequency edge of channels 12 and 13. At higher frequencies (such as around 775 GHz) differences can reach up to 4 K for certain profiles. HITRAN 2020 will include a completely updated ozone list where line intensities will be consistent from the microwave to the ultraviolet and intensely validated. Values may differ slightly to the one presented here, but the strongest lines should be the same (Iouli Gordon, Harvard & Smithsonian, personal communication, 2020)

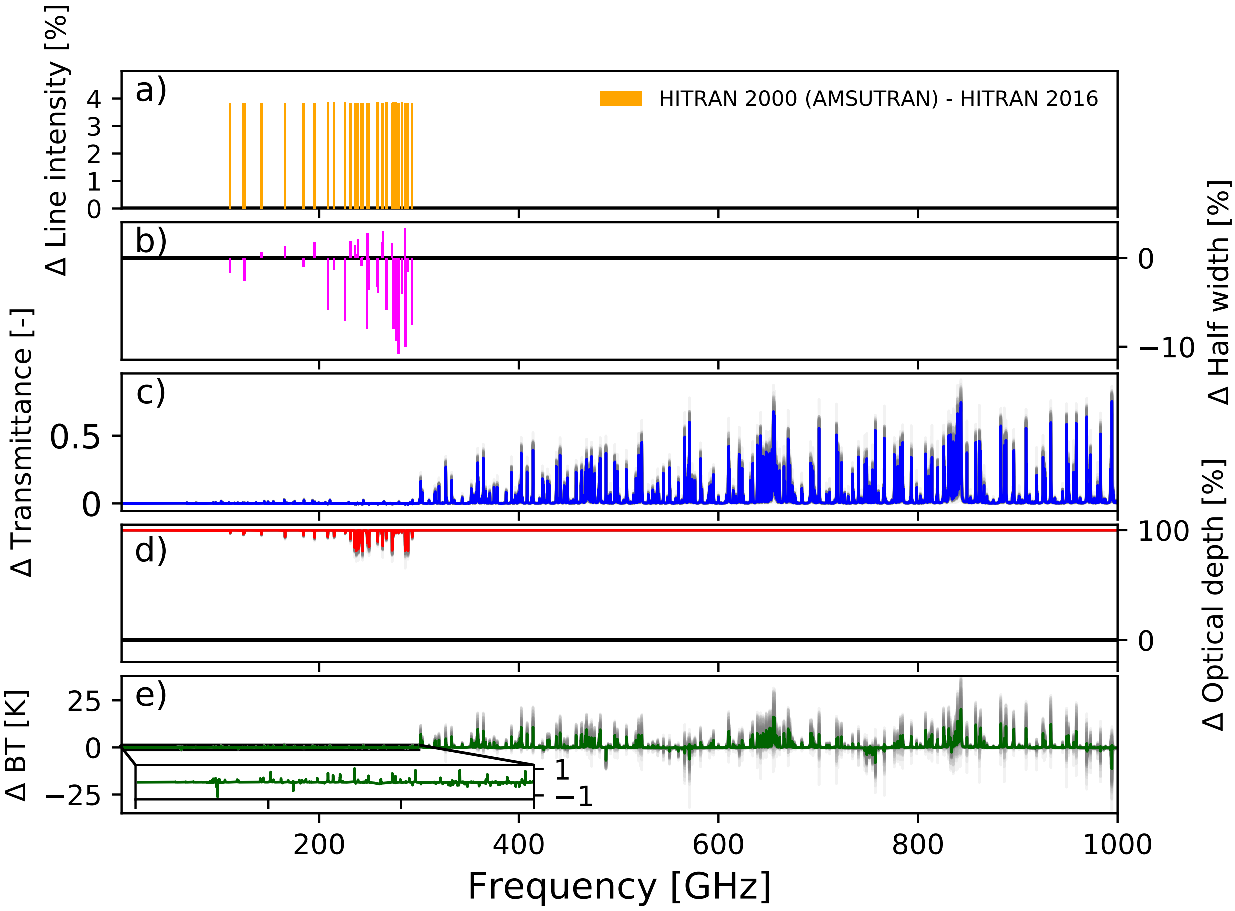

Figure 31: Ozone differences between AMSUTRAN and the HITRAN 2016 database. a) Percentage difference in line intensity at 296 K for the 35 lines included in AMSUTRAN. b) Percentage difference in total half-width. c) Ozone transmittance differences for 83 diverse atmospheric profiles (grey lines) and their mean (blue line). d) Percentage optical depth ozone differences for 83 diverse atmospheric profiles (grey lines) and their mean (red line). e) Brightness temperature differences for 83 diverse atmospheric profiles (grey lines) and their mean (green line) due to the change in ozone, zoomed in for the 0–300 GHz range.

4.5 Ozone lines summary

- Ozone should be included at sub-mm wavelengths due to the increasing intensity of line transitions, which is a more important parameter than broadening due to their sharp peaking in the stratosphere. Omission leads to monochromatic differences of up to 40 K at high frequencies.
- Ozone intensities at all wavelengths up to the infrared were scaled down by 4 % in HITRAN 2004 and have not been modified since. The justification for the scaling has recently been called into question for the microwave/sub-mm region by Birk et al. (2019).
- The present analysis shows a mean difference of around 3%, rather than the expected 4%, between JPL and HITRAN/AER line intensities for the principle isotopologue $^{16}O_3$.
- The Gamache et al. (2017) TIPS value for $^{16}O_3$ at 296 K, which is used by HITRAN is also thought to be in error and it is recommended to preferentially use the one provided in the S&MPO database.

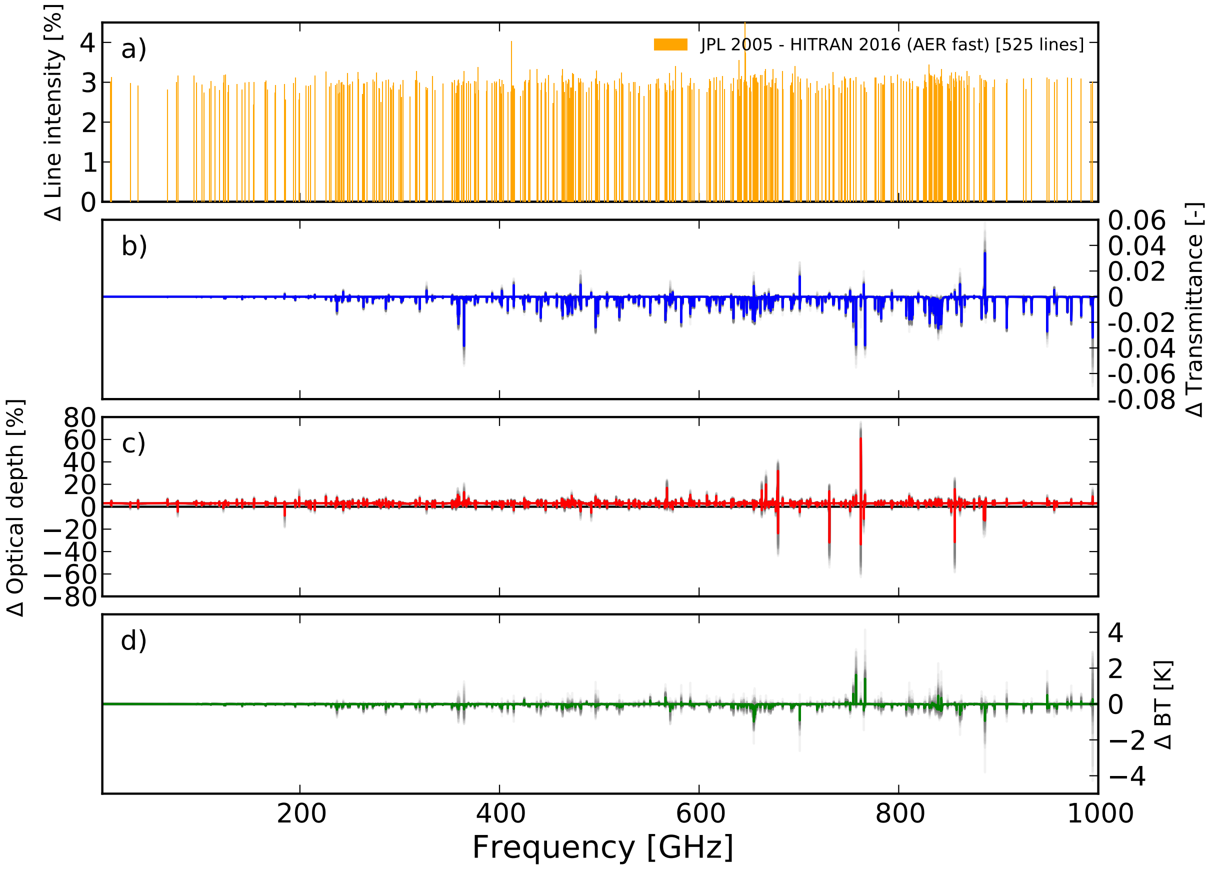

Figure 32: Differences between the AER 3.5 'fast' configuration of $^{16}O_3$ ozone lines and those from JPL 2005 version 4 database for corresponding lines. a) Percentage difference in line intensity. b) Difference in transmittance for 83 diverse atmospheric profiles (grey lines) and their mean (blue line) due to ozone only. c) Percentage optical depth differences for 83 diverse atmospheric profiles (grey lines) and their mean (red line) for ozone only; d) TOA brightness temperature differences for 83 diverse atmospheric profiles (grey lines) and their mean (green line).

- A new ozone line list based on 'correct' 2005 JPL values and subsetted for the AER 'fast' database has been created in the course of this work and is recommended for use. This list will be available in the HITRAN 2020 database with minor alterations.
- Differences between this new list and the un-modified AER lines can reach up to 4 K at high frequencies, but in general no more than 0.2 K in ICI channels.

5 Oxygen

The 60-GHz oxygen band between 50 and 70 GHz is of vital importance for temperature sounding by microwave satellite instruments due to the stratification of line intensities which provides information on the vertical temperature profile. The band comprises a series of a few tens of observable fine structure transitions between sublevels (typically 37 are used in models) caused by the splitting of the rotational levels with rotational angular momentum N, through interaction with the electronic spin of the molecule. One transition originating from the lowest energy level sits outside the band at 118.75 GHz. The first rotational transition doesn't occur until above 368 GHz. The transitions are weak yet the abundance of oxygen is large yielding absorption comparable in size to that of water vapour. The close proximity of the lines in the 60-GHz complex give rise to non-negligible line mixing (overlap interference), which affects absorption to the extent that each line cannot be modelled as if it were isolated. Parameters for the sub-millimetre rotational lines can be found in Golubiatnikov and Krupnov (2003) and more recently Drouin et al. (2010).

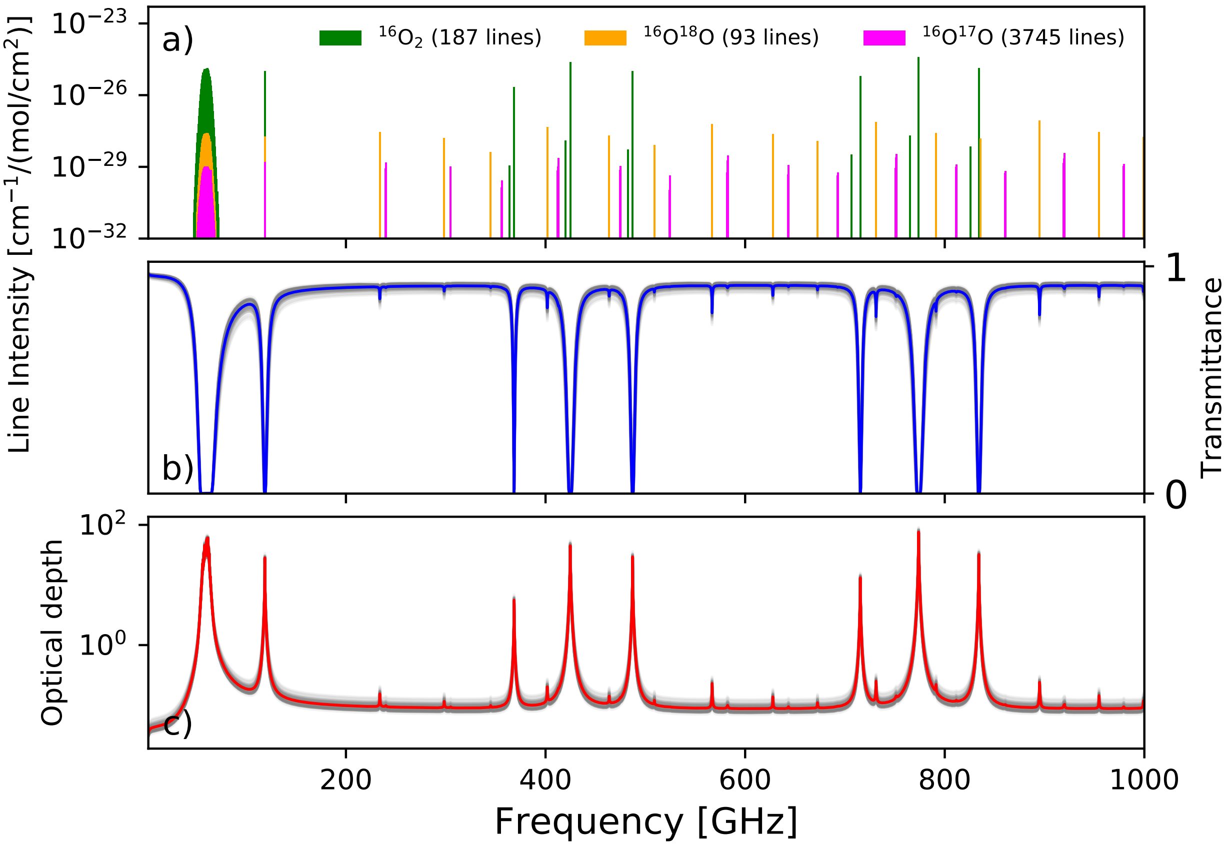

Figure 33: Line intensity at 296 K of the 4025 oxygen lines in HITRAN 2016 below 1000 GHz. b) Surface-to-space transmittance and c) surface-to-space optical depth, for 83 diverse atmospheric profiles (grey lines) and their mean (bold line) for oxygen lines only, with no line mixing.

5.1 HITRAN 2016

Figure 33a shows the position and intensities of 4025 O_2 lines available in the HITRAN 2016 line catalogue below 1000 GHz for the first three isotopologues of oxygen, 93% of which are from the least abundant $^{16}O^{17}O$ molecule. The intensities and half-widths are calculated by a semi-empirical model described in Mackie et al. (2011, not published) and were last updated in the HITRAN 2012 revision (Rothman et al., 2013). Line positions were updated in the HITRAN 2016 revision from Yu et al. (2014) using a 'Dunham fit' method with new observations. Based on measurements from Drouin (2007), temperature dependencies for the air-broadened half-widths are set to one of three values, 0.97, 0.86 or 0.72 depending on the lines value of N. Line mixing coefficients are not explicitly provided in the HITRAN database for this region (though mixing effects are incorporated in the derivation of line width parameters for the oxygen A-band around 762 nm).

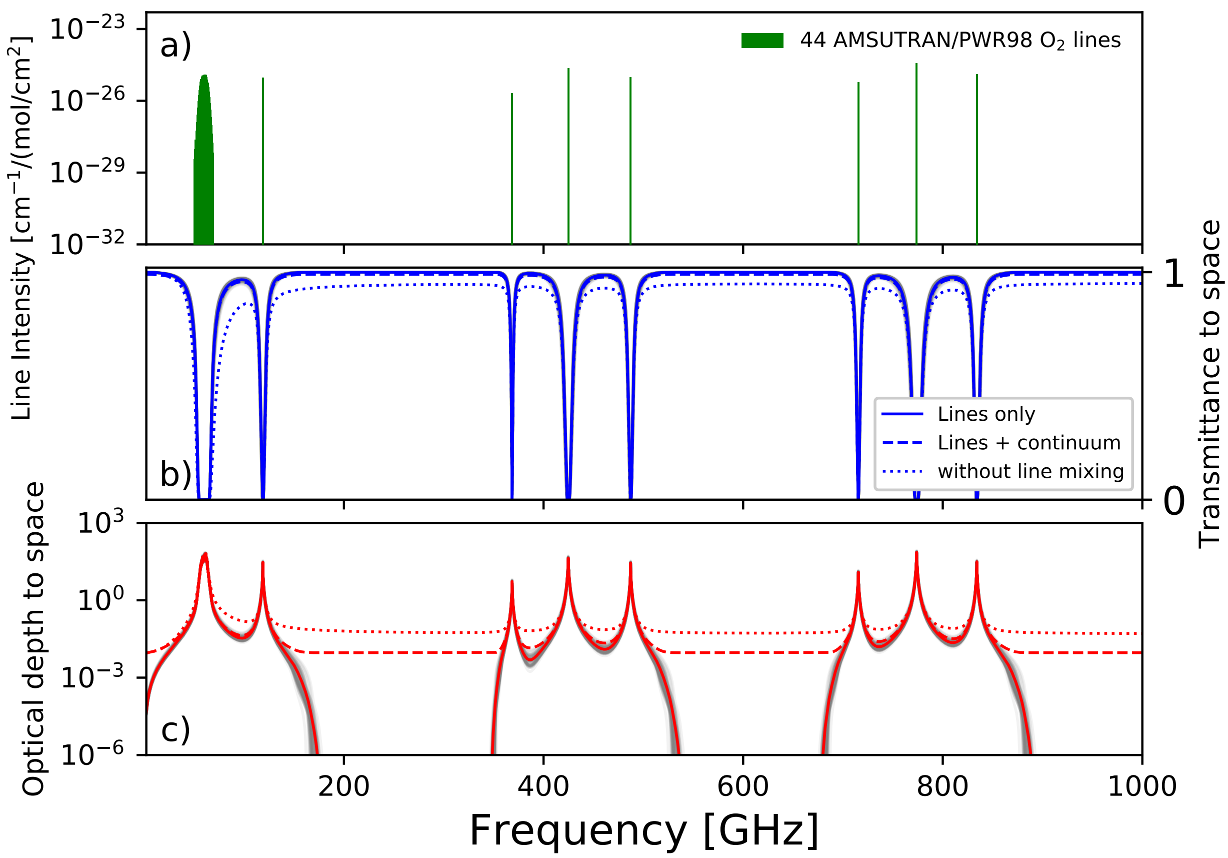

Figure 34: a)Line intensities at 296 K for the 44 oxygen lines in AMSUTRAN. b) Surface-to-space transmittance and c) surface-to-space optical depth, for 83 diverse atmospheric profiles (grey lines) and their mean (bold line) for oxygen lines only, for oxygen lines and the oxygen continuum (dashed line) and both without the line mixing parameterisation (dotted line).

5.2 Absorption models

The MPM92 model (Liebe et al., 1992) supersedes MPM89 for oxygen as it incorporates new improved laboratory measurements. The same parameters are included in PWR98 and reported in Rosenkranz (1993), but use a slightly different parameterisation. The MPM models include six of the higher frequency rotational lines as well as the aforementioned 38 fine structure lines. PWR17 and PWR19 contain 11 rotational lines below 1000 GHz and ATM includes six below and 31 above. The positions and strengths of the lines included in AMSUTRAN are shown in Figure 34a.

The broadening of oxygen lines can be described by an air component and a water vapour component, where the latter is sometimes incorporated via a scaling factor, r_{w2a}, applied to the air half-width and is assumed to have no temperature dependence. The total half-width is thus given by:

$$\gamma_{O_2} = \gamma_{air}(p_{dry}\theta^{n_{air}} + r_{w2a}p_{wv}\theta) \tag{10}$$

Line mixing is included as a modification to the original VVW lineshape via the pressure induced interference, δ_i, which in Equation 5 is a first-order function of pressure. In its simplest form it is equal to:

$$\delta_i = y_i p \theta^{n_{air}} \tag{11}$$

but the pressure term may include other effects such as the water vapour contribution (the term in parentheses in Equation 10), which is the case in PWR17 and PWR19. y_i may be a function of temperature and in the MPM formulation it is defined as:

$$y_i = (a_5 + a_6\theta) \tag{12}$$

where a_5 and a_6 are coefficients specified for each line.

Many models also include a parameterisation for non-resonant oxygen absorption, which arises from the relaxation (Debye) spectrum of the magnetic moment of oxygen below 10 GHz. The effect of the Liebe et al. (1992) oxygen continuum is shown in Figure 34c (dashed line).

5.3 Line mixing

At the centre of the 60-GHz band line mixing acts to increase absorption between 56 and 63 GHz, which has little to no effect on the transmittance as it is already at zero (Figure 34b). It does, however, have a noticeable effect at higher frequencies, where transmittances are increased in the line wings by around 0.05 (5%) which can perpetuate all the way up to 1000 GHz, a far larger difference than the spread due to the different atmospheric profiles (grey lines). It is interesting that parameters associated with a localised band of lines spanning 20 GHz at 60 GHz can have such a far reaching influence that acts to decrease absorption and strictly speaking models should apply a line cutoff, but this is often not done because the effects are not significant. It should be noted that the line mixing parameterisation is empirically derived and so there is a certain amount of uncertainty in its formulation. It has also been shown in Tretyakov et al. (2005) that experimental values in this band systematically deviated from the first order predictions derived. The latter formulation is such that values of negative absorption are possible, which the MPM configuration resets to zero, as can be seen in the zero optical depth regions between the three bands of oxygen lines in Figure 34c. A subsequent study by Makarov et al. (2011) developed the MPM line mixing approach to a second order function of pressure which the authors found to reduce residual errors from observations to within 2% or less within the 60 GHz band, however its performance at higher frequencies is unknown. The extended line-shape in this case takes the form:

$$F(\nu) = \frac{\nu}{\nu_i}\left[\frac{\gamma_i(1+g_iP^2)+\delta_i(\nu-\nu_i-\delta\nu_iP^2)}{(\nu-\nu_i-\delta\nu_iP^2)^2+\gamma_i^2} + \frac{\gamma_i(1+g_iP^2)-\delta_i(\nu+\nu_i+\delta\nu_iP^2)}{(\nu+\nu_i+\delta\nu_iP^2)^2+\gamma_i^2}\right] \quad (13)$$

where g_i and $\delta\nu_i$ are second order mixing coefficients. g_i is associated with a correction to line intensities and $\delta\nu_i$ is associated with a correction to line central frequencies. Later analysis revealed minor systematic overestimation of the absorption in the far wings of the band due to experimental errors, so the parameters were updated using corrected methods in Makarov et al. (2020). More recent studies derive a more general (non-perturbative) method for calculating the mixing using the Energy Corrected Sudden (ECS) model Makarov et al. (2013, 2018, 2020). The PWR19 model includes second order mixing with parameters from Makarov et al. (2018).

5.4 118.75 GHz (N = 1-)

The inclusion of four channels on MWI surrounding 118.75 GHz with various offsets between 1.2 and 3.2 GHz prompts a special focus on this line that is rarely used in satellite remote sensing. The lower sub level of the $N = 1$ rotational state results in this strong fine structure line outside of the 60-GHz band. It is relatively isolated which in principle makes it easier to measure, compared to the 60-GHz complex, however it is still subject to line mixing from the former. Though the advantages have been discussed for some time (Croom, 1971), only recently are satellite instruments beginning to make use of it. The 118.75 GHz literature is reviewed here for line intensity and broadening parameters applicable to a VVW line-shape, omitting those related to line mixing. Rosenkranz and Cimini (2019) tentatively estimate that the TOA brightness temperature differences between using the VVW and speed dependent line-shape to be between 0.05 K at the line centre, and up to 0.15–0.2 K around ± 2 GHz, using MWI geometry and laboratory measurements of speed dependent parameters from Koshelev et al. (2017).

118.75 GHz line intensity

Figure 35 shows line intensities from various sources. One of the earliest studies by Gamache et al. (1998) yielded a value of 0.9956e^{-26} cm^{-1}/(molecules/cm^2), which was included in the HITRAN 2004 catalogue and was also used in the broadening study of fine structure lines by Tretyakov et al. (2005). Both AMUSTRAN and AER model have adopted these parameters, however there are slight differences in value due to the former using supplementary parameters derived specifically to fit the MPM parameterisation, however they should both be the same. The updated measurements of Tretyakov et al. (2007) produce a line intensity of 0.973e^{-26} cm^{-1}/(molecules/cm^2) with a wide 3% uncertainty, from the fit to different temperatures. The authors explain the 2% reduction relative to the HITRAN 2004 value by the 98% declared purity of the oxygen sample used in

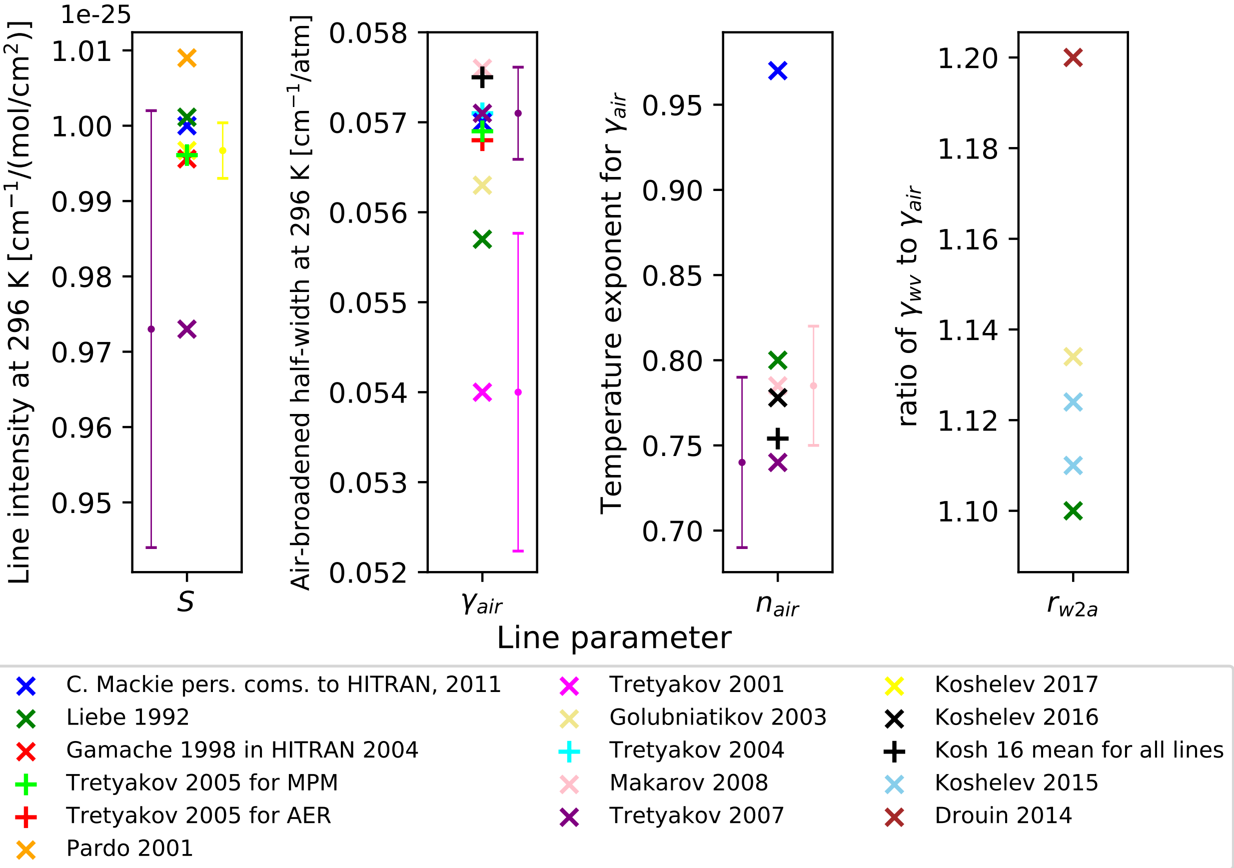

Figure 35: Comparison of line intensity, air-broadened half-width, temperature exponent and ratio of water to air broadening parameters across different studies for the 118.75 GHz line. Error bars show quoted uncertainties on the adjacent values where provided.

their resonator spectrometer, however, this result appears low compared to other values. HITRAN has included a line intensity of 1.000e^{-25} cm^{-1}/(molecules/cm^2) since the 2012 release, which is based on the global absorption model of C. Mackie, though there is no reference available.

Koshelev et al. (2017) uses a RAD spectrometer for low pressures and resonator spectrometer for high pressures to measure the speed dependence of the 118.75 GHz line, however, the study reports that accurate measurements of the line intensity is only possible with the latter. The intensity, recalculated to 296 K, is estimated to be 0.9967e^{-26} cm^{-1}/(molecules/cm^2), from the mean value presented in Koshelev et al. (2017, Figure 8.). The total uncertainty calculated from all sources is 0.37%. The total spread of values is around 3.6%, reducing to 1.3% when the low Tretyakov et al. (2007) value is omitted, and less than 1% when the higher Pardo et al. (2001a) is removed.

118.75 GHz air-broadened half-width

The MPM92 half-width is equivalent to 0.0557 cm-1/atm, which is included in the ATM model. The first direct measurement of the 118.75 GHz line broadening parameters in a laboratory using atmospheric air was by Tretyakov et al. (2001), who obtained a half-width of 0.0540 cm-1/atm with a 3% fitting error, the lowest value considered here. Following this Golubiatnikov et al. (2003) used a RAD spectrometer to measure the broadening of multiple molecules, resulting in a value of 0.0563 cm-1/atm for dry air. The subsequent work by Tretyakov et al. (2004) further increased it to 0.0571 cm-1/atm, which was also the value of the parameter obtain by Tretyakov et al. (2007) to 3 significant figures. The intermittent study by Tretyakov et al. (2005), which is widely used (e.g. by AER and AMSUTRAN) as it also cover the 60 GHz lines, uses the same values for 118.75 GHz as Tretyakov et al. (2004). However, through reprocessing and conversion of units some precision is lost, and 0.0568 cm-1/atm and 0.0569cm -1/atm end up in the AER database, and AMSUTRAN, respectively.

Table 8: Spectroscopic parameters of the 118.75 GHz line from databases and LBL models. Where applicable, values of line intensity (S) and half-width (γ_{air}) have been adjusted from their reference temperature of 300 K to 296 K for consistency. Sources for the data are given in the footnotes.

Parameter	ν	S	γ_{air}	n_{air}	$\mathbf{r}_{w2a}$	n_{self}	δ_{air}
$units$	GHz	$\frac{cm^{-1}}{molecules \times cm^2}$	$\frac{cm^{-1}}{atm}$	-	-	-	$\frac{cm^{-1}}{atm}$
118.75 GHz							
HITRAN 2016	118.750341[a]	1.000e-25[b]	0.0570[c]	0.97[d]	-	-	-
HITRAN 2012	118.750341	1.000e-25[b]	0.0570[c]	0.97[d]	-	-	-
GEISA 2019	118.750341[a]	1.000e-25[b]	0.0570[c]	0.97[d]	-	-	-
AER 3.8	118.750341[a]	9.956e-26[e*]	0.0568[f]	0.80[g]	-	-	-
MPM92/PWR93	118.7503	1.001e-25	0.0557	0.80	1.1	-	-
AMSUTRAN	118.750336	9.961e-26[h*]	0.0569[i]	0.80[g]	1.1	-	-
ATM	118.750343	1.009e-25[j]	0.0557[g]	0.80[g]	1.1[g]	-	-
PWR17	118.7503	9.692e-26[k*]	0.0575[l]	0.80	1.2	-	-
PWR19	118.7503	9.692e-26[k*]	0.0575[l]	0.754[m]	1.2	-	-

[*] All of these line intensities report to originate from HITRAN 2004 (Gamache et al., 1998) but convert to different values. Only AER 3.8 is directly from the database.

Shortly after, Makarov et al. (2008) used improved experimental apparatus to yield 0.0576 cm -1/atm; the highest result considered here. Years later Koshelev et al. (2016) repeated the experiment at pressures 300 times lower, made possible by more accurate equipment, and obtained the exact same result for the 118.75 GHz line indicating that possible systematic errors are minimised. This value was incorporated into the PWR17 and PWR19 models. A value of 0.0570 cm-1/atm is included in HITRAN 2016, 2012 and GEISA 2019 (C. Mackie, Global intensity model, private communication to HITRAN, 2011).

[a] Yu et al. (2014) [b] C. Mackie, Global intensity model, private communication (2011) [c] C. Mackie, Semi-empirical model for ΔN=0 transitions within ground electronic state, private communication (2011) [d] X$^3\sum_g^-$–X$^3\sum_g^-$ transitions with N'=1 were given a temperature-dependence of 0.97 Drouin (2007) [e] Gamache et al. (1998) in HITRAN 2004 [f] Tretyakov et al. (2005) reprocessing of Tretyakov et al. (2004) [g] Liebe et al. (1992) [h] Tretyakov et al. (2005) conversion of Gamache et al. (1998) in HITRAN 2004 to MPM coefficients [i] Tretyakov et al. (2005) conversion of Tretyakov et al. (2004) to MPM coefficients [j] Pardo et al. (2001a) [k] Rothman et al. (2005) [l] Koshelev et al. (2016) [m] Koshelev et al. (2016) mean value over all fine structure lines

These 11 studies give half-widths with a range of 6.4%, however, if the three earlier studies are removed, as Figure 35 suggests they are outside the main cluster, the remaining values are within 1.4% of each other. Going even further, if the two highest values are also omitted, the remaining six are within 0.5 % of each other and this strongly suggests the true half-width lies in the vicinity of 0.057 cm^{-1}/atm.

118.75 GHz temperature dependence of half-width

Two consecutive experiments by Tretyakov et al. (2007) and Makarov et al. (2008), where the second made a significant update to the apparatus with a climate chamber providing accurate temperatures between 243–333 K, produced temperature exponent values of 0.74 and 0.785, respectively. The uncertainties quoted overlap each other. More recently, Koshelev et al. (2016) determine a new value of 0.778 using a RAD spectrometer, which is very close to previous Makarov et al. (2008) result. PWR19 incorporates a value of 0.754 from the same study, which is the mean value in order to apply to all the oxygen fine structure lines. The small range of these three results suggests that the value of 0.97 used in HITRAN 2016, 2012 and GEISA 2019, which is based on measurements from (Drouin, 2007) and is the same number given to all N'=1 transitions in HITRAN (Drouin, 2007), is too high. On the other hand, the value of 0.8 from Liebe et al. (1992), which is applied to all fine structure transitions and is used by five models in Table 8, may only be slightly over-estimated.

118.75 GHz water to air broadening ratio

MPM and ATM models include a ratio of 1.1 from the Liebe et al. (1992) parameterisation, whereas the later PWR17 and PWR19 models update this to 1.2 based on the results presented in (Drouin et al., 2014). The line databases do not specify a value of broadening by water vapour. Golubiatnikov et al. (2003) calculate half-widths for water vapour and air that correspond to a ratio of 1.134. Koshelev et al. (2015) derive a value of 0.0639 cm-1/atm for the pressure broadening of the line by water vapour (incidentally this is the same as the one calculated by Golubiatnikov et al. (2003)), which when converted to a ratio using either the air broadened half-width from Tretyakov et al. (2005), or Koshelev et al. (2016), gives 1.124, or 1.110, respectively.

5.5 Zeeman effect

In addition to the overlapping effects of oxygen lines at low altitudes due to pressure broadening, at high altitudes its behavior is further complicated due to Doppler broadening and the splitting of oxygen lines into several smaller ones by the Zeeman effect in the presence of a geomagnetic field (Zeeman, 1896). One of the consequences of this is that the line has a wider range of influence than if it were not split. For RTTOV, a separate version of AMSUTRAN has been developed to include the complex nature of Zeeman splitting for existing satellite instruments with high peaking channels in the 60-GHz band, i.e. SSMIS, AMSU-A and ATMS. This version of AMSUTRAN applies the widely-used coherency matrix method of Lenoir (1967), which treats oxygen as a 'Hund case (b)' molecule, and follows the Rosenkranz and Staelin (1988) formulation of the line-by-line model developed by Rosenkranz to incorporate both Doppler broadening and Zeeman splitting into the spectral calculation.

Figure 36 shows an example of the Zeeman split transmittances calculated by AMSUTRAN for various satellite viewing geometries. In general the extent of the perturbation does not exceed 2 MHz from the line centre, yet

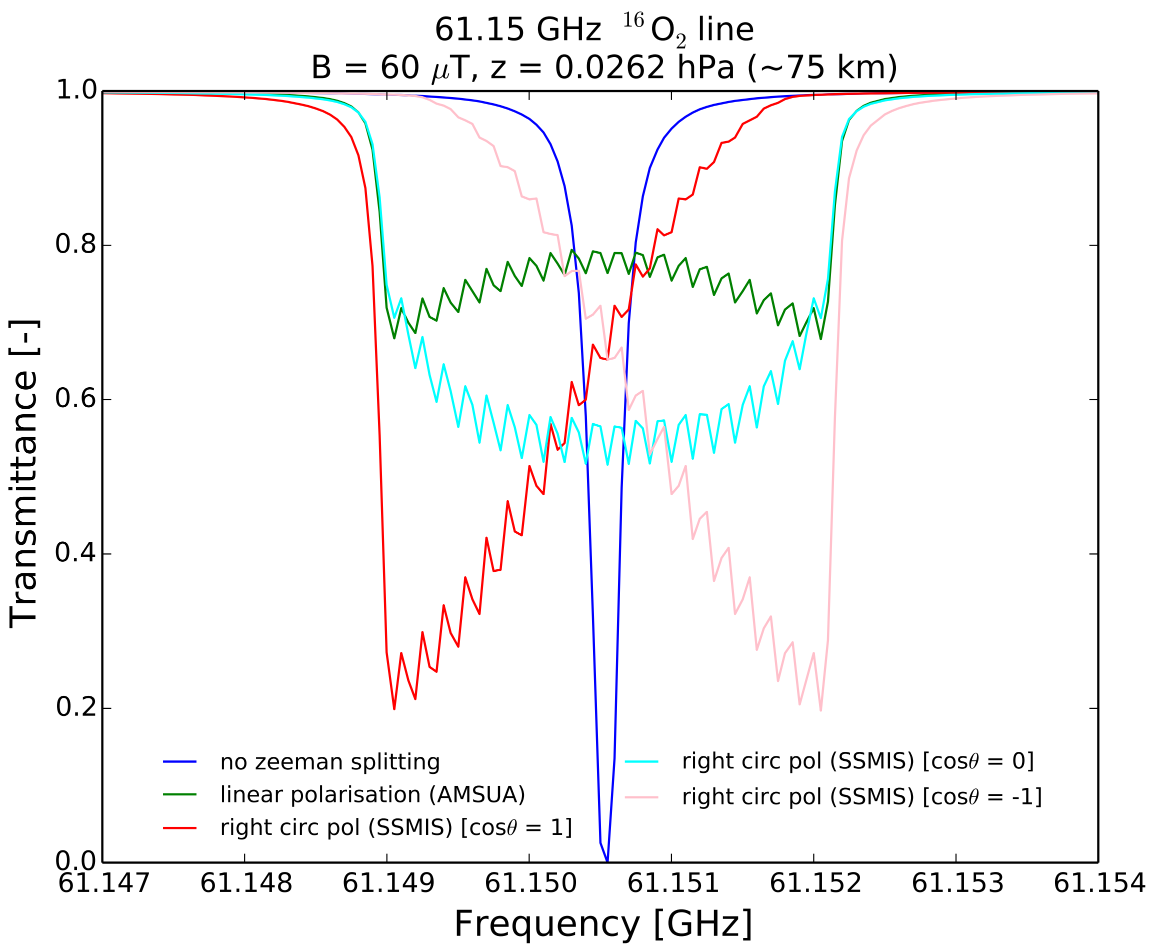

Figure 36: Zeeman affected transmittance spectrum from 0.0262 hPa (75 km) to space in the vicinity of the 9+ $^{16}O_2$ line at 61.15 GHz with the application of a magnetic field of 60 μT and receiver geometry representing either linear polarisation, like AMSU-A (green line), or right circular polarisation, like SSMIS where the geomagnetic field is either perpendicular to the viewing path (cyan line), or parallel to it (red and purple lines). θ is the angle between the magnetic field and viewing path. The un-split oxygen line is shown for reference (blue line).

the difference in measured brightness temperature can be several kelvin. Currently AMSUTRAN only calculates the Zeeman effect for 34 lines in the spin rotation band, 33 between 51 and 68 GHz and the 118.75 GHz line, and the current treatment is sufficient for these transitions. However, the Hund case (b) approximation becomes problematic for the higher frequency transitions and it becomes necessary to include the off-diagonal elements of the fine structure Hamiltonian and higher order Zeeman interactions (Drouin et al., 2010). The recent work of Larsson et al. (2019) presents updated coefficients using these detailed calculations, which could provide scope for future improvement in this respect.

5.6 Oxygen lines summary

- Line mixing implemented in the 60 GHz oxygen band has a proportionally greater effect in the line wings. The MPM formulation used in AMSUTRAN, which only includes first order terms, acts to decrease absorption by a relatively constant amount of 5% (transmittance) up to and beyond 1000 GHz. The inclusion of the MPM92 non-resonant oxygen formulation partly compensates for this reduction ensuring that there is always non-zero oxygen absorption between bands of lines.

- Recent work has sought to improve the parameterisation of line mixing by either incorporating higher order terms, which can be done in the MPM formulation, or implementing a new more physically based formulation called Energy Corrected Sudden (ECS) model.
- The range of 118.75 GHz values for line intensity is 3.6% (but more likely less than 1% if two outliers are removed), for air-broadened half-widths is 6.4% (but more likely 1.4% if earlier studies are omitted), and for the air temperature exponent is constrained between 0.745 and 0.8.
- The ratio of water-to-air broadened half-width likely lies between 1.1 and 1.2.
- The TOA brightness temperature differences at 118.75 GHz between the VVW and the speed dependent line-shape are estimated to be between 0.05–0.2 K.
- High peaking oxygen lines are subject to splitting in the presence of a magnetic field, which broadens their influence by around 2 MHz either side of the line centre. This could be particularly important for high-peaking channels such as channel 16 on MWS.

6 Recommendations and Uncertainties

It is challenging to objectively determine what could be considered the best spectroscopy for the spectral regions relevant to MetOp-SG, because the definitive test requires satellite observations of the channels themselves, many of which have no precedent and will be present on a spaceborne platform for the first time. The previous three sections have shown there are multiple values available for any one spectroscopic parameter particularly for those associated with water vapour, even within the limits of this report, and hence multiple solutions are possible. It is beyond the scope of this work to construct the optimum combination of parameter values for each line, which is instead left to the model developers, and it is recommended to use a complete model that has already been through the selection process. Of the nine collections of parameters presented here most have some aspects or omissions that do not align with every requirement of the project. For example, the HITRAN database is updated semi-regularly, every four years, but many parameters are theoretically derived and apply to many lines at once, rather than focusing on every line individually. And although the GEISA database has developed an empirical-based evaluation system to screen candidate parameters, this has been restricted to the infrared so far. Additionally, neither of these databases provides a complementary water vapour continuum, which is very important for the spectral region considered. The microwave models, AMSUTRAN and ATM, which have heritage in the MPM series are less regularly updated, so many parameters may be out of date.

6.1 Recommended models

Table 9: Key features and differences between AER (MonoRTM v5.4, line file v3.8, MT-CKD v3.5) and the PWR19 model.

Feature	AER	PWR19
Updates	Active on-going work to refine parameters	Regularly updated with new parameters
Spectral range	Microwave to ultra-violet	Microwave to sub-millimetre
Sources	Field campaigns constrain key parameters	Majority from various laboratory studies
Lineshape	Voigt using the Humlíček (1982) approximation	VVW with optional speed-dependent shape for the 22.23, 118.75 and 183.31 GHz lines
H_2O lines	Hundreds included, nine below 1000 GHz constrained: 22.23, 183.31, 325.15, 380.19, 556.93, 620.70, 752.03, 916.17, 987.92	16 included: 22.23, 183.31, 321.22, 325.15, 380.19, 439.15, 443.01, 470.88, 474.68, 556.93, 620.70, 658.00, 752.03, 916.17
Pressure shifts	Air-broadened	Air and self-broadened
H_2O continuum	MT-CKD model at 300 GHz increments updated regularly based on new campaigns	Turner et al. (2009) continuum parameters adjusted slightly for new line parameters
O_2 lines	Tretyakov et al. (2005) parameters	Parameters from various recent studies
Line mixing	First order from Tretyakov et al. (2005)	Second order from Makarov et al. (2018)
Uncertainties	Few specific estimates and HITRAN ranges	Most can be sourced from original study

Two complete models with very different philosophies stand out as suitable choices for future analysis, the latest version of the AER model, MonoRTM (version 3.8 line database and MT-CKD 3.5 continuum); and the newest Rosenkranz model, PWR19. Relevant key features are listed in Table 9. Both models benefit from being regularly updated with new parameters, however, these are obtained via different experimental methods. As described in section 2.2.2, AER uses dedicated field campaigns to constrain key parameters empirically, whereas lines in the Rosenkranz models are mostly formed from parameters taken from various laboratory studies, see section 2.1.5. This provides a good opportunity to test two sets of parameters that originate from independent sources, giving a further measure of uncertainty to the resulting radiative quantities.

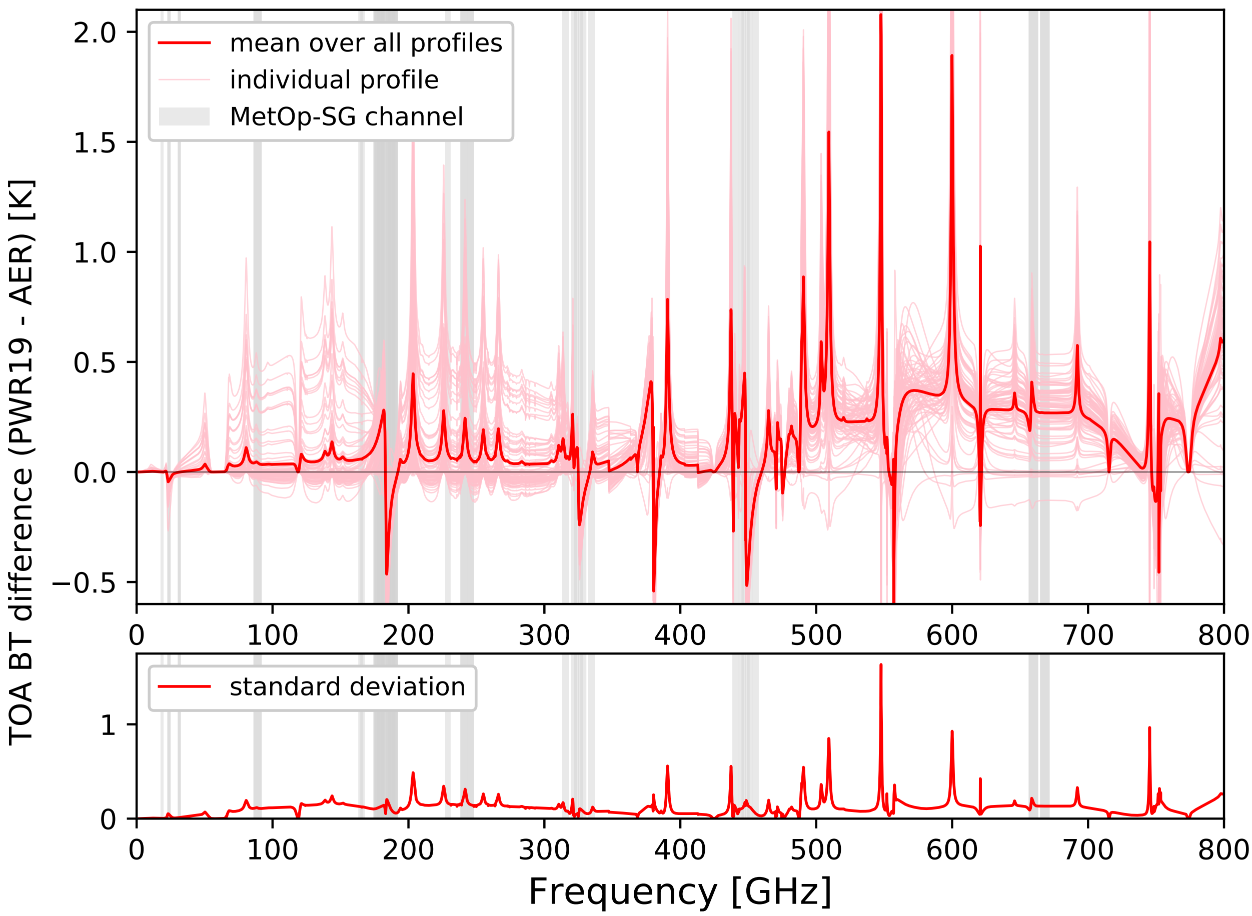

Figure 37: TOA brightness temperature differences between PWR19 and the AER model (AER v3.8 lines and MT-CKD 3.5 continuum), due to water vapour only. Simulations are made using the 83 diverse atmospheric profile with nadir viewing geometry and an emissivity of 1. The coverage of MetOp-SG channels are shaded grey.

Figure 37 presents the differences in TOA brightness temperature produced by the two models, purely due to their native water vapour parameters and absorption schemes, where all other aspects are held constant. These are by no means the most dissimilar of all the models considered in Section 3.3 (Figure 23), but there are some features worth noting. Omission of minor lines in the PWR19 model results in localised differences of up to 3 K at frequencies between the MetOp-SG channels. This may only be of concern to MWS channel 24 at 229 GHz and ICI channel 4 at 242.3 GHz, where a HDO line at 225.9 GHz, and two at 241.56 and 241.97 GHz, encroach on the lower passband of each respective channel producing differences up to around 1 K in some atmospheric profiles. Within the channels that straddle prominent lines, different parameters, particularly pressure-induced shifts, are responsible for high positive and negative fluctuations but these tend to compensate over the full swath. In window regions, mean brightness temperatures are consistently higher for the PWR19 model, which corresponds to the slightly weaker continuum absorption resulting in emission from lower, warmer levels of the troposphere. These differences are markedly elevated between 500–700 GHz, with a relatively constant separation of 0.3 K. At lower frequencies the mean is below 0.1 K, but individual, very humid profiles can diverge by up to 0.5 K.

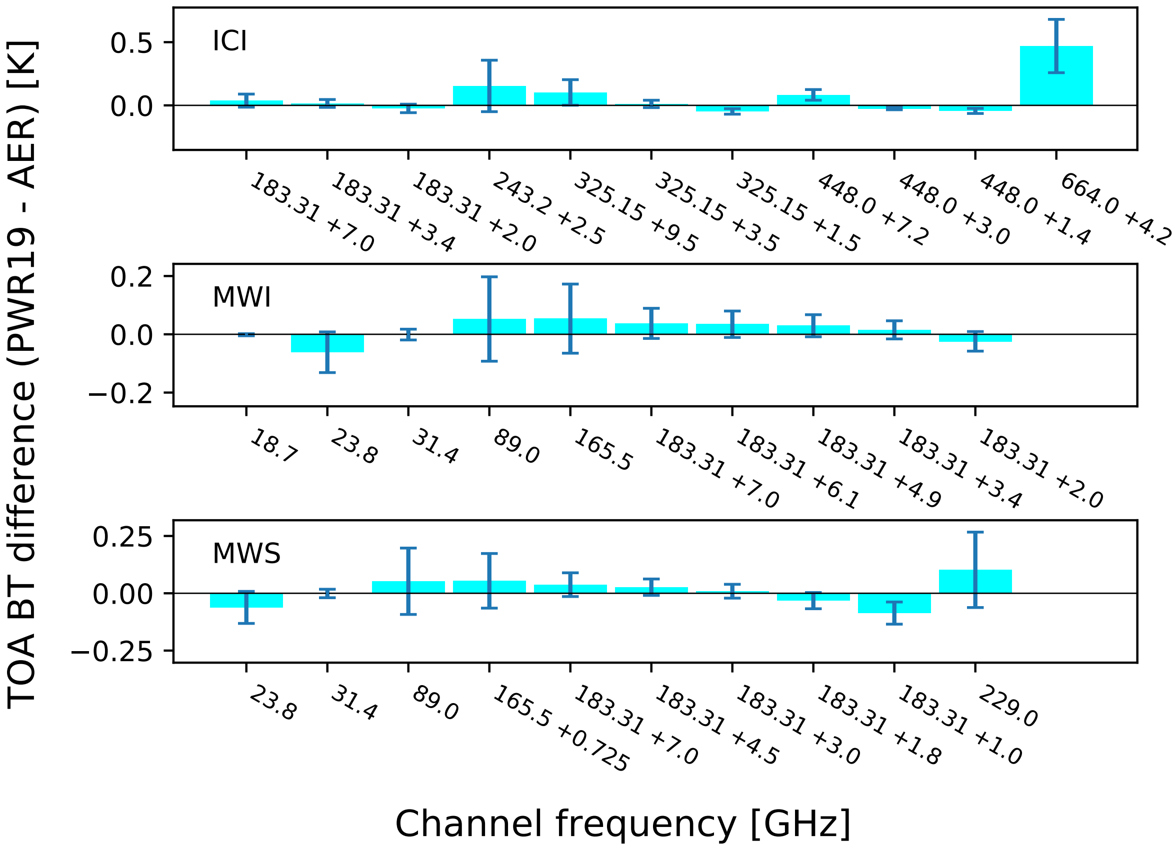

Figure 38: TOA brightness temperature differences in MetOp-SG water vapour channels between PWR19 and the AER model (AER v3.8 lines and MT-CKD 3.5 continuum), due to water vapour only. The mean (cyan bars) and standard deviation (blue error bars) of the difference for each channel is the average of 83 diverse atmospheric profiles and six satellite viewing angles using an emissivity of 1.

Figure 38 shows the differences averaged over MetOp-SG channels that are affected by water vapour. These simulations are different to those presented in Figure 37 as they include six satellite zenith angles, rather than restricting the geometry to nadir. Apart from the 664 and 243 GHz channels on ICI, all mean and standard deviations are below 0.25 K. The biggest variabilities are in window channels, including the aforementioned, which are primarily affected by the water vapour continuum.

6.2 Parameter uncertainties

Uncertainties estimated for each of the water vapour parameters adopted by AER 3.8 (MT-CKD 3.5) and PWR19 are listed in Tables 10 and 11 below the parameter values. These are determined from the literature where available, apart from MT-CKD continuum coefficients at 296 K, which are estimated via personal communication (E.Mlawer, 2021). The tables are incomplete as not all parameter uncertainties are provided in the original studies, which is particularly notable for the temperature exponents, n_{air} and n_{self}. Independent analysis can be used to subjectively estimate absent and constrain ranges of uncertainties, such as in Cimini et al. (2018).

Full resonant line frequencies, ν, are not included as a separate parameter in Table 10 because the sources are unknown for PWR19 lines and the AER 3.8 22.235 GHz line. Based on the HITRAN 2012 database, the remaining AER 3.8 line frequencies are taken from Lanquetin et al. (2001), and all have an uncertainty that lies between 0.0003 and 0.003 GHz (0.00001 – 0.0001 cm^{-1}), according to HITRAN uncertainty codes. These codes, described in Rothman et al. (2005, Table 5.), refer to the range of uncertainties in the parameter values, for example $\geq$5% and $<$10%. Where AER lines can be associated with HITRAN ranges it is evident that even the lower limit tends to be high compared to the corresponding PWR19 uncertainty. This is because PWR19 often selects its values from laboratory studies dedicated to a particular parameter and/or line, so the uncertainty is more tightly constrained, whereas HITRAN values are more conservative because the methods used to calculate the value often apply to many lines. Within the range of laboratory studies themselves, larger uncertainties tend to come from those that inter-compare multiple studies to deduce a value (Tretyakov, 2016; Gamache and Hartmann, 2004), whereas data from a single laboratory study may be more modest, i.e. describing one standard deviation of the fit (Koshelev et al., 2007; Tretyakov et al., 2013a).

Even when AER line-widths are derived from constrained atmospheric measurements rather than HITRAN line lists it is notable that the uncertainties are still significantly larger than PWR19 values. For example, the AER 3.8 uncertainties for the 22.235, 183.31, 556.94 and 752.03 GHz air-broadened half-widths (γ_{air}) are 3%, 3%, 4.1% and 4.9%, respectively, whereas the equivalent PWR19 estimates are 0.68%, 0.51%, 0.43% and 1.12%. The latter percentages are determined from either: the total error budget, which includes fit error, pressure uncertainty and temperature uncertainty (Koshelev et al., 2018a); expert assessment of different experiments across multiple studies (Tretyakov, 2016); or one standard deviation of the fit error (Golubiatnikov et al., 2008; Koshelev, 2011); for each of the four lines, respectively. The 3% uncertainties that AER places on the 22.235 and 183.31 GHz parameters are based on sensitivity tests involving assumptions made in the complex implementation of the Robert-Bonamy (CRB) theory (Payne et al., 2008), which is used to calculate the half-widths. Uncertainties for the 556.94 and 752.03 GHz line parameters are given by the percentages that correspond to the ratio of AER 3.8 to HITRAN 2012 air-broadened half-widths (Mlawer et al., 2019). The difference between AER 3.8 and PWR19 parameters themselves are often as big as the corresponding AER uncertainty, apart from the line intensities where the particular values included approximate each other to within 1%.

Table 10: Spectroscopic parameters for the six key water vapour lines considered in this report from the AER 3.8 line database and the PWR19 model. Where available in the original study, associated uncertainties are listed below each parameter with the corresponding percentage in parentheses (unless only a percentage is provided). References for data are given in the footnotes. A separate temperature dependence for self-broadened half-width (n_{self}) is not specified for AER lines so is set to the same value as the corresponding temperature dependence of air-broadened half-width (n_{air}). Original values are converted to consistent units where necessary and all temperature dependent parameters are shown at 296 K.

Parameter	S	γ_{air}	n_{air}	γ_{self}	n_{self}	δ_{air}	δ_{self}
units	$\frac{cm^{-1}}{molecules \times cm^2}$	$\frac{cm^{-1}}{atm}$	-	$\frac{cm^{-1}}{atm}$	-	$\frac{cm^{-1}}{atm}$	$\frac{cm^{-1}}{atm}$
22.235 GHz							
AER 3.8	4.348e-25[a]	0.0917[b]	0.65[?]	0.385[c]	0.65[?]	-0.800e-3[?]	-
	0.5%	0.00275 (*3%*)[g]	-	*>20%*	-	0.989e-3 (*121.9%*)[d]	-
PWR19	4.454e-25[e]	0.0912[f]	0.76[g]	0.449[f]	1.2[h]	-1.115e-3[f]	27.51e-3[f]
	1%	0.00062 (*0.68%*)	-	0.00148 (*0.33%*)	0.5 (*41.67%*)	0.127e-3 (*11.40%*)	0.303e-3 (*1.10%*)
183.31 GHz							
AER 3.8	7.691e-23[a]	0.1025[b]	0.71[i]	0.519[c]	0.71[i]	-2.700e-3[g*]	-
	0.5%	0.00238 (*3%*)[g]	-	*≥10% <20%*	-	0.989e-3 (*36.79%*)[j]	-
PWR19	7.736e-23[e]	0.0995[h]	0.77[g]	0.499[h]	0.78[h]	-2.433e-3[h]	5.830e-3[h]
	1%	0.0005 (*0.51%*)	-	0.0127 (*2.5%*)	0.08 (*10.26%*)	0.254e-3 (*10.42%*)	0.761e-3 (*13.04%*)
325.15 GHz							
AER 3.8	9.012e-23[a]	0.0944[k]	0.73[?]	0.507[c]	0.73[?]	-2.000e-3[?]	-
	0.5%	*≥5% <10%*	*≥5% <10%*	*≥10% <20%*	*≥5% <10%*	*≥0.001 < 0.01*	-
PWR19	9.077e-23[e]	0.0962[l]	0.64[m]	0.471[l]	0.74[n]	-0.439e-3[l]	44.7e-3[l]
	1%	0.00071 (*0.74%*)	0.09 (*14.06%*)	0.00071 (*0.16%*)	-	0.167e-3 (*38.10%*)	0.020e-3 (*0.45%*)
448.00 GHz							
AER 3.8	8.625e-22[s]	0.0889[j]	0.65[o]	0.467[p]	0.65[n]	-3.100e-3[?]	-
	≥5% <10%	*≥5% <10%*	*≥2% <5%*	*≥2% <5%*	*≥2% <5%*	*≥0.001 < 0.01*	-
PWR19	8.633e-22[e]	0.0883[q*]	0.70[r]	0.440[q]	0.67[n]	-3.291e-3[q]	-20.786e-3[q]
	≥1% <2%	0.0333 (*0.96%*)		0.00076 (*0.17%*)	-	0.43e-3 (*11.04%*)	0.89e-3 (*4.27%*)
556.94 GHz							
AER 3.8	5.207e-20[s]	0.1103[b]	0.75[r]	0.487[p]	0.75[r]	6.800e-3[?]	-
	≥5% <10%	*4.1%*	*<1%*	*≥1% <2%*	*<1%*	*≥0.001 < 0.01*	-
PWR19	5.238e-20[e]	0.1053[s]	0.75[q]	0.481[s]	1.00[n]	6.326e-3[s]	-57.22e-3[s]
	≥1% <2%	0.00045 (*0.43%*)	*<1 %*	0.0051 (*1.06%*)	-	0.45e-3 (*7.17%*)	2.56e-3 (*4.47%*)
752.03 GHz							
AER 3.8	3.433e-20[t]	0.1072[b]	0.77[r]	0.463[p]	0.77[r]	8.500e-3[?]	-
	≥5 % <10 %	*4.9 %*	*<1 %*	*≥1 % <2 %*	*<1 %*	*≥0.001 < 0.01*	-
PWR19	3.454e-20[e]	0.1052[u]	0.77[q]	0.459[u]	0.84[n]	5.48e-3[u]	-29.66e-3[u]
	≥1 % <2 %	0.0012 (*1.12%*)	*<1 %*	0.0038 (*0.83%*)	-	0.68e-3 (*12.5%*)	0.76e-3 (*2.56%*)

[*] Values originating from the same study may differ, check sections on individual line parameters for details.
[?] Source unknown.

[a] Clough et al. (1973) [b] Mlawer et al. (2019) [c] Gamache and Hartmann (2004) [d] uncertainty provided in Tretyakov (2016, Table 3.) [e] Lodi et al. (2011) [f] Koshelev et al. (2018a), note uncertainties come from the total error budget percentage in Table 3. [g] Payne et al. (2008) [h] Tretyakov (2016) [i] Ma et al. (2010) [j] uncertainty stated in Tretyakov (2016, Table 3.) [k] Jacquemart et al. (2005) in Rothman et al. (2013) [l] Koshelev et al. (2007) [m] Colmont et al. (1999) [n] Liebe and Layton (1987) [o] Birk and Wagner (2012) [p] Cazzoli et al. (2008) [q] Tretyakov et al. (2013a) [r] Gamache and Laraia (2009) [s] Golubiatnikov et al. (2008) [t] Martin et al. (2016) [u] Koshelev (2011)

Table 11: Spectroscopic parameters of the water vapour vapour continuum models used by AER (MT-CKD 3.5) and PWR19 (Turner et al., 2009). Square brackets contain the range of values produced by frequency dependent formulations, and temperature dependent in the case of n_s. Where available, the associated uncertainties are listed below each parameter, with the corresponding percentage in parentheses, unless only a percentage is provided. C_s and C_f are calculated for a temperature of 296 K.

Parameter units	$\mathbf{C}_s$ (dB/km)/(GHz^{2}hPa^2) x10^{-8}	$\mathbf{C}_f$	$\mathbf{n}_s$ –	$\mathbf{n}_f$ –
MT-CKD 3.5	6.46* [6.23–6.62]	0.269* [0.262–0.297]	5.84* [4.66–7.12]	0.0
	10%[v]	*5%*[v]	-	-
PWR19	6.55†	0.258	4.50	0.0
	1.49 (*22.78%*)[w]	0.0232 (*9.01%*)[w]	0.6 (13.33%)[x]	0.8[x]

* mean value over all frequencies between 2–1000 GHz, and all profile temperatures for n_s
† adjusted from 300 K to 296 K using the corresponding value of n_s

The PWR19 continuum uncertainties presented in Table 11 relate to the relative uncertainties in the scaling factors applied to the original Rosenkranz (1998) coefficients derived by Turner et al. (2009), which are 0.79(18) and 1.11(10) for C_s and C_f, respectively. There is only a small increase of 0.003 dB/km/GHz^{2}hPa^2 (x 10^{-8}) between the Turner et al. (2009) and the PWR19 C_f coefficient, and negligible change to C_s, to account for modifications to water vapour lines, so it is judged acceptable to retain the same uncertainties. The uncertainties attached to the temperature exponents are not those derived from the original Liebe and Layton (1987) study, which would be 0.3 and 0.4 for n_s and n_f, respectively, but are instead from Cimini et al. (2018), where they have been increased, partially to overlap with the values and uncertainties presented in Koshelev et al. (2011). The MT-CKD coefficients, which employ a more complicated frequency interpolation routine, show the full range of possible values in brackets next to the mean result over the 2–1000 GHz region.

6.3 Recommendations to spectroscopists

This literature review has illuminated certain areas where spectroscopy is either absent or lacking in the microwave/sub-millimetre regions, which would benefit from an increased focus, not only for MetOp-SG, but for radiative transfer developers in general and end users. These gaps could be addressed with dedicated laboratory experiments, targeted expert assessment of measured data, radiative closure studies performed in the real atmosphere, or even a collaboration between members of the different communities to combine approaches.

As discussed in section 3.1.2, and is evident from Figures 8–14, there have been multiple studies aimed at describing the 22.235 and 183.31 GHz water vapour lines as these are heavily used in microwave radiometry, but sub-millimetre lines have not been subject to the same scrutiny. Although each of the four lines centred at 325.15, 448.00, 556.94 and 752.03 GHz benefits from a dedicated laboratory study performed in the last two

[v] E.Mlawer personal communication, 2021 [w] Turner et al. (2009) [x] Cimini et al. (2018)

decades, it is clear that robust parameter values and accurate uncertainties require more than one experiment to constrain them. Studies such as Tretyakov et al. (2013a), which derives the same quantity using two different sets of apparatus are favorable and show that experimental set-up tends to dominate results (see Figure 9, 448.00 GHz column). Even so, the quoted uncertainties associated with each set of values are specific to the experiment and often do not overlap with each other, hence it is difficult to judge objectively which one is more correct.

Recent approaches to quantifying absorption model uncertainty (Cimini et al., 2018), require more general estimates of the likely range of values associated with each spectroscopic parameter, thus total error budgets are more useful than a simple standard deviation of the fit, preferably with a breakdown of components such as in Koshelev et al. (2018a, Table 3). Subjective determination of parameters in review papers like Tretyakov (2016), which crucially consider multiple experiments from independent studies are ideal for this purpose, as the quoted uncertainties take account of the full spread of possible values. It would be beneficial to the community if this type of review were extended to sub-millimetre water vapour lines and key transitions from other molecules, the 118.75 GHz oxygen line for example.

In terms of particular quantities that require focus, there is a general lack of temperature dependencies for water vapour broadening parameters, specifically derived for the line in question. This is especially true for the self-broadened component (Figure 12), which is not included at all in the larger line lists. Where multiple options do exist, such as the dependency associated with the 183.31 GHz air-broadened half-width, the range of possible values is large and does not appear to converge over time. As these are some of the most challenging measurements to make the best strategy is to use the results of theoretical calculations validated by experiments (M. Tretyakov, personal communication, 2021). Multiple theoretical methods can enhance robustness, for example the CRB method used by Gamache e.g. Koshelev et al. (2021b), and ab initio potential calculations, e.g. Serov et al. (2021). Pressure shift parameters are also sparsely available and appear quite uncertain (Figures 13 and 14), whilst exerting a significant effect on absorption close to the line (Figure 15, difference between upper and lower panels). More measurements of pressure shifts and their associated temperature dependencies would be an asset to model developers. Additionally, providing parameters that describe the speed-dependent line-shape, which has been a new subject of investigation in the microwave in recent years, would also be welcome for sub-millimetre lines in order to fully test its radiative effects on MetOp-SG channels.

Section 3.2.3 concludes that, as yet, no complete water vapour continuum model exists that has been sufficiently validated for both the microwave and sub-millimetre regions up to 1000 GHz, and has also been derived at a range of temperatures and pressures characteristic of the real atmosphere. Such a model would require repeat measurements at a range of frequencies, as the frequency squared moderation of coefficients (Equation 8), may not apply throughout the region according to conflicting configurations in existing models. Simultaneous derivation of all four parameters including self and foreign coefficients (the latter using atmospheric air as the broadening component), and their respective temperature dependencies is preferable, as is using an up-to-date set of line parameters in the residual calculation.

Finally, we request if possible that parameters be calculated at a common set of local conditions to minimise convolving uncertainties attached to other quantities that are required to convert between units. For example, coefficients which are temperature dependent, such as broadening widths and pressure shifts, are typically defined at 296 K following HITRAN conventions, so adjustments from other measurement temperatures involve additional assumptions to be made about the temperature dependence of these quantities. Clearly stating the values of all parameters employed in calculations and presenting results with sufficient precision to allow small units to be accurately converted if necessary, is also valued.

6.4 Recommendations and Uncertainties summary

- Parameters from the latest AER (MonoRTM) and PWR19 models are recommended to take forward for further assessment as they are both regularly updated and diverse in terms of origin, via field campaigns and laboratory experiments, respectively.
- Uncertainties are not available for all line and continuum parameters (only H_2O is presented here) and those that are have variable meanings. AER uncertainties are in general more conservative than the corresponding PWR19 values.
- A list of requests is made to spectroscopists in order to steer future work. These include a focus on sub-millimetre line parameters for both VVW/Voigt and speed-dependent line-shapes, expert assessment across multiple studies to determine accurate parameter values and overall uncertainty estimates, more measurements of temperature exponents and pressure shift parameters that are line specific, and a suitable water vapour continuum model valid for frequencies from the microwave to 1000 GHz.

7 Summary and conclusions

Spectroscopic assumptions are the largest source of clear-sky differences between radiative transfer models and observations, which often far exceeds the inter-model spread of both LBL and fast models, reaching several kelvin in some satellite channels. However, the current skill of fast radiative transfer models, such as RTTOV, in reproducing the results of the underlying line-by-line codes is such that the difference between them is often negligible, apart from in extreme cases such as very dry profiles. Though models share many features they often develop in isolation and are built for specific purposes, hence inter-comparisons are invaluable in assessing the range of simulation results, re-evaluating procedures and catching errors.

Line parameters from two versions of HITRAN (2012, 2016), AER 3.8, GEISA 2019, AMSUTRAN, ATM and three versions of PWR (1998, 2017, 2019), were compared alongside those from recent studies for six water vapour lines sensed by 18 channels on MetOp-SG, water vapour continuum that is the majority constituent affecting 10 channels, and the 118.75 GHz oxygen line sensed by four channels on MWI. Most of the listed models and databases overlap with each other in some respect but when all parameters are taken together they are sufficiently different to make a reasonable estimate of how well the line is known.

The number of publications that focus on parameters of 22.235 and 183.31 GHz lines far exceeds those relating to the other four sub-millimetre water vapour lines, due to their prevalent use in remote sensing and established microwave technology. The 448.00 GHz line shows less spread in parameter values, though studies are limited in number. Comparison of parameters for these seven lines shows intensities are most well known, to within 2.5% when obvious outliers are removed; air-broadened half-widths are known to within 5%, but the equivalent parameter for self-broadening tend to be less constrained, with a spread between 3.5–9.5%. It should be noted that the ranges given in this review are not equivalent to the uncertainty attached to a parameter, which should be the total of all error sources in the experiment combined, and is usually far more modest. It is highly subjective to attach a number based on a range of results grouped together as this depends on which studies were included, the number available, and whether outliers can be discarded.

Air-broadened half-widths show a dominant effect on water vapour absorption; a larger value acts to reduce it in the line centre and increase it the wings. A crossover occurs at around 2-3 GHz where sensitivity to the size is low, coinciding with the location of many double passband channels on MetOp-SG. Interestingly, this may result in the channels being less sensitive to the choice of air-broadened half-width.

Temperature dependencies for water vapour half-widths are not well constrained, but the air-broadened temperature exponent for the 118.75 GHz oxygen line appears to be. Values for pressure-induced shifts can be very variable where available. Inspection of the spread for a particular parameter shows that some of the values from earlier studies, such as MPM, now appear to be outliers, and in one case such a value was preferentially chosen to be included in the latest HITRAN release, based on their system of selecting the last available theoretical result over experimental, even though it deviates strongly from others.

Values provided by more recent studies tend to converge towards each other, though most of the laboratory measurements originate from one research group at the Russian Acadamy of Sciences, so there could be a non-negligible amount of experimental bias. Robustness is enhanced, however, by repeating experiments with different apparatus, and this has been shown to often be the dominant source of differences. The group's work has benefited from increasing sensitivity of measurement techniques over time, but it would be good to increase diversity by seeing similar studies performed at other institutions, and involve real atmospheric campaigns. In-situ measurements are vital for constraining parameters for remote sensing purposes, as is ensuring consistency between dependent parts of the absorption, such as water vapour lines and continuum.

Eleven water vapour continuum models are compared, and although each of the four continuum coefficients exhibits a wide range of values, at least half evaluate to within 7% of each other when the total absorption is calculated, and further compensation occurs for the MPM based models when the appropriate underlying lines are added. Many combinations of parameters can therefore produce the same result. The range of TOA brightness temperatures possible due to the different continuum models considered is as much as 1.2 $\pm$0.6 K in the 200-300 GHz window, which coincides with channel 4 of ICI, and channel 24 of MWS. This is well beyond the error in the fast model parameterisation. The behavior of far wings of water lines at detunings beyond 150–300 GHz is possibly the biggest unknown in this part of the spectrum.

No one continuum parameterisation satisfies all of the requirements for MetOp-SG from a theoretical point of view, in terms of corresponding experimental conditions. For this it would be preferable that the foreign component is atmospheric air, that measurements are made at multiple frequencies that overlap with MetOp-SG channels (18 – 700 GHz) and that the experiment samples the full range of characteristic temperatures from the warm tropical surface to the very cold stratosphere. The MT-CKD model comes closest to this although there is lower confidence in values between 183 – 450 GHz, as there are no direct measurements to constrain the function here so it's extrapolated. But crucially it does have the advantage of simultaneously refining both lines and continua in the real atmosphere, on a near continual basis. For water vapour in the microwave and sub-millimetre this synergy is particularly important.

Ozone lines are numerous and show little variation on a local scale so parameters are calculated in bulk and availability is limited to one or two sources, typically HITRAN. It has recently been determined that a 4% discrepancy affecting microwave ozone line intensities entered the catalogue at the 2004 release, but is expected to be corrected for HITRAN 2020. It is jointly recommended to use the S&MPO TIPS value for ozone. A preliminary updated list based on JPL intensities shows local line differences of up to 4 K at high frequencies with respect to HITRAN 2016.

There has been much work in recent years dedicated to describing the non-Lorentzian behavior of the line-shape made possible by more accurate experimental techniques, which is very relevant to oxygen lines. Higher order line mixing, speed-dependent line-shapes and Zeeman effects provide a more complete theoretical description of absorption in the low pressure limit, adding a multitude of new parameters and challenges for models to incorporate and validate. New work has also recently been published in the last year updating the fine structure oxygen lines for MPM based absorption models such as AMSUTRAN. Accurate simulation of these effects are particularly important for high-peaking channels such as channel 16 on MWS, and the 118.75 GHz channels on MWI.

Two models: AER (MonoRTM) and PWR19, are recommended to take forward for further assessment as they fulfill critical requirements for MetOp-SG and include parameters values from very different sources. For future studies it is recommended that more sub-millimetre measurements be made, as it is becoming increasingly utilised by the atmospheric community and is likely to be more so in the future. It is also advised that estimates of the associated uncertainties be specific to the parameter in question and constrained as much as possible, whilst realistically representing the full range of possible values. Finally, while inter-model and parameter comparisons are essential, more radiative closure experiments are needed to meaningfully evaluate the real world applicability of the new spectroscopic parameters that are emerging in the laboratory.

Acknowledgements

We thank M. Tretyakov for their insight and recommendations, which have enhanced this report, and everyone else who contributed in some way.

Appendices

A Profile datasets

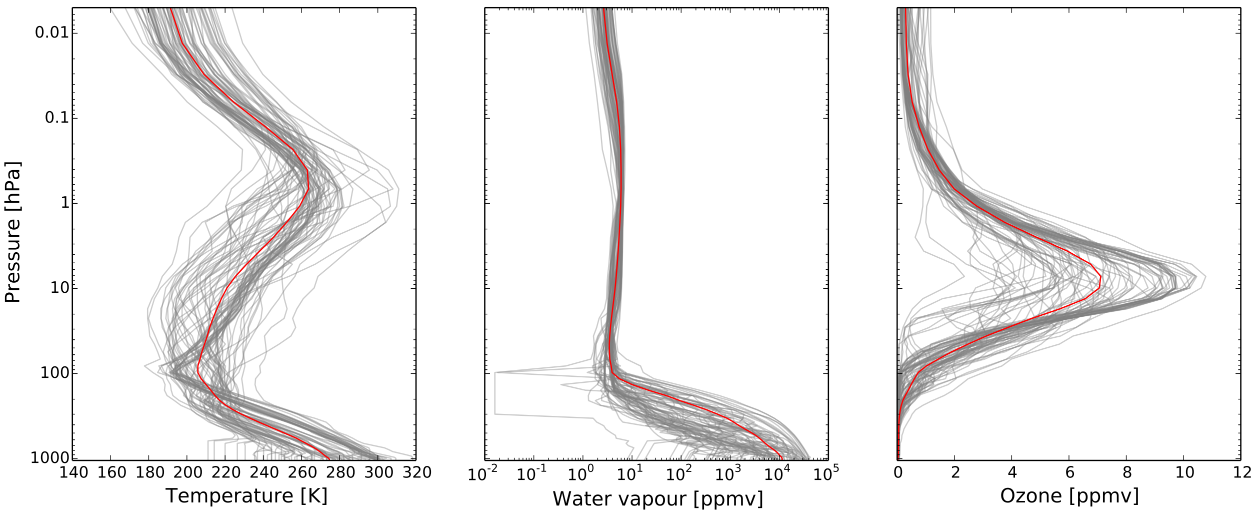

Figure 39: Atmospheric variables in the 83 profile, 54 level 'dependent' profile set that is used to create RTTOV coefficients. The mean profile is shown in red.

A set of 83 profiles covering a diverse range of global atmospheric conditions, originally created by Matricardi (2008), are the training set used for generating the transmittances that subsequently produce the fast model coefficients for RTTOV. These were selected from a large database of profiles on 91 levels generated by the experimental suite (cycle 30R2) of the ECMWF forecasting system, as described in Chevallier et al. (2006). The 81st, 82nd and 83rd profiles are the minimum, maximum and mean, respectively, of the initial database. The profiles have been interpolated to 54 levels between 0.005 and 1050 hPa, which has been shown by Saunders et al. (2013) to be a good compromise to reduce the burden of computation, whilst the levels have been chosen to provide adequate representation throughout the atmosphere and a smooth profile of pressure differences. The profiles consist of level values of: total pressure in hPa, temperature in K, volume mixing ratio (vmr) of water vapour in parts per million by volume, and the same for ozone, see Figure 39.

References

Accadia, C., Mattioli, V., Colucci, P., Schlüssel, P., D'Addio, S., Klein, U., Wehr, T., and Donlon, C. (2020). Microwave and sub-mm wave sensors: A European perspective. In *Satellite Precipitation Measurement. Advances in Global Change Research*, volume 67, pages 83–97. Springer, Cham.

Armante, R., Scott, N., Crevoisier, C., Capelle, V., Crepeau, L., Jacquinet, N., and Chédin, A. (2016). Evaluation of spectroscopic databases through radiative transfer simulations compared to observations. Application to the validation of GEISA 2015 with IASI and TCCON. *Journal of Molecular Spectroscopy*, 327:180–192.

Babikov, Y. L., Mikhailenko, S. N., Barbe, A., and Tyuterev, V. G. (2014). S&MPO–an information system for ozone spectroscopy on the WEB. *Journal of Quantitative Spectroscopy and Radiative Transfer*, 145:169–196.

Barlakas, V. and Eriksson, P. (2020). Three dimensional radiative effects in passive millimeter/sub-millimeter all-sky observations. *Remote Sensing*, 12(3):531.

Bergadá, M., Labriola, M., González, R., Palacios, M., Marote, D., Andrés, A., García, J., Sánchez-Pascuala, D., Ordóñez, L., Rodríguez, M., et al. (2016). The Ice Cloud Imager (ICI) preliminary design and performance. In *Microwave Radiometry and Remote Sensing of the Environment (MicroRad), 2016 14th Specialist Meeting on*, pages 27–31. IEEE.

Birk, M. and Wagner, G. (2012). n averaged as a function of J" for J" = 0 to 13 from: Temperature-dependent air broadening of water in the 1250–1750 cm^{-1} range. *Journal of Quantitative Spectroscopy and Radiative Transfer*, 113(11):889–928.

Birk, M., Wagner, G., Gordon, I. E., and Drouin, B. J. (2019). Ozone intensities in the rotational bands. *Journal of Quantitative Spectroscopy and Radiative Transfer*, 226:60–65.

Bobryshev, O., Buehler, S. A., John, V. O., Brath, M., and Brogniez, H. (2018). Is there really a closure gap between 183.31-ghz satellite passive microwave and in situ radiosonde water vapor measurements? *IEEE Transactions on Geoscience and Remote Sensing*, 56(5):2904–2910.

Brogniez, H., English, S., Mahfouf, J.-F., Behrendt, A., Berg, W., Boukabara, S., Buehler, S. A., Chambon, P., Gambacorta, A., Geer, A., et al. (2016). A review of sources of systematic errors and uncertainties in observations and simulations at 183 GHz. *Atmospheric Measurement Techniques*, 9(5):2207–2221.

Buehler, S., Courcoux, N., and John, V. O. (2006). Radiative transfer calculations for a passive microwave satellite sensor: Comparing a fast model and a line-by-line model. *Journal of Geophysical Research: Atmospheres*, 111(D20).

Buehler, S., Eriksson, P., Kuhn, T., Von Engeln, A., and Verdes, C. (2005). Arts, the atmospheric radiative transfer simulator. *Journal of Quantitative Spectroscopy and Radiative Transfer*, 91(1):65–93.

Buehler, S. A., Mendrok, J., Eriksson, P., Perrin, A., Larsson, R., and Lemke, O. (2018). Arts, the atmospheric radiative transfer simulator–version 2.2. *Geoscientific Model Development*, 11(4):1537–1556.

Cady-Pereira, K., Turner, E., and Saunders, R. (2018). Inter-comparison of line-by-line radiative transfer models MonoRTM and AMSUTRAN for microwave frequencies from the Top-Of-Atmosphere. *NWPSAF-MO-VS-057*.

Cazzoli, G., Puzzarini, C., Buffa, G., and Tarrini, O. (2007). Experimental and theoretical investigation on pressure-broadening and pressure-shifting of the 22.2 ghz line of water. *Journal of Quantitative Spectroscopy and Radiative Transfer*, 105(3):438–449.

Cazzoli, G., Puzzarini, C., Buffa, G., and Tarrini, O. (2008). Pressure-broadening in the THz frequency region: the 1.113 THz line of water. *Journal of Quantitative Spectroscopy and Radiative Transfer*, 109(9):1563–1574.

Chevallier, F., Di Michele, S., and McNally, A. P. (2006). *Diverse profile datasets from the ECMWF 91-level short-range forecasts*. European Centre for Medium-Range Weather Forecasts.

Cimini, D., Hocking, J., Angelis, F. D., Cersosimo, A., Paola, F. D., Gallucci, D., Gentile, S., Geraldi, E., Larosa, S., Nilo, S., et al. (2019). Rttov-gb v1. 0–updates on sensors, absorption models, uncertainty, and availability. *Geoscientific Model Development*, 12(5):1833–1845.

Cimini, D., Rosenkranz, P. W., Tretyakov, M. Y., Koshelev, M. A., and Romano, F. (2018). Uncertainty of atmospheric microwave absorption model: impact on ground-based radiometer simulations and retrievals. *Atmospheric Chemistry and Physics*, 18(20):15231–15259.

Clough, S., Kneizys, F., and Davies, R. (1989). Line shape and the water vapor continuum. *Atmospheric research*, 23(3-4):229–241.

Clough, S., Shephard, M., Mlawer, E., Delamere, J., Iacono, M., Cady-Pereira, K., Boukabara, S., and Brown, P. (2005). Atmospheric radiative transfer modeling: a summary of the AER codes. *Journal of Quantitative Spectroscopy and Radiative Transfer*, 91(2):233–244.

Clough, S. A., Beers, Y., Klein, G. P., and Rothman, L. S. (1973). Dipole moment of water from stark measurements of h2o, hdo, and d2o. *The Journal of Chemical Physics*, 59(5):2254–2259.

Colmont, J.-M., Priem, D., Wlodarczak, G., and Gamache, R. R. (1999). Measurements and calculations of the halfwidth of two rotational transitions of water vapor perturbed by n2, o2, and air. *Journal of molecular spectroscopy*, 193(2):233–243.

Conway, E. K., Gordon, I. E., Tennyson, J., Polyansky, O. L., Yurchenko, S. N., and Chance, K. (2020). A semi-empirical potential energy surface and line list for h 2 16 o extending into the near-ultraviolet. *Atmospheric Chemistry and Physics*, 20(16):10015–10027.

Coudert, L., Martin-Drumel, M.-A., and Pirali, O. (2014). Analysis of the high-resolution water spectrum up to the Second Triad and to J = 30. *Journal of Molecular Spectroscopy*, 303:36–41.

Coudert, L. H. (1999). Line frequency and line intensity analyses of water vapour. *Molecular Physics*, 96(6):941–954.

Croom, D. (1971). The 2.53 mm molecular rotation line of atmospheric o2. *Planetary and Space Science*, 19(7):777–789.

De Angelis, F., Cimini, D., Hocking, J., Martinet, P., and Kneifel, S. (2016). Rttov-gb–adapting the fast radiative transfer model rttov for the assimilation of ground-based microwave radiometer observations. *Geoscientific Model Development*, 9(8):2721–2739.

Drouin, B. J. (2007). Temperature dependent pressure induced linewidths of $o_2$16 and 18o16o transitions in nitrogen, oxygen and air. *Journal of Quantitative Spectroscopy and Radiative Transfer*, 105(3):450–458.

Drouin, B. J., Payne, V., Oyafuso, F., Sung, K., and Mlawer, E. (2014). Pressure broadening of oxygen by water. *Journal of Quantitative Spectroscopy and Radiative Transfer*, 133:190–198.

Drouin, B. J., Yu, S., Miller, C. E., Müller, H. S., Lewen, F., Brünken, S., and Habara, H. (2010). Terahertz spectroscopy of oxygen, O_2, in its 3Σ- g and 1Δ electronic states: THz Spectroscopy of O_2. *Journal of Quantitative Spectroscopy and Radiative Transfer*, 111(9):1167–1173.

Eriksson, P., Buehler, S., Davis, C., Emde, C., and Lemke, O. (2011). Arts, the atmospheric radiative transfer simulator, version 2. *Journal of Quantitative Spectroscopy and Radiative Transfer*, 112(10):1551–1558.

Eriksson, P., Rydberg, B., Mattioli, V., Thoss, A., Accadia, C., Klein, U., and Buehler, S. A. (2020). Towards an operational ice cloud imager (ici) retrieval product. *Atmospheric Measurement Techniques*, 13(1):53–71.

Eyre, J. (1991). A fast radiative transfer model for satellite sounding systems. *ECMWF Tech. Memo 176*.

Eyre, J., Kelly, G., McNally, A., Andersson, E., and Persson, A. (1993). Assimilation of tovs radiance information through one-dimensional variational analysis. *Quarterly Journal of the Royal Meteorological Society*, 119(514):1427–1463.

Flaud, J., Wagner, G., Birk, M., Camy-Peyret, C., Claveau, C., De Backer-Barilly, M., Barbe, A., and Piccolo, C. (2003). Ozone absorption around 10 μm. *Journal of Geophysical Research: Atmospheres*, 108(D9).

Flaud, J.-M., Camy-Peyret, C., Rinsland, C. P., Devi, V. M., Smith, M. A. H., and Goldman, A. (1990a). Improved line parameters for ozone bands in the 10-μm spectral region. *Applied optics*, 29(25):3667–3671.

Flaud, J.-M., Camy-Peyret, C., Rinsland, C. P., Smith, M. A. H., and Devi, V. M. (1990b). Atlas of ozone spectral parameters from microwave to medium infrared.

Fox, S., Lee, C., Moyna, B., Philipp, M., Rule, I., Rogers, S., King, R., Oldfield, M., Rea, S., Henry, M., et al. (2017a). ISMAR: an airborne submillimetre radiometer. *Atmospheric Measurement Techniques*, 10(2):477–490.

Fox, S., Mendrok, J., Eriksson, P., Ekelund, R., O'Shea, S. J., Bower, K. N., Baran, A. J., Harlow, R. C., and Pickering, J. C. (2019). Airborne validation of radiative transfer modelling of ice clouds at millimetre and sub-millimetre wavelengths. *Atmospheric Measurement Techniques*, 12(3):1599–1617.

Fox, S., Turner, E., Newman, S., and Harlow, C. (2017b). Evaluation of clear-sky spectroscopy using ISMAR and MARSS. *Met Office milestone report*.

Frisk, U., Hagström, M., Ala-Laurinaho, J., Andersson, S., Berges, J.-C., Chabaud, J.-P., Dahlgren, M., Emrich, A., Florén, H.-G., Florin, G., et al. (2003). The Odin satellite-I. Radiometer design and test. *Astronomy & Astrophysics*, 402(3):L27–L34.

Froidevaux, L., Livesey, N. J., Read, W. G., Jiang, Y. B., Jimenez, C., Filipiak, M. J., Schwartz, M. J., Santee, M. L., Pumphrey, H. C., Jiang, J. H., et al. (2006). Early validation analyses of atmospheric profiles from EOS MLS on the Aura satellite.

Gamache, R. R. (1985). Temperature dependence of n_2-broadened halfwidths of ozone. *Journal of Molecular Spectroscopy*, 114(1):31–41.

Gamache, R. R., Goldman, A., and Rothman, L. S. (1998). Improved spectral parameters for the three most abundant isotopomers of the oxygen molecule. *Journal of Quantitative Spectroscopy and Radiative Transfer*, 59(3-5):495–509.

Gamache, R. R. and Hartmann, J.-M. (2004). An intercomparison of measured pressure-broadening and pressure-shifting parameters of water vapor. *Canadian journal of chemistry*, 82(6):1013–1027.

Gamache, R. R. and Laraia, A. L. (2009). N_2-, O_2-, and air-broadened half-widths, their temperature dependence, and line shifts for the rotation band of $H_2^{16}O$. *Journal of Molecular Spectroscopy*, 257(2):116–127.

Gamache, R. R., Roller, C., Lopes, E., Gordon, I. E., Rothman, L. S., Polyansky, O. L., Zobov, N. F., Kyuberis, A. A., Tennyson, J., Yurchenko, S. N., et al. (2017). Total internal partition sums for 166 isotopologues of 51 molecules important in planetary atmospheres: Application to HITRAN2016 and beyond. *Journal of Quantitative Spectroscopy and Radiative Transfer*, 203:70–87.

Garand, L., Turner, D., Larocque, M., Bates, J., Boukabara, S., Brunel, P., Chevallier, F., Deblonde, G., Engelen, R., Hollingshead, M., et al. (2001). Radiance and jacobian intercomparison of radiative transfer models applied to hirs and amsu channels. *Journal of Geophysical Research: Atmospheres*, 106(D20):24017–24031.

Golubiatnikov, G. Y. (2005). Shifting and broadening parameters of the water vapor 183-ghz line (3 1 3-2 2 0) by h 2 o, o 2, n 2, co 2, h 2, he, ne, ar, and kr at room temperature. *Journal of Molecular Spectroscopy*, 230(2):196–198.

Golubiatnikov, G. Y., Koshelev, M., and Krupnov, A. (2003). Reinvestigation of pressure broadening parameters at 60-ghz band and single 118.75 ghz oxygen lines at room temperature. *Journal of Molecular Spectroscopy*, 222(2):191–197.

Golubiatnikov, G. Y., Koshelev, M., and Krupnov, A. (2008). Pressure shift and broadening of 110–101 water vapor lines by atmosphere gases. *Journal of Quantitative Spectroscopy and Radiative Transfer*, 109(10):1828–1833.

Golubiatnikov, G. Y. and Krupnov, A. (2003). Microwave study of the rotational spectrum of oxygen molecule in the range up to 1.12 THz. *Journal of Molecular Spectroscopy*, 217(2):282–287.

Gordon, I. E., Rothman, L. S., Gamache, R. R., Jacquemart, D., Boone, C., Bernath, P. F., Shephard, M. W., Delamere, J. S., and Clough, S. A. (2007). Current updates of the water-vapor line list in HITRAN: A new 'Diet' for air-broadened half-widths. *Journal of Quantitative Spectroscopy and Radiative Transfer*, 108(3):389–402.

Gordon, I. E., Rothman, L. S., Hill, C., Kochanov, R. V., Tan, Y., Bernath, P. F., Birk, M., Boudon, V., Campargue, A., Chance, K., et al. (2017). The HITRAN 2016 molecular spectroscopic database. *Journal of Quantitative Spectroscopy and Radiative Transfer*, 203:3–69.

Hewison, T. J., Cimini, D., Martin, L., Gaffard, C., and Nash, J. (2006). Validating clear air absorption models using ground-based microwave radiometers and vice-versa. *Meteorologische Zeitschrift*, 15(1):27–36.

Hocking, J., Vidot, J., Brunel, P., Roquet, P., Silveira, B., Turner, E., and Lupu, C. (2021). A new gas absorption optical depth parameterisation for rttov v13. *Geoscientific Model Development Discussions*, pages 1–28.

Humlíček, J. (1982). Optimized computation of the voigt and complex probability functions. *Journal of Quantitative Spectroscopy and Radiative Transfer*, 27(4):437–444.

Jacquemart, D., Gamache, R., and Rothman, L. S. (2005). Use of the semi-empirical coefficients of section 4.2.1: Semi-empirical calculation of air-broadened half-widths and air pressure-induced frequency shifts of water-vapor absorption lines. *Journal of Quantitative Spectroscopy and Radiative Transfer*, 96(2):205–239.

Jacquinet-Husson, N., Armante, R., Scott, N., Chédin, A., Crépeau, L., Boutammine, C., Bouhdaoui, A., Crevoisier, C., Capelle, V., Boonne, C., et al. (2016). The 2015 edition of the GEISA spectroscopic database. *Journal of Molecular Spectroscopy*, 327:31–72.

John, V. and Buehler, S. (2004). The impact of ozone lines on AMSU-B radiances. *Geophysical research letters*, 31(21).

Kidder, S. Q., Goldberg, M. D., Zehr, R. M., DeMaria, M., Purdom, J. F., Velden, C. S., Grody, N. C., and Kusselson, S. J. (2000). Satellite analysis of tropical cyclones using the advanced microwave sounding unit (amsu). *Bulletin of the American Meteorological Society*, 81(6):1241–1260.

Kikuchi, K.-i., Nishibori, T., Ochiai, S., Ozeki, H., Irimajiri, Y., Kasai, Y., Koike, M., Manabe, T., Mizukoshi, K., Murayama, Y., et al. (2010). Overview and early results of the Superconducting Submillimeter-Wave Limb-Emission Sounder (SMILES). *Journal of Geophysical Research: Atmospheres*, 115(D23).

Kim, E., Lyu, C.-H. J., Anderson, K., Vincent Leslie, R., and Blackwell, W. J. (2014). S-NPP ATMS instrument prelaunch and on-orbit performance evaluation. *Journal of Geophysical Research: Atmospheres*, 119(9):5653–5670.

Koshelev, M. (2011). Collisional broadening and shifting of the 211-202 transition of h216o, h217o, h218o by atmosphere gases. *Journal of Quantitative Spectroscopy and Radiative Transfer*, 112(3):550–552.

Koshelev, M., Delahaye, T., Serov, E., Vilkov, I., Boulet, C., and Tretyakov, M. Y. (2017). Accurate modeling of the diagnostic 118-ghz oxygen line for remote sensing of the atmosphere. *Journal of Quantitative Spectroscopy and Radiative Transfer*, 196:78–86.

Koshelev, M., Golubiatnikov, G. Y., Vilkov, I., and Tretyakov, M. Y. (2018a). Line shape parameters of the 22-ghz water line for accurate modeling in atmospheric applications. *Journal of Quantitative Spectroscopy and Radiative Transfer*, 205:51–58.

Koshelev, M., Serov, E., Parshin, V., and Tretyakov, M. Y. (2011). Millimeter wave continuum absorption in moist nitrogen at temperatures 261–328 K. *Journal of Quantitative Spectroscopy and Radiative Transfer*, 112(17):2704–2712.

Koshelev, M., Tretyakov, M. Y., Golubiatnikov, G. Y., Parshin, V., Markov, V., and Koval, I. (2007). Broadening and shifting of the 321-, 325-and 380-ghz lines of water vapor by pressure of atmospheric gases. *Journal of Molecular Spectroscopy*, 241(1):101–108.

Koshelev, M., Vilkov, I., Makarov, D., Tretyakov, M. Y., and Rosenkranz, P. (2021a). Speed-dependent broadening of the o2 fine-structure lines. *Journal of Quantitative Spectroscopy and Radiative Transfer*, 264:107546.

Koshelev, M., Vilkov, I., Makarov, D., Tretyakov, M. Y., Vispoel, B., Gamache, R., Cimini, D., Romano, F., and Rosenkranz, P. (2021b). Water vapor line profile at 183-ghz: Temperature dependence of broadening, shifting, and speed-dependent shape parameters. *Journal of Quantitative Spectroscopy and Radiative Transfer*, 262:107472.

Koshelev, M., Vilkov, I., and Tretyakov, M. Y. (2015). Pressure broadening of oxygen fine structure lines by water. *Journal of Quantitative Spectroscopy and Radiative Transfer*, 154:24–27.

Koshelev, M., Vilkov, I., and Tretyakov, M. Y. (2016). Collisional broadening of oxygen fine structure lines: The impact of temperature. *Journal of Quantitative Spectroscopy and Radiative Transfer*, 169:91–95.

Koshelev, M. A., Leonov, I. I., Serov, E. A., Chernova, A. I., Balashov, A. A., Bubnov, G. M., Andriyanov, A. F., Shkaev, A. P., Parshin, V. V., Krupnov, A. F., et al. (2018b). New frontiers in modern resonator spectroscopy. *IEEE Transactions on Terahertz Science and Technology*, 8(6):773–783.

Kuhn, T., Bauer, A., Godon, M., Buehler, S., and Künzi, K. (2002). Water vapor continuum: absorption measurements at 350 GHz and model calculations. *Journal of Quantitative Spectroscopy and Radiative Transfer*, 74(5):545–562.

Lanquetin, R., Coudert, L., and Camy-Peyret, C. (2001). High-lying rotational levels of water: an analysis of the energy levels of the five first vibrational states. *Journal of molecular spectroscopy*, 206(1):83–103.

Larsson, R., Lankhaar, B., and Eriksson, P. (2019). Updated Zeeman effect splitting coefficients for molecular oxygen in planetary applications. *Journal of Quantitative Spectroscopy and Radiative Transfer*, 224:431–438.

Lenoir, W. B. (1967). Propagation of partially polarized waves in a slightly anisotropic medium. *Journal of Applied Physics*, 38(13):5283–5290.

Liebe, H., Hufford, G., and Cotton, M. (1993). Propagation modeling of moist air and suspended water/ice particles at frequencies below 1000 GHz. In *In AGARD, Atmospheric Propagation Effects Through Natural and Man-Made Obscurants for Visible to MM-Wave Radiation 11 p (SEE N94-30495 08-32)*.

Liebe, H., Rosenkranz, P., and Hufford, G. (1992). Atmospheric 60 GHz oxygen spectrum: New laboratory measurements and line parameters. *Journal of Quantitative Spectroscopy and Radiative Transfer*, 48(5-6):629–643.

Liebe, H. J. (1989). MPM–An atmospheric millimeter-wave propagation model. *International Journal of Infrared and Millimeter Waves*, 10(6):631–650.

Liebe, H. J. and Dillon, T. A. (1969). Accurate foreign-gas-broadening parameters of the 22-ghz h2o line from refraction spectroscopy. *The Journal of Chemical Physics*, 50(2):727–732.

Liebe, H. J. and Layton, D. H. (1987). *Millimeter-wave properties of the atmosphere: Laboratory studies and propagation modeling*. US Department of Commerce, National Telecommunications and Information Administration.

Liljegren, J. C., Boukabara, S. A., Cady-Pereira, K., and Clough, S. A. (2005). The effect of the half-width of the 22 GHz water vapor line on retrievals of temperature and water vapor profiles with a twelve-channel microwave radiometer. *IEEE Trans. Geosci. Remote Sens*, 43(5):1102–1108.

Liu, Q., Weng, F., Han, Y., and van Delst, P. (2008). Community radiative transfer model for scattering transfer and applications. In *IGARSS 2008-2008 IEEE International Geoscience and Remote Sensing Symposium*, volume 4, pages IV–1193. IEEE.

Lodi, L., Tennyson, J., and Polyansky, O. L. (2011). A global, high accuracy ab initio dipole moment surface for the electronic ground state of the water molecule. *The Journal of chemical physics*, 135(3):034113.

Ma, Q., Tipping, R., and Gamache, R. (2010). Uncertainties associated with theoretically calculated n2-broadened half-widths of h2o lines. *Molecular Physics*, 108(17):2225–2252.

Mackie, C., Gordon, I., Rothman, L., Leshchishina, O., Kassi, S., Campargue, A., et al. (2011). Revision of spectral parameters for the bands of oxygen that involve ground x 3 σ g à and first excited a 1 δ g electronic states (in preparation). *J Quant Spectrosc Radiat Transfer*.

Makarov, D., Koval, I., Koshelev, M., Parshin, V., and Tretyakov, M. Y. (2008). Collisional parameters of the 118-GHz oxygen line: Temperature dependence. *Journal of Molecular Spectroscopy*, 252(2):242–243.

Makarov, D., Tretyakov, M. Y., and Boulet, C. (2013). Line mixing in the 60-GHz atmospheric oxygen band: Comparison of the MPM and ECS model. *Journal of Quantitative Spectroscopy and Radiative Transfer*, 124:1–10.

Makarov, D., Tretyakov, M. Y., and Rosenkranz, P. (2011). 60-GHz oxygen band: Precise experimental profiles and extended absorption modeling in a wide temperature range. *Journal of Quantitative Spectroscopy and Radiative Transfer*, 112(9):1420–1428.

Makarov, D., Vilkov, I., Koshelev, M., Aderkina, A., and Tretyakov, M. Y. (2018). Collisional Coupling of the Molecular Oxygen 16 O_2 Fine-Structure Lines Under Low Pressures. *Radiophysics and Quantum Electronics*, 60(10):808–823.

Makarov, D. S., Tretyakov, M. Y., and Rosenkranz, P. W. (2020). Revision of the 60-ghz atmospheric oxygen absorption band models for practical use. *Journal of Quantitative Spectroscopy and Radiative Transfer*, 243:106798.

Martin, M., Coudert, L., Pirali, O., and Balcon, O. (2016). Positions and intensities of water vapor transitions in 0–6000 cm à 1 region. *J Chem Phys*, in preparation.

Matricardi, M. (2007). *An inter-comparison of line-by-line radiative transfer models*. European Centre for Medium-Range Weather Forecasts.

Matricardi, M. (2008). *The generation of RTTOV regression coefficients for IASI and AIRS using a new profile training set and a new line-by-line database*. European Centre for Medium-Range Weather Forecasts.

Matsushima, F., Odashima, H., Iwasaki, T., Tsunekawa, S., and Takagi, K. (1995). Frequency measurement of pure rotational transitions of h2o from 0.5 to 5 thz. *Journal of molecular structure*, 352:371–378.

McClatchey, R. A., Benedict, W., Clough, S. A., Burch, D., and Calfee, R. F. (1973). AFCRL atmospheric absorption line parameters compilation. Technical report, Air Force Cambridge Research Labs HANSCOM AFB MA.

Melsheimer, C., Verdes, C., Buehler, S., Emde, C., Eriksson, P., Feist, D., Ichizawa, S., John, V., Kasai, Y., Kopp, G., et al. (2005). Intercomparison of general purpose clear sky atmospheric radiative transfer models for the millimeter/submillimeter spectral range. *Radio Science*, 40(1):1–25.

Mlawer, E., Turner, D., Paine, S., Palchetti, L., Bianchini, G., Payne, V., Cady-Pereira, K., Pernak, R., Alvarado, M., Gombos, D., et al. (2019). Analysis of water vapor absorption in the far-infrared and submillimeter regions using surface radiometric measurements from extremely dry locations. *Journal of Geophysical Research: Atmospheres*.

Mlawer, E. J., Payne, V. H., Moncet, J.-L., Delamere, J. S., Alvarado, M. J., and Tobin, D. C. (2012). Development and recent evaluation of the MT_CKD model of continuum absorption. *Philosophical Transactions of the Royal Society A: Mathematical, Physical and Engineering Sciences*, 370(1968):2520–2556.

Moradi, I., Goldberg, M., Brath, M., Ferraro, R., Buehler, S. A., Saunders, R., and Sun, N. (2020). Performance of radiative transfer models in the microwave region. *Journal of Geophysical Research: Atmospheres*, 125(6):e2019JD031831.

Odintsova, T., Tretyakov, M. Y., Pirali, O., and Roy, P. (2017). Water vapor continuum in the range of rotational spectrum of h2o molecule: New experimental data and their comparative analysis. *Journal of Quantitative Spectroscopy and Radiative Transfer*, 187:116–123.

Odintsova, T., Tretyakov, M. Y., Zibarova, A., Pirali, O., Roy, P., and Campargue, A. (2019). Far-infrared self-continuum absorption of h216o and h218o (15–500 cm- 1). *Journal of Quantitative Spectroscopy and Radiative Transfer*, 227:190–200.

Pardo, J. R., Cernicharo, J., and Serabyn, E. (2001a). Atmospheric transmission at microwaves (ATM): an improved model for millimeter/submillimeter applications. *IEEE Transactions on antennas and propagation*, 49(12):1683–1694.

Pardo, J. R. and Rayer, P. (2016). Atmospheric clear-sky radiative transfer model intercomparison at mm/submm wavelengths. *NWPSAF-MO-VS-056*.

Pardo, J. R., Serabyn, E., and Cernicharo, J. (2001b). Submillimeter atmospheric transmission measurements on mauna kea during extremely dry el nino conditions: implications for broadband opacity contributions. *Journal of Quantitative Spectroscopy and Radiative Transfer*, 68(4):419–433.

Payne, V. H., Delamere, J. S., Cady-Pereira, K. E., Gamache, R. R., Moncet, J.-L., Mlawer, E. J., and Clough, S. A. (2008). Air-broadened half-widths of the 22 and 183 GHz water-vapor lines. *IEEE Transactions on Geoscience and Remote Sensing*, 46(11):3601–3617.

Payne, V. H., Mlawer, E. J., Cady-Pereira, K. E., and Moncet, J.-L. (2011). Water vapor continuum absorption in the microwave. *IEEE Transactions on Geoscience and Remote Sensing*, 49(6):2194–2208.

Perrin, A., Puzzarini, C., Colmont, J.-M., Verdes, C., Wlodarczak, G., Cazzoli, G., Buehler, S., Flaud, J.-M., and Demaison, J. (2005). Molecular line parameters for the master (millimeter wave acquisitions for stratosphere/troposphere exchange research) database. *Journal of atmospheric chemistry*, 51(2):161–205.

Pickett, H., Poynter, R., Cohen, E., Delitsky, M., Pearson, J., and Müller, H. (1998). Submillimeter, millimeter, and microwave spectral line catalog. *Journal of Quantitative Spectroscopy and Radiative Transfer*, 60(5):883–890.

Podobedov, V., Plusquellic, D., Siegrist, K., Fraser, G., Ma, Q., and Tipping, R. (2008). New measurements of the water vapor continuum in the region from 0.3 to 2.7 THz. *Journal of Quantitative Spectroscopy and Radiative Transfer*, 109(3):458–467.

Robert, D. and Bonamy, J. (1979). Short range force effects in semiclassical molecular line broadening calculations. *Journal de Physique*, 40(10):923–943.

Rosenkranz, P. (1988). Interference coefficients for overlapping oxygen lines in air. *Journal of Quantitative Spectroscopy and Radiative Transfer*, 39(4):287–297.

Rosenkranz, P. (1993). Absorption of microwaves by atmospheric gases. John Wiley and Sons.

Rosenkranz, P. W. (1998). Water vapor microwave continuum absorption: A comparison of measurements and models. *Radio Science*, 33(4):919–928.

Rosenkranz, P. W. and Cimini, D. (2019). Speed dependence of 22-and 118-ghz line shapes for tropospheric remote sensing. *IEEE Transactions on Geoscience and Remote Sensing*, 57(12):9702–9708.

Rosenkranz, P. W. and Staelin, D. H. (1988). Polarized thermal microwave emission from oxygen in the mesosphere. *Radio Science*, 23(5):721–729.

Rothman, L., Barbe, A., Benner, D. C., Brown, L., Camy-Peyret, C., Carleer, M., Chance, K., Clerbaux, C., Dana, V., Devi, V. M., et al. (2003). The HITRAN molecular spectroscopic database: edition of 2000 including updates through 2001. *Journal of Quantitative Spectroscopy and Radiative Transfer*, 82(1-4):5–44.

Rothman, L. S., Gamache, R., Tipping, R., Rinsland, C., Smith, M., Benner, D. C., Devi, V. M., Flaud, J.-M., Camy-Peyret, C., Perrin, A., et al. (1992). The hitran molecular database: editions of 1991 and 1992. *Journal of Quantitative Spectroscopy and Radiative Transfer*, 48(5-6):469–507.

Rothman, L. S. and Gordon, I. (2006). Steps for Converting Intensities from the JPL (or CDMS) Catalog to HITRAN Intensities.

Rothman, L. S., Gordon, I. E., Babikov, Y., Barbe, A., Benner, D. C., Bernath, P. F., Birk, M., Bizzocchi, L., Boudon, V., Brown, L. R., et al. (2013). The HITRAN2012 molecular spectroscopic database. *Journal of Quantitative Spectroscopy and Radiative Transfer*, 130:4–50.

Rothman, L. S., Jacquemart, D., Barbe, A., Benner, D. C., Birk, M., Brown, L., Carleer, M., Chackerian Jr, C., Chance, K., Coudert, L. e. a., et al. (2005). The HITRAN 2004 molecular spectroscopic database. *Journal of Quantitative Spectroscopy and Radiative Transfer*, 96(2):139–204.

Rubens, H. and Aschkinass, E. (1898). Observations on the absorption and emission of aqueous vapor and carbon dioxide in the infra-red spectrum. *The Astrophysical Journal*, 8:176.

Ryadov, V. Y. and Furashov, N. (1966). The width of the water vapor absorption line λ= 0.92 mm. *Radiophysics and Quantum Electronics*, 9(6):621–623.

Saunders, R., Hocking, J., Rundle, D., Rayer, P., Matricardi, M., Geer, A., Cristina, L., Brunel, P., and Vidot, J. (2013). RTTOV-11 science and validation report; EUMETSAT NWP SAF. Technical report, NWPSAF-MO-TV-32.

Saunders, R., Hocking, J., Turner, E., Rayer, P., Rundle, D., Brunel, P., Vidot, J., Roquet, P., Matricardi, M., Geer, A., et al. (2018). An update on the RTTOV fast radiative transfer model (currently at version 12). *Geoscientific Model Development*, 11(7):2717–2737.

Schreier, F., Milz, M., Buehler, S. A., and von Clarmann, T. (2018). Intercomparison of three microwave/infrared high resolution line-by-line radiative transfer codes. *Journal of Quantitative Spectroscopy and Radiative Transfer*, 211:64–77.

Scribano, Y. and Leforestier, C. (2007). Contribution of water dimer absorption to the millimeter and far infrared atmospheric water continuum. *The Journal of chemical physics*, 126(23):234301.

Serov, E., Koshelev, M., Odintsova, T., Parshin, V., and Tretyakov, M. Y. (2014). Rotationally resolved water dimer spectra in atmospheric air and pure water vapour in the 188–258 GHz range. *Physical Chemistry Chemical Physics*, 16(47):26221–26233.

Serov, E., Odintsova, T., Tretyakov, M. Y., and Semenov, V. (2017). On the origin of the water vapor continuum absorption within rotational and fundamental vibrational bands. *Journal of Quantitative Spectroscopy and Radiative Transfer*, 193:1–12.

Serov, E., Stolarczyk, N., Makarov, D., Vilkov, I., Golubiatnikov, G. Y., Balashov, A., Koshelev, M., Wcislo, P., Thibault, F., and Tretyakov, M. Y. (2021). Co-ar collisions: ab initio model matches experimental spectra at a sub percent level over a wide pressure range. *Journal of Quantitative Spectroscopy and Radiative Transfer*, page 107807.

Shine, K. P., Ptashnik, I. V., and Rädel, G. (2012). The water vapour continuum: brief history and recent developments. *Surveys in Geophysics*, 33(3-4):535–555.

Slocum, D. M., Slingerland, E. J., Giles, R. H., and Goyette, T. M. (2013). Atmospheric absorption of terahertz radiation and water vapor continuum effects. *Journal of Quantitative Spectroscopy and Radiative Transfer*, 127:49–63.

Smith, M. (2001). Characterization of line broadening and shift parameters of ozone for spectroscopic databases. *56th International symposium on molecular spectroscopy, Ohio State University, June 11–15*, page Paper ME03.

Thomas, B., Brandt, M., Walber, A., Gibson, H., Philipp, M., Sonnabend, G., Benzazaa, M., Gonzalez, R., Bergada, M., Martinez, J., et al. (2014). Millimeter & sub-millimeter wave radiometer instruments for the next generation of polar orbiting meteorological satellites-MetOp-SG. In *Infrared, Millimeter, and Terahertz waves (IRMMW-THz), 2014 39th International Conference on*, pages 1–3. IEEE.

Tretyakov, M. Y. (2016). Spectroscopy underlying microwave remote sensing of atmospheric water vapor. *Journal of Molecular Spectroscopy*, 328:7–26.

Tretyakov, M. Y., Golubiatnikov, G. Y., Parshin, V., Koshelev, M., Myasnikova, S., Krupnov, A., and Rosenkranz, P. (2004). Experimental study of the line mixing coefficient for 118.75 ghz oxygen line. *Journal of Molecular Spectroscopy*, 223(1):31–38.

Tretyakov, M. Y., Koshelev, M., Dorovskikh, V., Makarov, D., and Rosenkranz, P. (2005). 60-GHz oxygen band: precise broadening and central frequencies of fine-structure lines, absolute absorption profile at atmospheric pressure, and revision of mixing coefficients. *Journal of Molecular Spectroscopy*, 231(1):1–14.

Tretyakov, M. Y., Koshelev, M., Koval, I., Parshin, V., Kukin, L., Fedoseev, L., Dryagin, Y. A., and Andriyanov, A. (2007). Temperature dependence of pressure broadening of the n= 1- fine structure oxygen line at 118.75 ghz. *Journal of Molecular Spectroscopy*, 241(1):109–111.

Tretyakov, M. Y., Koshelev, M., Vilkov, I., Parshin, V., and Serov, E. (2013a). Resonator spectroscopy of the atmosphere in the 350–500 ghz range. *Journal of Quantitative Spectroscopy and Radiative Transfer*, 114:109–121.

Tretyakov, M. Y., Parshin, V., Shanin, V., Myasnikova, S., Koshelev, M., and Krupnov, A. (2001). Real atmosphere laboratory measurements of the 118-ghz oxygen line: Shape, shift, and broadening of the line. *Journal of molecular spectroscopy*, 208(1):110–112.

Tretyakov, M. Y., Serov, E., Koshelev, M., Parshin, V., and Krupnov, A. (2013b). Water dimer rotationally resolved millimeter-wave spectrum observation at room temperature. *Physical Review Letters*, 110(9):093001.

Turner, D., Mlawer, E., Bianchini, G., Cadeddu, M., Crewell, S., Delamere, J., Knuteson, R., Maschwitz, G., Mlynczak, M., Paine, S., et al. (2012). Ground-based high spectral resolution observations of the entire terrestrial spectrum under extremely dry conditions. *Geophysical Research Letters*, 39(10).

Turner, D. D., Cadeddu, M. P., Lohnert, U., Crewell, S., and Vogelmann, A. M. (2009). Modifications to the water vapor continuum in the microwave suggested by ground-based 150-GHz observations. *IEEE Transactions on Geoscience and Remote Sensing*, 47(10):3326–3337.

Turner, E., Rayer, P., and Saunders, R. (2019). AMSUTRAN: A microwave transmittance code for satellite remote sensing. *Journal of Quantitative Spectroscopy and Radiative Transfer*.

Turner, E. C., Withington, S., Newnham, D. A., Wadhams, P., Jones, A. E., and Clancy, R. (2016). Simulation of submillimetre atmospheric spectra for characterising potential ground-based remote sensing observations. *Atmospheric Measurement Techniques*, 9(11):5461–5485.

Van Vleck, J. H. and Weisskopf, V. F. (1945). On the shape of collision-broadened lines. *Reviews of Modern Physics*, 17(2-3):227.

Vispoel, B., Cavalcanti, J. H., and Gamache, R. R. (2019). Modified complex robert-bonamy calculations of line shape parameters and their temperature dependence for water vapor in collision with n2. *Journal of Quantitative Spectroscopy and Radiative Transfer*, 228:79–89.

Wagner, G., Birk, M., Schreier, F., and Flaud, J.-M. (2002). Spectroscopic database for ozone in the fundamental spectral regions. *Journal of Geophysical Research: Atmospheres*, 107(D22):ACH–10.

Wang, D., Prigent, C., Aires, F., and Jimenez, C. (2017). A statistical retrieval of cloud parameters for the millimeter wave Ice Cloud Imager on board MetOp-SG. *IEEE Access*, 5:4057–4076.

Watson, J. K. G. (1977). Aspects of quartic and sextic centrifugal effects on rotational energy levers. *J. R. Durig, Ed, Amsterdam: Elsevier*, 6.

Wentz, F. J. and Meissner, T. (2016). Atmospheric absorption model for dry air and water vapor at microwave frequencies below 100 GHz derived from spaceborne radiometer observations. *Radio Science*, 51(5):381–391.

Yang, J., Ding, S., Dong, P., Bi, L., and Yi, B. (2020). Advanced radiative transfer modeling system developed for satellite data assimilation and remote sensing applications. *Journal of Quantitative Spectroscopy and Radiative Transfer*, 251:107043.

Yu, S., Drouin, B. J., and Miller, C. E. (2014). High resolution spectral analysis of oxygen. IV. Energy levels, partition sums, band constants, RKR potentials, Franck-Condon factors involving the X 3 Σ g-, a 1Δ g and b 1 Σ g+ states. *The Journal of chemical physics*, 141(17):174302.

Zeeman, P. (1896). On the Influence of Magnetism on the Nature of the Light Emitted by a Substance (Part I). *Communications from the Physical Laboratory at the University of Leiden*, 33:1–8.